UNIVERSIDADE DE SÃO PAULO
INSTITUTO DE FÍSICA DE SÃO CARLOS

Jesuel Marques Leal Junior

The lattice quark propagator at finite temperature

São Carlos

2024

Jesuel Marques Leal Junior

The lattice quark propagator at finite temperature

Thesis presented to the Graduate Program in Physics at the Instituto de Física de São Carlos da Universidade de São Paulo, to obtain the degree of Doctor in Science.

Concentration area: Theoretical and Experimental Physics

Advisor: Profa. Dra. Tereza Cristina da Rocha Mendes

Original version

São Carlos

2024

Leal Junior, Jesuel Marques
The lattice quark propagator at finite temperature / Jesuel Marques Leal Junior; advisor Tereza Cristina da Rocha Mendes -- São Carlos 2024.
166 p.

Thesis (Doctorate - Graduate Program in Theoretical and Experimental Physics) -- Instituto de Física de São Carlos, Universidade de São Paulo - Brasil , 2024.

1. QCD. 2. Lattice QCD. 3. Quark propagator. 4. QCD at finite temperature. 5. Landau gauge-fixing. I. Mendes, Tereza Cristina da Rocha, advisor. II. Title.

FOLHA DE APROVAÇÃO

Jesuel Marques Leal Júnior

Tese apresentada ao Instituto de Física de São Carlos da Universidade de São Paulo para obtenção do título de Doutor em Ciências. Área de Concentração: Física Teórica e Experimental

Aprovado (a) em: 18/04/2024

Comissão Julgadora

Dr(a).: Tereza Cristina da Rocha Mendes

Instituição: (IFSC/USP)

Dr(a).: Arlene Cristina Aguilar

Instituição: (UNICAMP/Campinas)

Dr(a).: Letícia Faria Domingues Palhares

Instituição: (UERJ/Rio de Janeiro)

Dr(a).: Antonio Duarte Pereira Junior

Instituição: (UFF/Niterói)

Dr(a).: Tobias Frederico

Instituição: (ITA/São José dos Campos)

Dedico essa tese a minha esposa Amanda
que é meu amor, meu centro e minha paz.

ACKNOWLEDGEMENTS

Agradeço à FAPESP pelo apoio financeiro através da bolsa no país (processo nº 2019/10913-0) e à que bancou minha estadia na Irlanda durante o BEPE (processo nº 2021/11101-9).

À minha orientadora, Professora Tereza Mendes, agradeço pela leitura atenta desta tese, pela liberdade que me deu no trabalho e pela confiança. Agradeço ao grupo do IFSC, composto pelo Professor Attilio Cucchieri, Rafael Tonhon, João Otavio Kül, Artur Soares, Sasa Salmen. Agradeço também grandemente aos membros anteriores do grupo: Willian Serenone, Leandro Viscardi, e em especial ao Matheus Cerqueira e Nelson Lachini, que se tornaram meus amigos, e com os quais compartilhei parte do meu tempo inicial no IFSC. Sem os excelentes trabalhos anteriores do grupo, minha vida de doutorando teria sido muito mais difícil, portanto deixo aqui o meu reconhecimento.

Agradeço aos outros membros do IFSC que de uma forma ou de outra acompanharam esse trabalho e estiveram em reuniões do seminário de altas energias: Professor Diogo Boito e seus alunos Fábio Oliani, Marcus Vinícius Gonzalez, Gabriel das Neves e Cristiane London. Outros amigos que fiz no IFSC, que me acompanharam nas disciplinas e em momentos de lazer em São Carlos, me apoiando de diversas maneiras são Felipe Cônsole, Ronaldo Araújo, Marcos Trivelato, Nícolas Morazotti, Julian Zanon, Laís dos Anjos e Rodrigo Dourado.

Agradeço à minha banca de qualificação pelos apontamentos que contribuíram para a evolução do meu trabalho e me fizeram procurar entender melhor o que estava fazendo. Fica aqui meu obrigado aos professores Luiz Agostinho Ferreira, Gastão Krein e Kanchan Khemchandani. Ao professor Agostinho também gostaria de agradecer por me permitir participar da sua disciplina como aluno ouvinte, o que contribuiu também de forma positiva em minha formação. Ao professor Gastão, assim como ao professor Bruno El-Bennich, juntamente com seus grupos de pesquisa, agradeço pelos seminários que participei em sua companhia no IFT-UNESP.

Na Irlanda fui recebido por minha amiga Ana Retore, que me ajudou muito a me acostumar com Dublin, includindo seu mercado imobiliário insano. Obrigado, Ana. Through her I made two more friends, Chiara Paletta and Aradhita Chattopadhyaya. In Maynooth, Dale Lawlor was immensely patient with my infinite stream of questions. I had the pleasure of sharing an office room with Phillip Cussen-Burke and Babatunde Ayeni. Aonghus McCabe, John Brennan, Kay Lehnert and Hannah O'Brennan helped me a lot and were always pleasant company. I have to thank Professors Paul Watts, Graham Kells and, of course, my supervisor there Prof. Jon-Ivar Skullerud. Besides Prof. Skullerud, I

must also thank the other members of the FASTSUM collaboration for allowing me to participate in their meetings and have access to their materials. Os professores Orlando e Paulo me receberam tão bem em Coimbra e devo agradecê-los pela ótima semana lá, assim como pela ajuda com meus códigos e dúvidas sobre QCD na rede. I thank them and also Prof. Ayşe Kızılersü for the nice discussions in the vertex meeting.

Agradeço à Wikipedia, ao Sci-hub/Libgen e a todas as outras iniciativas que tentam fazer com que o conhecimento chegue ao maior número possível de pessoas. Eles sabem que essa é a maneira mais efetiva de salvaguardar nossa sabedoria limitada sobre o universo, que, no final, é o que mais importa.

Devo um muito obrigado aos meus colegas do IFT que se tornaram amigos pessoais e que espero guardar para toda a vida: Natália Tenório e Jogean Matheus Carvalho. Vocês me ajudaram muito a manter a sanidade durante a pandemia em nossas discussões culturais e também nas mais descontraídas.

Aos meus amigos de graduação Santiago Giménez, Vinícius Pena, Caique Ronqui, Bleider Santos, Lu Xavier, Theo Motta e Ricardo Costa, agradeço por terem continuado ao meu lado, seja jogando, bebendo, trocando mensagens pelo celular sobre tudo e nada, ou simplesmente dando risada das coisas.

Agradeço aos meus amigos da escola Rafael Kawamura, Alberto Souza, Henrique Oliveira, Marcos Akira Ueda, Victor Nunes, Maria Eugênia Dela Rosa, Paulo Scheluchuak, Victor Hugo de Carvalho, Ingrid Person e Ana Lydia Carvalho. Nem consigo acreditar que já nos conhecemos há tanto tempo. Apesar de todas as provações, nossa amizade permanece, mesmo que de longe muitas vezes.

Meus novos amigos de AOE2, que também me ajudaram a encontrar diversão e motivos para gargalhar nesses anos tão difíceis e, por isso, merecem meu muito obrigado: Além de alguns já citados acima, Nando, Rodrigo, Marvin, Vagi, Valnir e Will.

Agradeço ao São Paulo Futebol Clube, que tem me dado muitas alegrias.

Agradeço à família da Amanda, dona Adeli, seu Doda, Josiane e Daiane, que me acolheram e que agora também são parte de mim. Agradeço especialmente à minha sobrinha Clarissa e aos meus sobrinhos Augusto e Benício, que me mostram o tanto de amor que tenho em mim.

A meus pais, que sempre fizeram tudo que estava em seu poder para me ajudar e me ver bem. Não consigo expressar em palavras todo o amor e gratidão que tenho por vocês.

Devo muitos agradecimentos à minha amada esposa e companheira Amanda, que me aguenta, faça chuva ou faça sol, e me apoia, sofre e se diverte comigo. Você me faz melhor.

"The world is dark, and knowledge is light,
a sparkling jewel to lead you through the night -
without it you would wander mystified,
Like Alexander lost without a guide;
But if you trust its light too much, despair
will be the sequel of pedantic care,
And if you underestimate this jewel
Despair will mark you as a righteous fool (...)"
Attar of Nishapur. Translation by Dick Davis and Afkham Darbandi

ABSTRACT

LEAL JUNIOR, J. M. **The lattice quark propagator at finite temperature**. 2024. 166p. Thesis (Doctor in Science) - Instituto de Física de São Carlos, Universidade de São Paulo, São Carlos, 2024.

Quantum Chromodynamics (QCD) is the theory currently used to describe the strong interaction between quarks and gluons. One of the characteristic features of the theory is its behavior at high energies, where the small coupling between the particles allows for the safe application of traditional quantum field theory techniques, such as perturbative expansions. Conversely, at low energies, the coupling grows and perturbative methods break down. The defining features in the low-energy regime are confinement and spontaneous chiral symmetry breaking. A satisfactory theoretical explanation of these infrared phenomena is still lacking, although a consensus has formed that the use of non-perturbative tools is imperative in their study. An interesting laboratory to explore confinement and chiral symmetry breaking is the environment described by QCD at high temperatures, as the theory is found to undergo chiral symmetry restoration and also a transition to a quark-gluon plasma. In this plasma the fundamental particles are found to be deconfined but strongly interacting. The Green's functions (also called N-point functions or correlators) of the theory encapsulate information relevant to the description of the aforementioned non-perturbative low-energy phenomena. The primary objective of this thesis was the calculation of a particular correlator, the quark propagator, in the vacuum and at finite temperatures. To this end, we have performed numerical simulations using the non-perturbative framework of Lattice Quantum Chromodynamics, which presents a discretized and Euclidean version of QCD, preserving the internal $SU(3)$ gauge symmetry of the theory exactly. We have used the quenched approximation and produced ensembles of gauge configurations for several lattice volumes and temperatures. The quark propagator was computed in the vacuum and at temperatures above the deconfinement transition. A necessary step in the study of correlators in general, and propagators in particular, is setting up a gauge fixing scheme. As a valuable by-product of this project, we have refined and optimized algorithms for $SU(3)$ gauge fixing to Landau gauge on the lattice. In this thesis, we present the approach of Lattice Quantum Chromodynamics, including the introduction of fermions on the lattice and the algorithms employed in the simulations. Our findings encompass the thermal effects on the quark propagator, as well as the results of the Landau gauge fixing optimizations.

Keywords: QCD. Lattice QCD. Quark Propagator. QCD at Finite Temperature. Landau Gauge-Fixing.

RESUMO

LEAL JUNIOR, J. M. **O propagador de quark na rede a temperatura finita**. 2024. 166p. Tese (Doutorado em Ciências) - Instituto de Física de São Carlos, Universidade de São Paulo, São Carlos, 2024.

A cromodinâmica quântica (QCD) é a teoria utilizada para descrever a interação forte entre quarks e glúons. Uma das características da teoria é seu comportamento a altas energias, em que o acoplamento pequeno entre as partículas permite o uso de técnicas tradicionais de teoria quântica de campos, como expansões perturbativas. Por outro lado, no regime de baixas energias, o acoplamento cresce e métodos perturbativos não funcionam. As características mais notáveis da teoria para baixas energias são o confinamento e a presença de quebra espontânea da simetria quiral. Uma explicação teórica satisfatória desses fenômenos do infravermelho ainda está por vir, apesar de se ter formado um consenso de que o uso de ferramentas não-perturbativas é obrigatório para o estudo dos mesmos. Um laboratório interessante para a exploração do confinamento e da quebra de simetria quiral é fornecido pelo ambiente descrito pela QCD a altas temperaturas, sob as quais a teoria realiza a restauração da simetria quiral e também a transição para um estado da matéria chamado plasma de quarks e glúons. No plasma, as partículas fundamentais se encontram desconfinadas, apesar de serem ainda fortemente interagentes. As funções de Green (também chamadas funções de N pontos ou correlatores) da teoria guardam informações relevantes para a descrição dos fenômenos não-perturbativos mencionados. O objetivo principal desta tese era o cálculo de um correlator em particular, o propagador do quark, no vácuo e a temperatura finita. Para esse fim, executamos simulações numéricas usando o arcabouço não-perturbativo da Cromodinâmica Quântica na Rede, no qual é utilizada uma versão discretizada e euclidiana da QCD que preserva a simetria interna de calibre $SU(3)$ da teoria exatamente. Utilizamos a aproximação *quenched* e produzimos configurações de calibre para diferentes volumes e temperaturas. O propagador do quark foi computado no vácuo e a temperaturas acima da transição de desconfinamento. Um passo necessário para o cálculo de correlatores em geral, e propagadores em particular, é estabelecer um esquema para fixação do calibre. Um valioso subproduto desse projeto foi o refinamento e otimização de algoritmos de fixação de calibre $SU(3)$ para o calibre de Landau na rede. Nesta tese, apresentamos a abordagem da Cromodinâmica Quântica na Rede, incluindo a introdução de férmions na rede e os algoritmos empregados nas simulações. Nossos resultados abarcam os efeitos térmicos no propagador de quark, assim como os resultados das otimizações da fixação de calibre de Landau.

Palavras-chave: QCD. QCD na Rede. Propagador do Quark. QCD a Temperatura Finita. Fixação de Calibre de Landau.

LIST OF FIGURES

LIST OF TABLES

CONTENTS

1 INTRODUCTION

The established description of the universe in terms of particles is done using the framework of quantum field theory (1–4). This includes three of the four known fundamental interactions, comprising the Standard Model of particle physics.* Particles are seen as excitation of fields that permeate the universe, which carry certain characteristic quantities known as quantum numbers. The Standard Model generally provides very accurate theoretical predictions for comparison with experiment, but there are still some challenges, markedly regarding its strong sector. Among these challenges is the description of matter under extreme conditions, e.g. the high-temperature limit, related to the expected conditions in the early universe and experimentally accessible nowadays in heavy-ion colliders.

Quantum chromodynamics, in short QCD, is the quantum field theory currently used to describe the strong interactions between quarks and gluons, the color-charged particles (5, 6). Its success is immense, ranging from describing correctly the behavior of scatterings between protons and electrons at high-energy, to hadron masses in the low-energy regime, with the help of non-perturbative approaches. These are necessary due to some unique features of QCD. Indeed, just like the other sectors of the Standard Model, the theory is based on a local gauge symmetry, but for QCD the gauge group is more restrictive, which introduces some major differences in behavior.

One of the characteristics of gauge field theories is that there is a universal coupling g, which controls the intensity of the interaction between the fundamental fields of quarks and gluons, which carry color charges. A result of the renormalization of quantum field theories is that the coupling is in general not constant, but changes with the energy scale. In particular, for non-Abelian gauge theories like QCD, it has been shown by Gross, Wilczek and Politzer (7, 8) that the coupling goes to zero for high energies for a sufficiently low number of quark flavors. This is asymptotic freedom, and it justifies the use of perturbation theory for calculations of high-energy phenomena, such as deep inelastic scatterings, which are studied experimentally at particle colliders. Conversely, the coupling grows, and, close to an infrared scale Λ, perturbation theory results are no longer convergent or reliable. For the case of quantum electrodynamics, a typical value for Λ_{QCD} is 200MeV and the corresponding length scale $1/\Lambda_{\mathrm{QCD}}$ is in the femtometer range, which is a typical size scale for light hadrons (1).

For the infrared regime, where the coupling is large, analytic calculations based solely on the QCD Lagrangian are impossible to perform, and one has to resort to non-

* The gravitational interaction is the exception, and its quantum mechanical treatment is still unsatisfactory.

pertubative tools. Such methods are based on other assumptions, expansions and/or modelings of the theory. Some examples of non-pertubative methods are lattice field theory, Schwinger-Dyson equations, QCD sum rules, Nambu-Jona-Lasinio models, chiral perturbation theory, the functional renormalization group, the framework of the large N_c limit and methods based on the AdS/CFT correspondence, such as holography.

Lattice QCD, which is our framework of choice for the thesis, is one of the most successful non-perturbative methods used to study QCD. It is based on the Euclidean discretized version of the theory for a 4-dimensional space-time lattice. This framework is well-suited for computer simulations with Monte Carlo methods and it has the advantage that the extension to study the high-temperature regime is straightforward. The lattice formulation allows the regularization of the theory, while keeping gauge symmetry intact. The same is not true for other symmetries, though, which are recovered as the continuum limit is taken, in a controlled way. Indeed, the lattice QCD approach has been extremely successful at calculating the physical ground-state spectrum of hadrons (9), hadronic contributions to electroweak processes (10), besides other observables such as hadronic form factors (11), and also non-perturbative determinations of the running coupling constant of QCD with errors at the sub-percent level (12). It has also been used to investigate the vacuum structure of QCD, beyond-standard-model theories and further aspects of new physics, even quantum gravity.

In addition to the phenomenologically interesting properties just mentioned, it is expected that QCD should, eventually, provide a first-principles theoretical explanation for the emergent phenomena observed in the hadronic world. Two of these are spontaneous chiral symmetry breaking and confinement, which are important themes of discussions in the strong-interaction community. Chiral symmetry breaking is responsible for the dynamically generated mass of hadrons and a non-vanishing value for the quark condensate $\langle \overline{q}q \rangle$. Informally, the "confinement" of color charges is the observation that quarks and gluons are not detected outside of their bound states. These two features of QCD have eluded a satisfactory detailed theoretical explanation since the 1970s, whilst it has become clear that the origin of both phenomena cannot be perturbative. Their sources must lie intrinsically in the low-energy non-perturbative realm of the theory.

Confinement is phenomenologically characterized by the absence of colored particles in the asymptotic states that reach detectors at the experimental facilities. The spectrum of the strong interaction contains only particles that are color singlets. The best known of these are the 2- and 3-valence quark bound states (the minimal number of quark fields to make up a color singlet), which produce the plethora of identified hadrons and mesons. There are also exotic states, which do not fit easily within the classical valence-quark-model scheme, such as the relatively recently discovered tetra- and pentaquarks or the gluon bound states, called glueballs, which have still to be unambiguously identified

experimentally. In fact, in their "Free Quark Searches" section, the authors of the Particle Data Group 2018 paper say

> Experiments show that it is at best difficult to "unglue" quarks. Accelerator searches at increasing energies have produced no evidence for free quarks, while only a few cosmic-ray and matter searches have produced uncorroborated events.

That color charge seems not to manifest itself at macroscopic scales is in stark contrast to regular electric charge. In QED, which is formally similar to QCD, the electromagnetic interactions have infinite range. This is due to the masslessness of the photon, which is the force carrier of electromagnetism. The internal symmetry group of QED is the Abelian group $U(1)$, which is the group of complex phases. This internal symmetry, by means of the Ward identity, in fact forbids the photon from acquiring a mass to all orders in perturbation theory. The source of the different behaviors of QED and QCD with regard to their starkly different phenomenology is thought to lie in the different internal symmetry groups. In particular, the non-Abelian character of the $SU(3)$ group of QCD produces a screening of the color charge due to the self-interactions of the carriers of the strong force, supporting the picture of asymptotic freedom at short distances, or high energies. In turn, at larger distances, or lower energies, the theory would predict an increased intensity for the interaction, sometimes referred to as infrared slavery.

The search for a more precise description of confinement has led to the formulation of the Kugo-Ojima (13) and Coulomb (14) confinement criteria, which are based on the absence of spontaneous breaking of a remnant gauge symmetry that is left after gauge fixing to Landau and Coulomb gauge, respectively. Other confinement criteria are formulated in the Gribov-Zwanziger formalism (15, 16), which are based on restrictions on the path integral to remove Gribov copies. Like the Kugo-Ojima formulation, the Gribov-Zwanziger scenario predicts a characteristic behavior for the propagators of gluons and of Faddeev-Popov ghosts in the infrared limit, which is confirmed by lattice simulations. More precisely (17), lattice results show that the gluon (resp., ghost) propagator attains a finite value (resp., has a free-field behavior) in the infrared limit, supporting the massive or decoupling picture for confinement predicted in the Gribov-Zwanziger formalism. Lattice results also show that the gluon spectral function violates positivity, which may be a further signal for confinement, since for a deconfined particle with a proper Källén-Lehmann representation, positivity must hold. For a more in-depth discussion of the scenarios and predictions of these frameworks, one can consult, for example, (18, 19).

In general, we can say that, no matter the framework, the effects of confinement and chiral symmetry breaking must be detectable in the correlators of the theory, as was the case for the propagators or 2-point functions in the aforementioned Gribov-Zwanziger

scenario. This must necessarily be the case, since the correlators encode all the information of a quantum field theory.

Many mechanisms have been proposed to explain confinement for non-Abelian gauge theories. Since it is a low-energy phenomenon, the mechanism should be non-perturbative in nature, as we pointed out before. Topologically non-trivial classical solutions of the field equations, which should contribute with a high weight in the path integral, present some candidates, such as monopoles (20–22), vortices (23, 24) and perhaps instantons (25–28). The issue remains, however, as an open problem (with a million dollar prize by the Clay Mathematics Institute for solving the mathematically related problem of a mass gap in Yang-Mills theories (29)) and hopefully a better understanding will come from investigating QCD propagators in extreme conditions, which bring about deconfinement and restoration of chiral symmetry

Indeed, it is compelling to believe that, in order to have a complete understanding of the inner workings of confinement and chiral symmetry breaking in QCD, the study of the behavior of the theory at high temperatures and/or densities will be helpful and may lead to insights on the underlying mechanisms. This is so because, in this regime, there occurs a transition to a state called "quark-gluon plasma", in which the particles of the theory are not confined to their bound states, the hadrons. Restoration of chiral symmetry in QCD is also expected to take place at high temperatures. Therefore, field theory in extreme conditions has become a "hot" topic in the community recently. This includes studies of the aforementioned systems at high temperature and high density, but also high electromagnetic fields, high chiral imbalance, and other conditions that may be important to account for phenomena in heavy-ion collisions and astrophysical systems. In the case of QCD, this is partly due to the interest arisen from the experimental observation of the "quark-gluon plasma" at the LHC and RHIC facilities, where some of these extreme conditions are met for fractions of a second in heavy-ion collisions. Furthermore, recent measurements became available on characteristics of the early universe and on the structure of compact stars, whose equation of state is now being restricted by observations from LIGO, Virgo, and KAGRA (30). These results also helped to catch the attention of physicists to the research area of quantum field theory in extreme environments.

Clearly, as we increase the temperature, the confinement scenario changes. In fact, there are indications (both theoretical and experimental) that a quark-gluon plasma may form under extreme conditions. The quark-gluon plasma is the state of matter where quarks and gluons are not confined to the interior of hadrons, but are instead quasiparticles in a hot medium. The extreme conditions that make possible the formation of such a phase are attained in high-energy collisions and should also have been present at the beginning of the universe for fractions of a second. Theoretically, the idea of a deconfinement transition of QCD at high temperature were already present in the 1970s (31, 32) and even

before (references therein). Even though there are now complex calculations of the critical transition temperature based on various methods, a pretty good value may be obtained from a simple estimate based on the bag model of QCD and the counting the degrees of freedom at the deconfined and confined phases. Indeed, the procedure produces a value for the transition of around $T_c \approx 150\,\mathrm{MeV}$, which is close to the value obtained in lattice simulations, although details such as the order of the transition differ (33). This suggests that counting the number of degrees of freedom plays an important role in the transition between a hadronic phase and a quark-gluon plasma (33). For the quenched case (see Sect. 3.1), theoretical results show that a first-order transition takes place at a temperature of $T_{c,\,\mathrm{quenched}} \approx 270\,\mathrm{MeV}$.

On the experimental side of the research on (de)confinement, we may cite the efforts at the LHC (34) and RHIC (35) facilities, in Europe and the United States respectively. Experiments conducted at these facilities have provided indications that a strongly interacting quark-gluon-plasma is indeed formed when colliding heavy ions with each other. As examples of quantities used as signatures of quark-gluon plasma formation, we may cite collective anisotropies in high multiplicity pA and pp collisions (36), the cumulants of the net multiplicity distributions (37), J/ψ suppression (25, 38), as well as the theoretical suppression of the ρ and φ peaks in the dilepton channel, which were in agreement with experimental trends (33).

A most interesting question is the relation between the deconfinement and chiral restoration transitions. In particular, another expectation from QCD at high-temperatures is that the vacuum of QCD passes through a transition and chiral symmetry becomes restored. In this phase, chiral symmetry will manifest itself in the Weyl-Wigner mode, with a vanishing of the chiral condensate order parameter, and constituent quarks becoming massless (33).

For the transition temperature, recent full dynamical lattice results quote a value of $T_c = 156.5 \pm 1.5\,\mathrm{MeV}$ (39) and $T_c = 155 \pm 1 \pm 8\,\mathrm{MeV}$ (40). A Dyson-Schwinger study quotes $T_c = 156.7\,\mathrm{MeV}$ (41) and a functional renormalization group result is $T_c = 156.3\,\mathrm{MeV}$ (42). Of course, it is an abuse to use the word "critical" temperature for this chiral transition, as there is no transition, strictly speaking. Today it is well established theoretically that a cross-over happens between the two phases and no divergences in the susceptibilities of the chiral order parameter, which would mark a second order transition, actually take place. The pseudocritical temperatures, quoted above, all refer to a peak of the susceptibility of the order parameter and other proxies for the cross-over. For example, in the context of the linear sigma model (see Sect. 2.1), the consequences of the restoration of chiral symmetry are that the π mesons become massive and degenerate with the σ meson, and the mass difference between baryon parity doublets vanishes (33).

There is an ongoing debate as to how (and if) the chiral and deconfinement transi-

tions are related. Despite some early indications that their (pseudo)critical temperatures roughly coincided (33, 43), there are now studies in which criticisms of the identification of the chiral transition with the deconfinement transition have been raised, for example in (44), where it is claimed that deconfinement would only happen at temperatures as high as 3 times the chiral transition temperature. An older study (45) cites a milder disagreement of 25 MeV between the chiral transition from the chiral condensate and the deconfinement transition as measured with Polyakov loops. The issue is not easily resolved, since the order parameter for confinement in pure-gauge theories, the Polyakov loop, is not a proper order parameter in full-QCD simulations, as the introduction of dynamical fermions breaks the associated global center symmetry explicitly. Although there have been some suggestions for alternative order parameters, none is widely accepted.

The remainder of this thesis is structured as follows: in Chapter 2 we provide the essentials of the theoretical framework of QCD and discuss a few phenomenological implications of chiral symmetry. Chapter 3 is devoted to the formulation of lattice QCD in the vacuum and at finite temperature. The subject of gauge fixing in the continuum and on the lattice is the focus of Chapter 4. In Chapter 5, we review how chiral symmetry is treated on the lattice and give an introduction to the main fermion discretizations used in propagator studies. We then present, in Chapter 6, the algorithms used to generate configurations, perform the gauge-fixing and the operator inversion necessary for the computation of the quark propagator. A review of the literature on quark propagators on the lattice is the subject of Chapter 7. Finally our own results are showcased in Chapter 8, after which we give our conclusions in Chapter 9.

2 QCD ESSENTIALS

Usually, a quantum field theory is given in terms of a Lagrangian density, which is a scalar function of the space-time coordinates that describes what are the degrees of freedom of a theory as well as its local and global internal symmetries, while keeping the space-time Lorentz symmetry invariance manifest (1, 5, 46). For QCD, the fermionic part of the QCD Lagrangian is given by

$$\mathcal{L}_F = \sum_f \overline{\psi}^{(f)}_{\alpha\, a}(x) \left[(\gamma_\mu)_{\alpha\beta} (\delta_{ab}\partial_\mu + \mathrm{i} A_\mu(x)_{ab}) + m^{(f)} \delta_{\alpha\beta}\delta_{ab} \right] \psi^{(f)}_{\beta\, b}(x), \tag{2.1}$$

where $m^{(f)}$ is the bare quark mass of quark flavor f, δ_{ab} denotes a Kronecker delta and γ_μ is the Dirac matrix associated with the Lorentz index μ. In our conventions, the Dirac gamma matrices γ_μ are

$$\gamma_1 = \begin{bmatrix} 0 & 0 & 0 & -i \\ 0 & 0 & -i & 0 \\ 0 & i & 0 & 0 \\ i & 0 & 0 & 0 \end{bmatrix}, \ \gamma_2 = \begin{bmatrix} 0 & 0 & 0 & -1 \\ 0 & 0 & 1 & 0 \\ 0 & 1 & 0 & 0 \\ -1 & 0 & 0 & 0 \end{bmatrix}, \gamma_3 = \begin{bmatrix} 0 & 0 & -i & 0 \\ 0 & 0 & 0 & i \\ i & 0 & 0 & 0 \\ 0 & -i & 0 & 0 \end{bmatrix}, \ \gamma_4 = \begin{bmatrix} 0 & 0 & 1 & 0 \\ 0 & 0 & 0 & 1 \\ 1 & 0 & 0 & 0 \\ 0 & 1 & 0 & 0 \end{bmatrix}$$

and $\gamma_{-\mu} = -\gamma_\mu$.

The bosonic part is given by

$$\mathcal{L}_G = \frac{1}{2g^2} \mathrm{tr}[F_{\mu\nu}(x) F^{\mu\nu}(x)], \tag{2.2}$$

where

$$F_{\mu\nu,\, ab}(x) = \partial_\mu A_{\nu,\, ab}(x) - \partial_\nu A_{\mu,\, ab}(x) + \mathrm{i}\, [A_\mu(x), A_\nu(x)]_{ab} \tag{2.3}$$

and g is the bare coupling constant. The trace is taken in color space, since the $A_\mu(x)$ fields are matrices. There is a metric tensor, that determines how indices are lowered ($g_{\mu\nu}$) and raised ($g^{\mu\nu}$). Since, as will be explained shortly, we are mostly concerned with Euclidean space, which has a trivial metric $g_{\mu\nu} = \delta_{\mu\nu}$, we will sometimes take the liberty of writing contracted indices at the same level (high or low). The complete Lagragian is $\mathcal{L} = \mathcal{L}_F + \mathcal{L}_G$.

As written above, we can identify the degrees of freedom of the theory as the fields $\psi(x)$, $\overline{\psi}(x)$ and $A_\mu(x)$. The first two are spinor fields associated to the spin-1/2 fermions of the theory: the quarks. They carry indices for Dirac space α, β and color indices a, b, for the fundamental representation of $SU(3)$, besides the spatial coordinate x. There is also an index (f) for the quark flavor: up, down, strange, charm, bottom, top in order of ascending mass $m^{(f)}$.

The gluons, which are bosons and the carriers of the strong interaction, are excitations of the $A_\mu(x)$ fields, and have a spin of 1. The gauge fields $A_\mu(x)$ are matrices in the algebra of $SU(3)$, and can thus be written in terms of components

$$A_\mu(x) = \sum_{i=1}^{8} A_\mu^{(i)}(x)\, T_i, \tag{2.4}$$

where the T_i form a basis for the 3×3 Hermitian traceless matrices, and can be taken, for example, as the Gell-Mann matrices. The $A_\mu^{(i)}(x)$ are real valued fields.

The bare coupling g controls the strength of the interaction. Let us note that the most familiar form for the QCD Lagrangian usually has the coupling appearing whenever there is a product of fields, thus making it clear that g is a universal coupling controlling the interaction between quarks and gluons and the gluons themselves. This more familiar format can be obtained by the substitution

$$\frac{A_\mu(x)}{g} \to A_\mu(x), \tag{2.5}$$

which is just a rescaling. We prefer the form above because it is what is usually adopted for QCD on the lattice, which is the framework for this thesis.

The parameters $m^{(f)}$ are interpreted as the bare quark masses. After renormalization, these would be identified with the physical quark masses at a particular renormalization scale. The fact that quarks are confined complicates the definition of a mass, since they present no asymptotic states. We will briefly comment on these complications later in Sect. 2.1.

Besides being invariant with respect to Poincaré transformations (translations, rotations, boosts), from which Lorentz transformations are a subset, the QCD Lagrangian is exactly invariant under local $SU(3)$ gauge transformations

$$\overline{\psi}(x) \to \overline{\psi}'(x) = \overline{\psi}'(x) g^\dagger(x) \tag{2.6}$$

$$\psi(x) \to \psi'(x) = g(x)\psi'(x), \tag{2.7}$$

provided that the field $A_\mu(x)$ transforms as

$$A_\mu(x) \to A'_\mu(x) = g(x) A_\mu(x) g^\dagger(x) + i(\partial_\mu g(x)) g^\dagger(x). \tag{2.8}$$

The QCD Lagrangian is formally similar to its quantum electrodynamics (in short QED) counterpart. The fundamental difference is in the underlying internal symmetry group: in the electrodynamics case, this is $U(1)$, the group of complex phases, which is Abelian, whereas the strong interactions are described by the non-Abelian group $SU(3)$. Due to the non-Abelianity of $SU(3)$, the commutators of A_μ gauge fields do not vanish. This causes 2.2 to contain, besides a kinetical term also present in QED, products of gauge

fields, which are associated to interaction vertices. Thus, for non-Abelian theories, the gauge field has self-interactions, which make the theory highly non-trivial even without fermions.

An alternative complete description of a quantum field theory can be given in terms of its correlation functions, also called Green's functions or N-point functions.

$$S_n(x_1, \ldots, x_N) = \langle \phi(x_1) \ldots \phi(x_N) \rangle, \tag{2.9}$$

where $\langle\rangle$ means the expectation value of the combination of ϕ fields in the vacuum of the theory, and ϕ stands generically for the ψ, $\overline{\psi}$ and A_μ degrees of freedom. A convenient way to express these correlators is by taking functional derivatives of a generating functional, which resembles a partition functional from statistical mechanics

$$Z[J] = \int \mathcal{D}\phi \, e^{iS[\phi, J]}, \tag{2.10}$$

where $S[\phi]$ is the action, given by

$$S[\phi, J] = \int d^4x \, \left[\mathcal{L}(x) + J(x)\phi(x) \right], \tag{2.11}$$

in which we included a term with a source $J(x)$. Again, we stress that ϕ stands here for a generic field, and in actuality for each field of the theory there will be a corresponding source function. The integration of 2.10 is performed for all possible configurations of the field. This is called a path-integral representation of the quantum field theory. The $\mathcal{D}\phi$ is an integration measure

$$\mathcal{D}\phi = \prod_x d\phi(x). \tag{2.12}$$

The correlators can be obtained by

$$\langle \phi(x_1) \ldots \phi(x_N) \rangle = \left(\frac{1}{Z[J]} \frac{\delta}{i\delta J(x_1)} \ldots \frac{\delta}{i\delta J(x_N)} Z[J] \right)_{J=0}. \tag{2.13}$$

The equivalence between the path-integral formulation and standard perturbative techniques of the canonical formalism has been demonstrated by Freeman Dyson, and is one of the milestones of quantum field theory. The derivation of this equivalence can be found in the modern quantum field theory textbooks, such as (1). This makes the path-integral formalism an alternative quantization prescription.

The lattice framework (described in detail in the Chap. 3) is based on discretizing the QCD Lagrangian in Euclidean (i.e., imaginary-time) space-time. The need for the Euclidean version of the theory in the lattice framework is the following: the Minkowski (i.e., real-time) formulation of QCD provided by the generating functional 2.10 is unfortunately not suitable for lattice simulations. In these simulations, configurations of fields are

generated in a stochastic fashion. The "weight" of the configurations provided by the Minkowski Lagrangian is

$$dP[\phi] = \frac{e^{iS[\phi]}}{Z}, \tag{2.14}$$

which is in general complex due to the exponential, and thus not a proper statistical weight. We perform a transformation called a Wick rotation $t \to i\tau$, and transform the action correspondingly to an Euclidean action $iS[\phi] \to -S_E[\phi]$. The metric for performing contractions is now trivial $g_{\mu\nu} = \delta_{\mu\nu}$, and the fields will be defined in an Euclidean space. The Wick rotation prevents us from performing "real-time" simulations, and we are thus forced to focus on energy levels and matrix elements of operators of the quantum field theories. For example, it can be shown that, when calculating Euclidean correlators between two operators, one gets (46)

$$\langle \mathcal{O}_2(\tau)\mathcal{O}_1(0)\rangle = \sum_n \langle 0|\mathcal{O}_2|n\rangle\langle n|\mathcal{O}_1|0\rangle e^{-\tau E_n}, \tag{2.15}$$

where E_n are the energy levels, $|0\rangle$ is the vacuum state and $|n\rangle$ are the states of energy E_n that have a non-zero overlap with the operators $\mathcal{O}_1$ and $\mathcal{O}_2$. The energy levels can then be extracted from this formula and from them the masses of hadronic states.

The relationship between Euclidean correlators, also called Schwinger functions, and the the Minkowski ones, called Wightmann functions, is an analytical continuation. The Osterwalder–Schrader reconstruction clarifies the relation between the two groups of correlators, as long as the Euclidean ones satisfy a set of axioms (47–49). In general, Euclidean correlators obey simpler properties and are easier to manipulate than their Minkowski counterparts (50), in part because the causal structure is absent for the Euclidean formulation.

Another advantage of the lattice formulation is that the lattice spacing between the discretized space-time points provides an ultraviolet regulator to the theory and, because of this, no infinities appear. One studies how the discretized theory approaches the continuum by taking the lattice spacing to zero, while having only to deal with finite numbers at all times.

2.1 Chiral symmetry

Another important aspect of the QCD Lagrangian that, to a great extent, determines the spectrum of light hadrons, is the approximate chiral symmetry of the theory. Let us begin our discussion of chiral symmetry for one flavor of quark coupled to a Yang-Mills gluonic sector. The Lagrangian density function is then given by

$$\mathcal{L}(\psi, \overline{\psi}, A) = \overline{\psi}\left[\gamma_\mu\left(\partial_\mu + iA_\mu\right) + \mathbb{1}m\right]\psi = \overline{\psi}\mathcal{M}\psi, \tag{2.16}$$

where the spatial dependence of the ψ and $\overline{\psi}$ fields has been suppressed to reduce cluttering. A chiral transformation is a global transformation given by

$$\psi \to \psi' = e^{i\alpha\gamma_5}\psi, \quad \overline{\psi} \to \overline{\psi}' = \overline{\psi}e^{i\alpha\gamma_5}. \tag{2.17}$$

The constant α is real and the Dirac-space matrix $\gamma_5 = \gamma_1\gamma_2\gamma_3\gamma_4$ anti-commutes with all other γ_μ. If the chiral transformation is applied to the fermionic Lagrangian, we obtain

$$\overline{\psi}\left[e^{i\alpha\gamma_5}e^{-i\alpha\gamma_5}\gamma_\mu\left(\partial_\mu + iA_\mu\right) + e^{i\alpha\gamma_5}e^{i\alpha\gamma_5}m\right]\psi = \overline{\psi}\left[\gamma_\mu\left(\partial_\mu + iA_\mu\right) + e^{2i\alpha\gamma_5}m\right]\psi, \tag{2.18}$$

which shows that, unless $m = 0$, the chiral transformation does not represent a symmetry of this Lagrangian. We notice that the fact that the first term is invariant under chiral transformations boils down to its anti-commutativity with γ_5. Thus, we can condense the condition to decide whether or not a particular fermionic operator $\mathcal{M}$ is chiral symmetric in a simple equation

$$\{\mathcal{M}, \gamma_5\} = 0. \tag{2.19}$$

Even though the up- and down-quark mass parameters in the QCD fermionic Lagrangian do not vanish, they have values of $2.16^{+0.49}_{-0.26}\,\mathrm{MeV}$ for the up quark and $4.67^{+0.48}_{-0.17}\,\mathrm{MeV}$ for the down quark in nature (51). These values are small in comparison to, for example, $\Lambda_{\mathrm{QCD}} \approx 200\,\mathrm{MeV}$, a scale which we alluded to already, and is commonly used to define the limits of perturbation theory in QCD. Even the strange-quark, with a mass of $93^{+11}_{-5}\,\mathrm{MeV}$, may be considered relatively light by this argument. These masses can be extracted, for example from the hadronic invariant mass spectrum in semihadronic τ decay, normalized to the leptonic τ decay rate(51)

$$\frac{dR_\tau}{ds} = \frac{d\Gamma/ds(\tau^- \to \text{hadrons} + \nu_\tau(\gamma))}{\Gamma(\tau^- \to e^-\overline{\nu}_e\nu_\tau(\gamma))}, \tag{2.20}$$

where $s = q^2$ is the invariant hadronic mass. The experimental results are matched to theoretical predictions done at a particular renormalization scheme, usually $\overline{\mathrm{MS}}$, which then allows the values of QCD parameters to be extracted at a particular renormalization scale, which, for the numbers presented above, is $\mu = 2\,\mathrm{GeV}$.

Given the relatively small values of quark mass, we should expect an approximate version of chiral symmetry to be manifest in reality. The Noether current associated to the chiral transformation is given by

$$j_{5\,\mu}(x) = \overline{\psi}(x)\gamma_\mu\gamma_5\psi(x), \tag{2.21}$$

which is conserved for exact chiral symmetry

$$\partial^\mu j_{5\,\mu} = 0. \tag{2.22}$$

The associated charge is obtained in the usual way

$$Q_5 = \int d^3x j_{5\,0}(x). \tag{2.23}$$

When adding a flavor structure on top of the approximate chiral symmetry of the QCD Lagrangian, one obtains a rich pattern of possible states and different ways of breaking the symmetry explicitly, by having each flavor have its own non-vanishing mass, all the same mass or all massless fermions. This also introduces global "rotations" among different flavors, which gives rise to the symmetries of the "eightfold way", a systematic classification scheme proposed by Ne'eman and Gell-Mann to explain the symmetries observed experimentally for the plethora of hadrons detected (52, 53). This classification, and the associated patterns, can be derived from the representations of the $SU(3)$ flavor group, which extends the isospin $SU(2)$ group of pions and nucleons.

The "eightfold way" classification later developed into the idea of a quark model in which the hadrons are described as bound states of constituent quarks. These in turn, as understood today, are the bare current quarks that one would obtain in a free theory, with well-defined quantum numbers, dressed by all the complicated non-perturbative QCD dynamics, as seen at low energy. This model works well for the low-lying QCD spectrum and its success is one of the pillars of the interpretation of the hadronic world in terms of the QCD degrees of freedom. Lattice QCD, for example, usually follows the quark model in hadron spectrum calculations by using correlators with minimal quark content combining into color singlets and with the correct quantum numbers of the hadron to be studied.

One feature of the phenomenology of QCD is that the bound states of its spectrum are heavy in comparison to the Λ_{QCD} scale that we used as a standard to declare that quark masses are light. In fact, the word hadron comes from the Ancient Greek word "ἁδρός", which means "stout". For the case of the proton, for example, there is then a naïve disagreement with the experimental observations, which portray the up and down quarks as light and the quark model, which portray the proton as a bound state of the said quarks. It has been believed since the 1970s that the key to this puzzle is the kind of "dressing" that the constituent quarks receive from the QCD interactions.

To reconcile the (approximate) chiral symmetry of the Lagrangian with the experimental observations, we must understand the manifestations of symmetries in nature. There are two modes that the chiral symmetry of a theory could manifest itself: the Wigner-Weyl and Nambu-Goldstone modes. The Wigner-Weyl mode assumes that the vacuum state is annihilated by the chiral charge operator (54)

$$Q_5|0\rangle = 0, \tag{2.24}$$

and it says that, when applied to a state in the spectrum of the theory, the chiral charge operator, which is a pseudoscalar object, should produce another state with the same mass and spin, but opposite parity

$$Q_5|m, s, p, +\rangle = -|m, s, p, -\rangle. \tag{2.25}$$

Thus we should observe a mass degeneracy in the form of parity doublets for the massive states of the spectrum. This is not the case when examining the hadronic spectrum. Let us take the example of the nucleon, which has a mass of around 940 MeV. The closest candidate in the spectrum for a would-be chiral partner, N^*, has a mass of 1535 MeV, which cannot be considered degenerate with the nucleon in any possible way. This difference is just too big also to be attributed to the small breaking caused by explicit quark masses. The alternative mode of realization of chiral symmetry is the Nambu-Goldstone mode, which postulates that the vacuum state or ground state is not a symmetric state with respect to the chiral charge. It is said to be spontaneously broken

$$Q_5|0\rangle \neq 0. \tag{2.26}$$

Although the mechanism behind this breaking is not completely understood, somehow the fields, parameters and symmetries of the non-Abelian $SU(3)$ gauge theory combine in such a way that the breaking eventually occurs: even though chiral symmetry is approximately respected by the QCD Lagrangian, the vacuum of the theory does not respect it at all. As a result, the constituent up and down quarks obtain dynamically generated masses of the order of $m_N/3$, where m_N is the nucleon mass, in such a way that the masses add up to the full mass of the proton or neutron.

One could hope that chiral symmetry breaking can somehow be explained and its effects taken into account by using standard perturbative quantum field theory techniques. However, this is not the case, and this is an intrinsic low-energy non-perturbative effect in QCD. One of the hints to its non-perturbative nature are that the mass corrections which come from higher-order perturbative calculations are always proportional to the mass itself. If one starts with a massless fermion theory, the perturbative corrections will not generate masses, as is expected to happen in QCD.

One framework which shows how the dynamical generation of mass might come about is the linear sigma model, proposed by Gell-Mann and Lévy, (55). This can be viewed as an effective model, or, in order words, a model that may be expected to hold for sufficiently low energies and that could be, in principle, derived from another more fundamental theory by integrating out the high-energy degrees of freedom. A simplified version is given by the Lagrangian

$$\mathcal{L} = \frac{1}{2}(\partial_\mu \sigma)^2 + \frac{1}{2}(\partial_\mu \vec{\pi})^2 + \frac{\mu^2}{2}(\sigma^2 + \vec{\pi}^2) - \frac{\lambda}{4}(\sigma^2 + \vec{\pi}^2)^2, \tag{2.27}$$

where $\vec{\pi} = (\pi_1, \pi_2, \pi_3)$ are an $SU(2)$ isospin triplet and σ is an isospin singlet field. The parameters μ and λ can have values such that a minimum of the potential develops which is different from the trivial vacuum ($\vec{\pi} = 0\,, \sigma = 0$). This is the famous "Mexican hat" potential. In fact, the σ field develops a non-vanishing vacuum expectation value

$$\sigma \to \sigma + v, \tag{2.28}$$

with $v = \mu/\sqrt{\lambda}$. When this is the case, we also get that the σ particles, associated to that field, develop a mass $m_\sigma = \sqrt{2\mu^2}$, whereas the π fields remain massless.

This model is analogous to the Higgs mechanism, which gives mass to the elementary particles of the standard model. Both are instances of Goldstone's theorem, which states that, to each continuous symmetry that is broken spontaneously, there corresponds a massless particle, called a Goldstone boson (56). In the case of QCD with up and down quarks, these bosons are identified with the three pions, which have masses much lower than Λ_{QCD}, and in particular much lower than those of the nucleons. In the same fashion as the Higgs model, one may add a coupling between the σ field and nucleon fields ψ_N, in such a way that these particles now obtain a dynamically generated mass.

The pion states would be created from the vacuum by the pseudoscalar chiral charge operator

$$Q_5|0\rangle = |\pi, -\rangle, \tag{2.29}$$

as the pions have the same quantum numbers as the operator object. As the charge commutes with the Hamiltonian of QCD, they do not cost energy to be generated, which is particular to massless particles. The small but non-vanishing observed mass of the pions is expected to come from the fact that chiral symmetry is in fact explicitly, albeit mildly, broken by the up and down quark mass terms in the Lagrangian. These effects can also be included in the sigma model as well. In nature, the $\pm\pi$ masses are 139.57061(20) MeV, whereas the neutral pion has a mass of 134.9768(5) MeV, the difference coming from the electroweak coupling only.

The sigma particle itself has never been observed unambiguously, however a candidate for it is the $f_0(500)$ particle, with a mass given in the PDG of between 450 and 600 MeV. The reason for the large uncertainty is the extremely quick decay, which takes place through the strong interaction. This particle decays into two pions predominantly and has a huge width, estimated to be between 400 and 700 MeV by the PDG collaboration (57).

The vacuum expectation value v of the linear sigma model may be interpreted using the degrees of freedom of QCD as a quark condensate $\langle\overline{q}q\rangle$, meaning that the true interacting lowest energy state of QCD is not a true vacuum in the strict sense of being completely empty, but has instead quark pairs populating it. A quark condensate transforms like a mass term, which means that it breaks chiral symmetry. If $\langle\overline{q}q\rangle$ acquires a non-vanishing value, this is an indication that chiral symmetry is spontaneously broken. It is thus used as an order parameter for this symmetry breaking, and is important when discussing QCD at non-zero temperatures, as chiral symmetry is expected to be recovered for sufficiently extreme thermal conditions.

The actual value for the condensate can be estimated via the phenomenological

Gell-Mann-Oakes-Renner relation

$$f_\pi^2 m_\pi^2 = -2 \langle \overline{q} q \rangle (m_u + m_d), \tag{2.30}$$

or by other means, such as the trace of the quark propagator for zero quark mass. It can also be expressed from the partition function of theory, in which case it is expressed as

$$\langle \overline{q} q \rangle = \frac{1}{V} \frac{\partial \ln Z}{\partial m}, \tag{2.31}$$

where Z is the partition function, V is the volume and m the corresponding quark mass. A second derivative gives the susceptibility of the condensate. This last definition is particularly well suited for a thermodynamical setting.

As for the actual value of the condensate at zero temperature, the authors of (6) cite $m_q \langle \overline{q} q \rangle \approx -(100\text{MeV})^4$ from a QCD Sum Rules fit, and, if the average PDG masses for the up and down quark are used for m_q, one gets $\langle \overline{q} q \rangle \approx -(310\,\text{MeV})^3$. This may be compared with a quenched lattice result of $\langle \overline{q} q \rangle \approx -(270\,\text{Mev})^3$, by (58), whereas an unquenched calculation (59) quotes $\langle \overline{q} q \rangle \approx -(255\,\text{Mev})^3$ and another (60) $\langle \overline{q} q \rangle \approx -(234\,\text{MeV})^3$, the three of which use the $\overline{MS}$ renormalization scheme at renormalization scale $\mu = 2\,\text{GeV}$.

3 LATTICE QCD

Our presentation in this chapter is based largely on (25, 46, 50). We start our discussion of the lattice QCD formulation by supposing that we have a discretized Euclidean four-dimensional space-time, which for simplicity we assume, in order to maintain hypercubic symmetries: that is, we have sites with coordinates that are multiples of some lattice constant a, which has dimensions of a length and measures the distance between consecutive sites

$$x_\mu = an_\mu, \quad n_\mu = 0, 1, ..., N_\mu - 1, \tag{3.1}$$

where μ is a Lorentz index that labels the dimensions of the problem. Henceforth we will use the index n to refer to lattice sites, where the four Euclidean components are understood. In the notation we have also added the restriction that our lattice will have a finite volume. If we succeed in crafting a sensible theory on this lattice structure, we can ask ourselves what is its behavior as the volume is increased to ∞ in all directions, and what is its behavior as the lattice constant a is made to vanish.

As mentioned before, the building principle of lattice field theory is to maintain exact invariance under the internal gauge transformations, even when breaking most of the space-time symmetries of the theory. In the case of QCD, we want to maintain the internal $SU(3)$ local gauge symmetry of the continuum Lagrangian. Wilson proposed a way to do this in (61), and the key element of this formalism is the link variable, which we may think of as the parallel-transport operator acting on the gauge-field vector between two sites of the lattice, as we soon show. For now, let us worry about pure-gauge theory, without the fermions, which add many more complications, and which will be explored later, in Chap. 5.

A link variable $U_\mu(n)$ is defined for each site n and direction μ, and one can thus think of it as being defined on the edges between the sites. Their name comes from them linking two neighboring sites. The link variables are taken to be elements of the symmetry group under consideration in the fundamental representation, so each link variable is a 3×3 complex matrix, with determinant 1 and whose inverse is its Hermitian conjugate.

The gauge transformations we are interested in are local, which means that, at each site, we may allow for a different gauge transformation element $g(n)$. The gauge transformations are also given by elements of $SU(3)$. The link variables will transform according to

$$U_\mu(n) \to U'_\mu(n) = g(n)U_\mu(n)g^\dagger(n + \hat{\mu}), \tag{3.2}$$

where $\hat{\mu}$ is the unit vector in the μ direction, which implies that $n + \hat{\mu}$ is the neighboring site in that direction. Since all matrices in the right-hand side of Eq. 3.2 are elements of

$SU(3)$, by the definition of the group, $U'_\mu(n)$ is also a member of $SU(3)$. We also define a backward link connecting a site to its neighbor at position $n - \hat{\mu}$ by

$$U_{-\mu}(n) \equiv U^\dagger_\mu(n - \hat{\mu}), \tag{3.3}$$

which is also a member of $SU(3)$, since the Hermitian conjugation operation is equivalent to taking the inverse of the group element, and all inverses of the elements must also be part of the group. A gauge transformation will act accordingly as

$$\begin{aligned} U'_{-\mu}(n) &= (g(n-\hat{\mu})U_\mu(n-\hat{\mu})g^\dagger(n))^\dagger \\ &= g(n)U^\dagger_\mu(n-\hat{\mu})g^\dagger(n-\hat{\mu}) = g(n)U_{-\mu}(n)g^\dagger(n-\hat{\mu}). \end{aligned} \tag{3.4}$$

If we want a Lagrangian, and consequently an action, that exhibits exact gauge-symmetry, we need to create combinations of link variables that are invariant under gauge transformations. One way of doing this is by considering closed paths, since the transformation at the "head" of the link variable will cancel the one at the "tail" of the next link down the path, until we get back where we started. The simplest non-trivial closed path on the lattice is the plaquette, which winds around with the shortest possible route

$$U_{\mu\nu}(n) \equiv U_\mu(n)U_\nu(n+\hat{\mu})U_{-\mu}(n+\hat{\mu}+\hat{\nu})U_{-\nu}(n+\hat{\nu}). \tag{3.5}$$

We can see explicitly what a gauge transformation does to a plaquette

$$\begin{aligned} U'_{\mu\nu}(n) &= U'_\mu(n)U'_\nu(n+\hat{\mu})U'_{-\mu}(n+\hat{\mu}+\hat{\nu})U'_{-\nu}(n+\hat{\nu}) \\ &= g(n)U_\mu(n)g^\dagger(n+\hat{\mu})g(n+\hat{\mu})U_\nu(n+\hat{\mu})g^\dagger(n+\hat{\mu}+\hat{\nu}) \\ &\quad g(n+\hat{\mu}+\hat{\nu})U_{-\mu}(n+\hat{\mu}+\hat{\nu})g^\dagger(n+\hat{\nu})g(n+\hat{\nu})U_{-\nu}(n+\hat{\nu})g^\dagger(n) \\ &= g(n)U_\mu(n)U_\nu(n+\hat{\mu})U_{-\mu}(n+\hat{\mu}+\hat{\nu})U_{-\nu}(n+\hat{\nu})g^\dagger(n) = g(n)U_{\mu\nu}(n)g^\dagger(n). \end{aligned} \tag{3.6}$$

By taking the trace we have then an invariant under gauge transformations

$$\mathrm{tr}\left[U'_{\mu\nu}(n)\right] = \mathrm{tr}\left[g(n)U_{\mu\nu}(n)g^\dagger(n)\right] = \mathrm{tr}\left[U_{\mu\nu}(n)\right], \tag{3.7}$$

due to the cyclic property of the trace.

There is a continuum object related to the link variables, the so-called Wilson line

$$U_P\left(x, y; A\right) = P\left\{e^{i\int_{C_{xy}} A\cdot dz}\right\} = P\left\{e^{-i\int_0^1 \frac{dz^\mu}{ds} A_\mu(z(s))\, ds}\right\}. \tag{3.8}$$

The path C_{xy}, between continuum points x and y, has coordinates $z(s)$, where s is a parameter running from 0 to 1, with $z(0) = x$ and $z(1) = y$. The path-ordering operator is there to ensure that the product of group elements is performed properly, with the elements ordered by the corresponding value of s.

To elucidate the relationship between the link variable and the Wilson line, we can perform a gauge transformation in the relativistic four-potential $A_\mu(z)$ and calculate the corresponding gauge transformation of $U_P(x,y)$. First we note that the Wilson line obeys the first order differential equation

$$\frac{dU_P(x(s),y;A)}{ds} = \left[-i\frac{dx(s)^\mu}{ds}A_\mu(x(s))\right]U_P(x(s),y;A), \tag{3.9}$$

where we now write x in terms of a parameter s. This may be rewritten by noticing that

$$\frac{d}{ds} = \left(\frac{dx^\mu(s)}{ds}\right)\frac{\partial}{\partial x^\mu}, \tag{3.10}$$

which leads to

$$\left(\frac{dx^\mu(s)}{ds}\right)\frac{\partial U_P(x(s),y;A)}{\partial x^\mu} + \left[i\left(\frac{dx(s)^\mu}{ds}\right)A_\mu(x(s))\right]U_P(x(s),y;A) = 0, \tag{3.11}$$

where we can identify the covariant derivative as $D_\mu(A) = \partial_\mu + iA_\mu(x)$ and write

$$\left(\frac{dx^\mu(s)}{ds}\right)D_\mu(A)U_P(x(s),y;A) = 0. \tag{3.12}$$

We are emphasizing the $A_\mu(x)$ dependence of the covariant derivative because this will be important in what follows. Eq. 3.12 must hold for any field $A_\mu(x)$: in particular, it must hold for a gauge-transformed field $A'_\mu(x)$ as well

$$\left(\frac{dx^\mu(s)}{ds}\right)D_\mu(A')U_P(x(s),y;A') = 0. \tag{3.13}$$

Let us now calculate

$$\left(\frac{dx^\mu(s)}{ds}\right)D_\mu(A')g(x)U_P(x(s),y;A)\,g^\dagger(y), \tag{3.14}$$

where g is the gauge transformation which transforms between A and A' (see Eq. 2.8)

$$A'_\mu(x) = g(x)A_\mu(x)g^\dagger(x) + i\left[\partial_\mu g(x)\right]g^\dagger(x), \tag{3.15}$$

The corresponding transformation for the covariant derivative is

$$D_\mu(A') = g(x)D_\mu(A)g^\dagger(x) \rightarrow D_\mu(A')g(x) = g(x)D_\mu(A), \tag{3.16}$$

where we used the unitarity of $g(x)$. This allows us to rewrite the expression in 3.14 as

$$\left(\frac{dx^\mu(s)}{ds}\right)g(x)D_\mu(A)U_P(x(s),y;A)\,g^\dagger(y) = g(x)\left[\left(\frac{dx^\mu(s)}{ds}\right)D_\mu(A)U_P(x(s),y;A)\right]g^\dagger(y), \tag{3.17}$$

but the expression in square brackets is 0 because of Eq. 3.12. So, we conclude that $g(x)U_P\left(x(s),y;A\right)g^\dagger(y)$ is a solution to Eq. 3.13, as well as $U_P\left(x(s),y;A'\right)$, by definition. Now, since this is a first-order differential equation, it has a single solution if the boundary conditions are fixed, as is the case here. Thus, we can state that

$$U_P\left(x(s),y;A'\right)=g(x)U_P\left(x(s),y;A\right)g^\dagger(y), \tag{3.18}$$

which is the gauge transformation of the Wilson line that we were seeking. If we choose $x=an$ and $y=x+a\hat{\mu}$ and take the path between them as a straight segment, we can approximate Eq. 3.8 as

$$U_P\left(an,a(n+\hat{\mu});A\right)=e^{iaA_\mu(n)}. \tag{3.19}$$

By looking at this relation, it is tempting to identify the link variable as this elementary Wilson line

$$U_\mu(n)\equiv e^{iaA_\mu(n)}. \tag{3.20}$$

By these arguments, we are thus led to write the lattice action in terms of the smallest closed loop (i.e. the plaquette $U_{\mu\nu}$ in Eq. 3.5) obtained from links around a point n, which is guaranteed to be gauge-invariant. The actual gauge action that was proposed by Wilson has some extra terms, which are there to ensure that we get to the correct result in the continuum limit

$$S_G[U]=\beta\sum_{n\in\Lambda}\sum_{\mu<\nu}\mathrm{Re\ tr}[\mathbb{1}-U_{\mu\nu}(n)]=\beta\sum_{n\in\Lambda}\sum_{\mu<\nu}\mathrm{tr}\left\{\mathbb{1}-\frac{1}{2}\left[U_{\mu\nu}(n)+U^\dagger_{\mu\nu}(n)\right]\right\}, \tag{3.21}$$

where the last form shows that clockwise and anticlockwise plaquettes are included symmetrically. In order to see what we obtain in a naïve continuum limit from this action, we can use Eq. 3.20. Let us first express the plaquette $U_{\mu\nu}(n)$ in terms of the A field. In order to do this we need to use the Baker-Campbell-Hausdorff formula

$$e^Ae^B=e^{A+B+\frac{1}{2}[A,B]+\text{terms with powers higher than 2}}. \tag{3.22}$$

We omit the higher-order terms, because we are interested in the small-a behavior of the expression, and those terms would contain higher powers of a, which we neglect. Applying the formula to the case of the plaquette, one obtains

$$\begin{aligned}U_{\mu\nu}(n)=\exp\Big\{&ia\Big[A_\mu(n)+A_\nu(n+\hat{\mu})-A_\mu(n+\hat{\nu})-A_\nu(n)\Big]\\&+\frac{a^2}{2}\Big[-[A_\mu(n),A_\nu(n+\hat{\mu})]-[A_\mu(n+\hat{\nu}),A_\nu(n)]+[A_\mu(n),A_\mu(n+\hat{\nu})]\\&\quad+[A_\mu(n),A_\nu(n)]+[A_\nu(n+\hat{\mu}),A_\mu(n+\hat{\nu})]+[A_\nu(n+\hat{\mu}),A_\nu(n)]\Big]\Big\}.\end{aligned} \tag{3.23}$$

We assume the fields are smooth and one can perform a Taylor series in order to deal with the A's evaluated at different sites

$$A_\nu(n+\hat{\mu})=A_\nu(n)+a\,\partial_\mu A_\nu(n)+\mathcal{O}(a^2). \tag{3.24}$$

Terms in the first row of Eq. 3.23 evaluate to

$$A_\mu(n) + A_\nu(n) + a\partial_\mu A_\nu(n) - A_\mu(n) - a\partial_\nu A_\mu(n) - A_\nu(n) = a\partial_\mu A_\nu(n) - a\partial_\nu A_\mu(n) \quad (3.25)$$

and the terms involving commutators become

$$\begin{aligned}\frac{a^2}{2}\Big[&- [A_\mu(n), A_\nu(n)] - [A_\mu(n), A_\nu(n)] + [A_\mu(n), A_\mu(n)] \\ &+ [A_\mu(n), A_\nu(n)] + [A_\nu(n), A_\mu(n)] + [A_\nu(n), A_\nu(n)]\Big] \\ &= -\frac{a^2}{2}\, 2\,[A_\mu(n), A_\nu(n)] = -a^2[A_\mu(n), A_\nu(n)], \end{aligned} \quad (3.26)$$

by keeping the lowest powers of a that arise in the expansion. We arrive then at

$$U_{\mu\nu}(n) \approx \exp(ia^2(\partial_\mu A_\nu(n) - \partial_\nu A_\mu(n) + i[A_\mu(n), A_\nu(n)])), \quad (3.27)$$

and can recognize the field-strength tensor in the exponent (see Eq. 2.3)

$$F_{\mu\nu}(n) = \partial_\mu A_\nu(n) - \partial_\nu A_\mu(n) + i[A_\mu(n), A_\nu(n)]. \quad (3.28)$$

Expanding Eq. 3.27 in powers of a^2, we get

$$U_{\mu\nu}(n) \approx \mathbb{1} + ia^2 F_{\mu\nu}(n) - \frac{a^4}{2} F_{\mu\nu}(n)F_{\mu\nu}(n), \quad (3.29)$$

which implies that

$$\text{tr Re}[\mathbb{1} - U_{\mu\nu}(n)] = \frac{a^4}{2}\text{tr}[F_{\mu\nu}(n)F_{\mu\nu}(n)], \quad (3.30)$$

where we used that $F_{\mu\nu}(n) = \sum_i F^{(i)}_{\mu\nu}(n)T_i$ is in the algebra of $SU(3)$, which implies that it is traceless and the components $F^{(i)}_{\mu\nu}(n)$ are real. We also notice that the lattice spacing factors together with the sum over lattice sites is a discretization of the space-time integration

$$a^4 \sum_{n\in\Lambda} \to \int d^4x, \quad (3.31)$$

so that, for the Wilson gauge action, Eq. 3.21, we end up with

$$S_G[A] = \int d^4x\, \frac{\beta}{4} \sum_{\mu\nu} \text{tr}\left[F_{\mu\nu}(x)F_{\mu\nu}(x)\right]. \quad (3.32)$$

The constant β can then be fixed to match the continuum expression correctly. Its value needs to be

$$\beta = \frac{2N_c}{g^2} = \frac{6}{g^2}, \quad (3.33)$$

where g is the continuum bare coupling and $N_c = 3$ is the number of colors in the theory.

Note that one may include larger loops in the action to further reduce lattice artifacts and thus obtain results closer to the continuum limit with the same lattice spacing. This is the philosophy of improvements to the lattice action. One can, for example,

include, besides the plaquettes, which have length 4, loops of length 6, such as rectangles, and obtain the Lüscher-Weisz gauge action (62). This new formulation would have the same continuum limit as the previous one, and would thus be part of the same class of universality, from a statistical mechanics point of view.

Since the Wilson pure-gauge action (with plaquettes only) is already correct to order $\mathcal{O}(a^2)$, improvements are not as critical. Improvement is much more decisive when dealing with fermions, especially when a particular kind of fermionic discretization is used, called Wilson fermions, which contain errors of $\mathcal{O}(a)$. We will explore this theme further when we introduce fermions on the lattice in Chap. 5.

Since in simulations we will be constrained to a finite volume, we have to decide what to do at the borders of the lattice. We will implement periodic boundary conditions, since this simplifies the theoretical analysis and reduces finite-volume effects by maintaining the discrete translation symmetry of the lattice. For the direction $\mu = 1$, corresponding to extent N_1, one has

$$U_1(n_1 = N_1, n_2, n_3, n_4) = U_1(n_1 = 0, n_2, n_3, n_4), \tag{3.34}$$

and likewise for all other directions.

Up to now we have described one way to construct a pure-gauge theory on the lattice. We may add fermions to the theory, but on the lattice the construction of a fermionic action is a delicate business and will be explored in more depth in Chap. 5. For now, we only say that fermion actions have the following form

$$S_F[\overline{\psi}, \psi, U] = \sum_{m,n\in\Lambda} \overline{\psi}(m)\mathcal{M}(m, n; U)\psi(n) = a^4\overline{\psi}\mathcal{M}[U]\psi, \tag{3.35}$$

in which the operator $\mathcal{M}$ is the inverse of the fermion propagator $\mathcal{M}^{-1} = S$, $\overline{\psi}$ and ψ are Grassmann valued anticommuting fields. The path-integral representation of the full partition function in terms of the Euclidean action is given by

$$Z = \int \mathcal{D}U\mathcal{D}\psi\mathcal{D}\overline{\psi}\, e^{-\left(S_G[U]+S_F[\overline{\psi},\psi,U]\right)}. \tag{3.36}$$

The measures of integration are: the Haar measure for the link variables

$$\mathcal{D}U = \prod_{n\in\Lambda}\prod_{\mu} dU_\mu(n), \tag{3.37}$$

which implements the integration over the group manifold of $SU(3)$ for each discretized site, and for the Grassmann fields

$$\mathcal{D}\psi\mathcal{D}\overline{\psi} = \prod_{n\in\Lambda}\prod_{\alpha,c} d\psi_{\alpha,c}(n)d\overline{\psi}_{\alpha,c}(n). \tag{3.38}$$

The integration over the fermionic fields can be performed exactly, using standard formulas for Grassmann-variable integration (1, 46). We obtain for Z

$$Z = \int \mathcal{D}U \left[e^{-S_G[U]} \int \mathcal{D}\psi\mathcal{D}\overline{\psi} e^{-\overline{\psi}\mathcal{M}[U]\psi}\right] = \int \mathcal{D}U \left[e^{-S_G[U]}\det[\mathcal{M}[U]]\right]. \tag{3.39}$$

Expectation values are calculated as

$$\langle \mathcal{O} \rangle = \frac{1}{Z} \int \mathcal{D}U \mathcal{D}\psi \mathcal{D}\overline{\psi}\, e^{-\left(S_G[U]+S_F[\overline{\psi},\psi,U]\right)} \mathcal{O}[\overline{\psi},\psi,U]. \tag{3.40}$$

We assume that the operator whose expectation value is being calculated is expressed in terms of products of quark bilinears

$$\mathcal{O}_k \left[\overline{\psi}(m_k), \psi(n_k)\right] = \overline{\psi}_{\alpha_k}(m_k) \Gamma_{k,\,\alpha_k\beta_k} \psi_{\beta_k}(n_k),$$

where Γ is a Dirac-space matrix. Then, one can use Wick's theorem when integrating over the fermionic fields to obtain

$$\left\langle \prod_{k=1}^{n} \mathcal{O}_k \right\rangle = \int \mathcal{D}U \, \frac{e^{-S_G[U]} \det\mathcal{M}[U]}{Z} \times \left[(-1)^n \left(\sum_{P(1,2,\ldots,n)} \mathrm{sign}(P) \prod_k (S_{m_k,n_{P_k}}[U])_{\alpha_k\beta_{P_k}} \right) \prod_{k'} \Gamma_{k',\alpha_{k'},\beta_{k'}} \right], \tag{3.41}$$

where the sum runs over all permutations of the numbers $(1, 2, \ldots, n)$, $\mathrm{sign}(P)$ gives the sign of the permutation and $S_{n,m}[U]$ is the quark propagator for a particular field configuration

$$S_{n,m}[U] = \frac{1}{\det\mathcal{M}[U]} \int \mathcal{D}\psi \mathcal{D}\overline{\psi}\, e^{-\overline{\psi}\mathcal{M}[U]\psi} \psi(n)\overline{\psi}(m) = \mathcal{M}^{-1}_{nm}[U]. \tag{3.42}$$

3.1 Quenched approximation

In a lattice setting, the exact calculation of $\det[\mathcal{M}[U]]$ in 3.39 is an expensive operation. The operator $\mathcal{M}$ has $(4 \times 3 \times \mathrm{Volume})^2$ complex entries, which for a lattice of size 32^4, for example, would give approximately 158 trillion complex numbers. This is a naïve counting, since $\mathcal{M}$ is sparse for most Dirac operators used in practice, because only entries corresponding to nearest neighbors are included. But, even taking into account the sparsity of the matrix, the task of calculating the determinant in exact closed form is unthinkable. In fact, a simulation in lattice gauge theory usually consists in producing configurations of link variables and evaluating expectation values by sampling, as will be explained further in 6.1. The determinant of $\mathcal{M}$ influences the evolution of the algorithms to generate the configurations, and, conversely, it needs to be calculated for every single gauge configuration at each step of the generation algorithm, since it depends itself on U.

There are nowadays specialized algorithms to take this fermion determinant into account in simulations exactly. When performing a numerical lattice calculation using these methods, one speaks of a dynamical fermion simulation. These simulations, which are much more expensive than pure-gauge simulations, take into account all the effects coming from the fermionic degrees of freedom and are absolutely necessary for precision physics and if one wishes to obtain agreement with experimental values at the sub-percent level.

An alternative to this problem is to neglect the effects of the determinant, in the hope that the fermionic dynamics is not essential to the physics that one is looking at. This is the so-called "quenched approximation", where one takes $\det[\mathcal{M}] = 1$. In the past, most simulations had to be done in this approximation or they would not have been done at all. Nowadays, the quenched approximation is still in use, for example, for exploratory studies or studies that envisage a conceptual breakthrough, rather than precision.

Moreover, there is some theoretical basis for the quenched approximation. The simplest argument is based on counting the degrees of freedom of the theory. QCD contains a larger amount of gluonic degrees of freedom than fermionic ones. There is also the OZI rule and the approximate linearity of Regge trajectories, which indicate that quark loops would only contribute a small effect to some observables (50). Perhaps more convincing is the argument given *a posteriori*, based on the success of the approximation to produce the light hadron spectrum in good agreement with the experimental data (63), indicating that at least a part of the effects of quenching can be reabsorbed in the definition of the gauge coupling g.

One known drawback of the quenched approximation is that, since quarks are not taken into account in the action, the axial anomaly is absent, making the η' an extra Goldstone boson, where in reality is has a mass larger than the nucleon (33, 46). The quenched approximation is also undesirable when studying aspects of the phase transition in QCD thermodynamics, as mentioned in the Introduction.

When calculating propagators in a quenched approximation, what is effectively being done is to separate the valence quark masses from the external propagators from the sea quark masses of the determinant. The sea quark masses are taken to infinity, in such a way that they decouple from the theory. One then evaluates the valence quark propagators in a pure-gluon background.

3.2 Scale setting

In pure-gauge theory on the lattice we just have one parameter to vary: the inverse coupling β. One may wonder how to determine the lattice spacing in physical units, since everything on the lattice is written in terms of dimensionless quantities. The way to proceed to is to numerically calculate some observable that can be related to experimental results. Then one obtains the lattice spacing by matching. Of course, this will only give reliable results if the lattice spacing is sufficiently small, because, for large lattice spacings, one should expect lattice artifacts to dominate.

We must notice first that there is only hope of obtaining a continuum limit for a lattice quantum field theory if the associated statistical mechanical partition function, given by the integral over the Boltzmann exponential of the lattice action, contains a

second-order phase transition. These transitions are characterized by the divergence of correlation lengths. In fact, the largest correlation length will have the following relationship with the smallest mass of the spectrum of the theory (25)

$$\xi = \frac{1}{m}. \tag{3.43}$$

If the smallest mass in the spectrum of the theory is to have a finite value, the corresponding value in lattice units $\hat{m} = am$ must vanish as we approach the continuum limit $a \to 0$. Conversely, the associated correlation length in lattice units $\hat{\xi} = \frac{\xi}{a}$ will diverge. If the statistical mechanical system does not contain any region in the space of the action coefficients where criticality is achieved, then there is no hope that a continuum limit will be realized. Conversely, if the continuum limit exists, all lattice lengths will tend to infinity (and masses tend to 0, respectively) as it is approached.

More precisely, if a physical observable Θ has mass dimension d_Θ, then we should be able to write it as

$$\Theta(g, a) = \left(\frac{1}{a}\right)^{d_\Theta} \hat{\Theta}(g), \tag{3.44}$$

where $\hat{\Theta}$ denotes the lattice equivalent of the said observable, which can be obtained numerically. In order to obtain the continuum limit, we must drive the couplings, here represented by g, to their critical values g^*, so that the physical value of Θ will be

$$\Theta(g, a) = \left(\frac{1}{a}\right)^{d_\Theta} \hat{\Theta}(g) \overset{a\to 0,\, g\to g^*}{\longrightarrow} \Theta_{\text{physical}}. \tag{3.45}$$

The framework to understand changes in the ultraviolet cutoff a with the corresponding changes in the coupling is the renormalization-group. We aim at obtaining a relationship of the type $g(a)$ or $\beta(a)$ in this formalism. This relationship expresses how the coupling runs as the ultraviolet regulator (the lattice spacing) changes, in such a way as to keep physical observables unchanged, which should be true sufficiently close to the continuum limit. The invariance of the observables with respect to changes in the lattice spacing is expressed in the following renormalization group equation (25, 46)

$$\frac{d\Theta(g(a), a)}{d\ln(a)} = \left(\frac{\partial}{\partial \ln(a)} - \beta(g)\frac{\partial}{\partial g}\right)\Theta(g, a) = 0, \tag{3.46}$$

where the β-function* was defined by

$$\beta(g) \equiv -\frac{\partial g}{\partial \ln(a)}. \tag{3.47}$$

One can interpret the renormalization-group equation on the lattice as saying that we need to fine-tune the couplings (and, in general, all Lagrangian parameters), as we change

* It is unfortunate that the inverse temperature, the inverse coupling and the β-function are all written with the same Greek letter, however this is quite standard notation, so we feel compelled to stick to it. We hope that throughout this text it will be clear which one is meant.

the spacing, so as to keep physics constant. For a broader presentation of renormalization as pertaining to lattice field theories, one can consult Sects. 1.6 and 1.7 of (50).

In order to determine the β-function on the lattice, we may calculate, for example, the potential between a static (that is, infinitely heavy) quark and static antiquark in lattice perturbation theory as powers of g. The potential has the following form (25,64,65)

$$V(R,g,a) \approx -\frac{g^2(a)}{4\pi R}\, C_1 \left\{ 1 + \frac{g^2(a)}{(4\pi)^2}\, \frac{11N_c}{3}\, \left[\ln\left(\frac{R^2}{a^2}\right) + C_2 \right] \right\}, \tag{3.48}$$

where C_1 and C_2 are constants, and R is the separation between the quark and the antiquark. By using this for $\Theta(g,a)$ in Eq. 3.46, we may obtain an approximation to the β-function for small g

$$\beta(g) \approx -\beta_0 g^3, \tag{3.49}$$

where

$$\beta_0 = \frac{1}{(4\pi)^2} \left(\frac{11N_c}{3}\right). \tag{3.50}$$

One could, in principle, improve on this by calculating expressions with a higher number of loops in lattice perturbation theory. This approach is, however, extremely cumbersome due to the complicated structure of the Feynman rules on the lattice. One may resort to the universality or renormalization scheme independence of the first two coefficients of the beta function expansion (5,25,64),

$$\beta(g) = -\beta_0 g^3 - \beta_1 g^5 + \mathcal{O}(g^7), \tag{3.51}$$

meaning that their values are the same both on the lattice and in regular continuum perturbation theory. In fact, 3.50 is the same result obtained in usual continuum perturbation theory (1). The next coefficient is

$$\beta_1 = \frac{1}{(4\pi)^4} \left(\frac{34N_c^2}{3}\right), \tag{3.52}$$

for $SU(N_c)$ without dynamical quarks. Universality also entails that the use of the potential between static quarks was merely illustrative and another observable would have given the same coefficients. Integrating out the β-function to obtain the relationship between the lattice spacing and the coupling results in

$$a(g) \equiv \frac{1}{\Lambda_L} R(g), \quad R(g) = (\beta_0 g^2)^{-\frac{\beta_1}{2\beta_0^2}} e^{-\frac{1}{2\beta_0 g^2}} (1 + \mathcal{O}(g^2)). \tag{3.53}$$

The lattice dimensionful integration constant Λ_L can be used to set the scale, by fixing a value for g at some a. This constant is renormalization-scheme-dependent[†] and different from the continuum Λ_{QCD}, but both are related, as clarified by lattice perturbation theory

[†] One can check (64) for the same argument but using other quantities, such as the string tension and glueball masses.

(25, 66). The fact that the formula for $a(g)$ contains a term of the form e^{-1/g^2} is seen as a hint that non-perturbative contributions are included in the result (25, 64), since such a term does not have a Taylor series in g.

There are also mean-field improved renormalization schemes that extend the convergence of the lattice perturbation theory for weak-coupling expansion presented above by removing tadpole diagrams (67, 68). A non-perturbative scheme has been proposed by integrating the two- or three-loop renormalization equation numerically (64, 69). More on this subject can be found in (70).

We can derive from 3.53 that the critical value for the gauge coupling is $g \to 0$, or conversely $\beta \to \infty$, and the continuum limit is obtained for large β (see Eq. 3.33). This is a lattice version of asymptotic freedom: as one delves into smaller and smaller lattice spacings, one is able to probe the finer details of the ultraviolet regime of the theory, and the gauge coupling is correspondingly found to vanish in this limit, tending to a free theory. The value $g = 0$ is also a root of the β-function and is thus a fixed point in the space of the renormalization-group couplings.

With 3.53 in mind, we can now substitute the relationship between the spacing and the coupling in Eq 3.45, to derive that, close to the continuum limit, the lattice version of a physical quantity should obey

$$\hat{\Theta}(g) \overset{g\to 0}{\approx} \hat{C}_\Theta \, R^{d_\Theta}(g). \tag{3.54}$$

This is the asymptotic-scaling relationship for the observable Θ, from which one can obtain $\hat{C}_\Theta$ from the known $R(g)$. Moreover, the physical value of the observable is found to be

$$\Theta_{\text{physical}} = \hat{C}_\Theta \, \Lambda_L^{d_\Theta}, \tag{3.55}$$

and one sees that the mass scale Λ_L provides a way to express dimensionful quantities from the lattice. Even though Λ_L is undetermined without input from the world external to a lattice QCD simulation, one can obtain ratios of observables from the simulation alone. If the continuum limit is close, so that the relation 3.54 is valid for a pair of observables, we obtain that two observables with the same mass dimension are going to obey

$$\frac{\Theta_{1,\text{physical}}}{\Theta_{2,\text{physical}}} = \frac{\hat{C}_{\Theta_1}}{\hat{C}_{\Theta_2}}. \tag{3.56}$$

When performing a numeric calculation on available computers, we have to worry about other issues. If we want to study a system at constant physics, we should preferably keep the lattice volume unchanged, especially since we do not know *a priori* what are the finite-size effects. The physical volume in a finite-volume lattice simulation is given by

$$V = a^4 N_{\text{spatial}}^3 N_{\text{temporal}}. \tag{3.57}$$

If we decrease the lattice spacing, as mandated in order to obtain the continuum limit, but keep the same number of lattice points, we will also be decreasing the physical volume. In order to keep the physical volume constant for a decreasing lattice spacing, we must increase the number of lattice points. This can only be done up to a certain point, since more lattice points require more computational power, and the available resources are finite. For a given lattice volume, the correlation length will not be able to grow to be larger than the available memory and this restricts the values of β for which the behavior in 3.54 will be verified. One is thus constrained to a "scaling window", where the relation is obeyed.

One more issue that has to be taken into consideration in practice is "critical slowing down". Many algorithms for generating configurations in lattice field theory suffer from a difficulty of convergence as one approaches the continuum limit, because their convergence is tied in one way or another to the correlation lengths of the system, which diverge as we have discussed at the start of this section. This causes the correlation between subsequent configurations in a Monte Carlo simulation, for example, to become very large and one needs to discard more configurations when measuring numerically expensive quantities on the lattice, which leads to a reduction of the statistics and consequently to an increase of the errors. The simulation cost is expected to quickly grow with a power of the lattice size. In fact, the slowing down is also present for gauge-fixing algorithms (71) and algorithms that deal with the inversion of the Dirac operator, due to the small values of the associated eigenvalues close to the continuum limit. This phenomenon contributes in further restricting the accessible scaling window.

The renormalization-group discussion provides the background for understanding the relationship between the Lagrangian parameters and the lattice spacing. In practice, however, the values of coupling that are used for numeric simulations in the $SU(3)$ pure-gauge (or quenched) case, $\beta \approx 6.0$, $g \approx 1$, preclude one from using the actual formulas presented above without caution. A procedure that is better tailored for the range used in practice is the Necco-Sommer scheme, which is also based on obtaining the lattice spacing from the static potential between a quark and antiquark, but giving more emphasis to non-relativistic quantum knowledge (72). It is well established that heavy quarkonia can be studied using non-relativistic potentials and the Schrödinger equation in regular quantum mechanics. From these studies, one obtains that the force between quarks in the limit that they are infinitely heavy is given by

$$F(r_0)\, r_0^2 = 1.65, \tag{3.58}$$

when $r_0 \approx 0.5\,\mathrm{fm}$. We can model the interaction between these quarks with a potential of the form

$$V(r) = A + \frac{B}{r} + \sigma r. \tag{3.59}$$

Using that $F(r) = dV(r)/dr$ gives

$$F(r_0)\, r_0^2 = -B + \sigma r_0^2 = 1.65, \tag{3.60}$$

which can be solved for r_0 to yield

$$\frac{r_0}{a} = \frac{0.5\,\mathrm{fm}}{a} = \sqrt{\frac{1.65 + B}{a^2\sigma}} \quad \rightarrow \quad a = 0.5\,\mathrm{fm}\sqrt{\frac{a^2\sigma}{1.65 + B}}. \tag{3.61}$$

The dimensionless constants B and $a^2\sigma$ can be determined numerically from a lattice calculation of the correlators of two Polyakov loops, which will be defined later on in Sect. 3.3.1. One then fits the potential to the form

$$aV(an) = aA + \frac{B}{n} + a^2\sigma n, \tag{3.62}$$

thus obtaining the constants, which can be inserted back into Eq. 3.61. In this way, a can be read off.

By varying β in the simulation, we can find out how the spacing will change with the coupling. The authors of (73), along the lines of the procedure above, produced the following parameterization for $a(\beta)$, valid for $SU(3)$ quenched/pure-gauge theory in the range $5.7 < \beta < 6.92$

$$a(\beta) = r_0 e^{f(\beta)}, \tag{3.63}$$

with

$$f(\beta) \equiv -1.6804 - 1.7331(\beta - 6.0) + 0.7849(\beta - 6.0)^2 - 0.4428(\beta - 6.0)^3. \tag{3.64}$$

We choose to work with this scheme, given in 3.63, since it is better suited for the coupling values used in practice by us.

3.3 QCD at finite temperature on the lattice

In studies of finite-temperature systems, the partition function plays a pivotal role. For quantum systems, in particular, it is defined as

$$Z(T) = \mathrm{tr}\left[e^{-\beta H}\right] \tag{3.65}$$

and it admits a path-integral representation as

$$Z(T) = \int D[\Phi] e^{-S_E^\beta[\Phi]}, \tag{3.66}$$

where $S_E^\beta[\Phi]$ is the finite-temperature Euclidean action and Φ represents the collection of all fields that make up the degrees of freedom of the theory. The Euclidean action is the integral of the Euclidean Lagrangian density, and the temperature is given as the inverse of a finite "imaginary-time" extent $\beta = \frac{1}{T}$ (with $k_B = 1$ in natural units) for this integration

$$S_E[\Phi] = \int_0^\beta \int_{\mathrm{Volume}} d^3x\, \mathcal{L}_E[\Phi(x)]. \tag{3.67}$$

The bosonic gluon fields, moreover, are required to obey periodic boundary conditions, which comes from the trace in Eq. 3.65.

Naïvely, for sufficiently high temperatures, one might think that non-perturbative effects should be absent in QCD, since the typical energy scales are also high and this would allow perturbation theory to be applicable. In fact, however, this is not necessarily so. One instance of the failure of perturbation theory for high temperatures is the Linde problem, which states that perturbative quantum field theory at finite temperature breaks down due to infrared divergences from order g^6 onward, since, above this, all orders of perturbation theory start to contribute equally (74, 75). Actually, as evidenced by the fact that the quark-gluon plasma appears to behave as a nearly perfect liquid, QCD seems to be strongly coupled at least up to temperatures as high as 450 MeV. The upshot is that, in order to have a correct picture of the deconfinement and chiral-restoration transitions and a description of the quark-gluon plasma, one must include non-perturbative effects. These arguments support the use of lattice QCD as the ideal tool to research this topic. Lattice simulations show, in particular, that a convergence to the Stefan-Boltzmann limit (when the particles can be considered free) for QCD matter is slow and is attained only for extremely high temperatures $\gg 600$ MeV (76), thus justifying the need for non-perturbative techniques *a posteriori*.

In the continuum, one usually takes the volume to ∞, but, in the lattice simulations, we are always restricted to finite volume. The "imaginary-time direction" on the lattice is also always finite, and if zero-temperature results are needed, one has to take β to be large together with the volume. If, on the other hand, one is interested in finite-temperature physics, one fixes β as one allows the volume to grow. The inverse temperature on the lattice is then given by

$$\beta = aN_T, \tag{3.68}$$

where a is again the lattice spacing and N_T the number of sites in the T direction. From this, one sees that one has two options when trying to control the temperature on the lattice: either change the spacing or change the number of points in the T direction. The first option gives us the ability to change the temperature continuously, albeit with the disadvantage that changes in the volume will also result [‡]. The second option, keeping a fixed and changing N_T, will allow us to change the temperature by discrete amounts only.

[‡] Unless one uses anisotropic lattices, with different temporal and spatial spacings, which is a rather clumsy formalism which we will not explore in this work

3.3.1 Center symmetry and Polyakov loops

One important quantity to describe confinement on the lattice will be the Polyakov loop. It is given by

$$L(\vec{m}) = \mathrm{tr}\left[\prod_{j=0}^{N_t-1} U_t(\vec{m},t)\right], \tag{3.69}$$

which means that it is a closed circuit of links along the temporal direction for a given spatial position $\vec{m}$. Since it is a closed loop due to the periodic boundary conditions, it is automatically gauge-invariant.

The importance of it is linked to a calculation of the excess free energy of a single static-quark test charge in the surrounding gluon medium. The partition function of a static quark at spatial position $\vec{m}$ for a pure-gauge theory is given by (18, 77, 78)

$$Z_Q = \mathrm{tr}_{q(\vec{m})} e^{-\beta H} = \sum_n \left\langle \psi_n(1 \text{ quark}, \vec{m}) | e^{-\beta H} | \psi_n(1 \text{ quark}, \vec{m}) \right\rangle \tag{3.70}$$

$$= \int \mathcal{D}U \, \mathrm{tr}\left[L(\vec{m})\right] e^{-S[U]}. \tag{3.71}$$

From this, it follows that the expectation value of the trace of the Polyakov loop is related to the free-energy difference between a scenario with and without a static quark

$$\langle L(\vec{m}) \rangle = \langle L \rangle = \frac{1}{Z} \int \mathcal{D}U \, L(\vec{m}) e^{-S[U]} = \frac{Z_Q}{Z} = e^{-\frac{F_Q - F_0}{T}}, \tag{3.72}$$

where

$$L = \frac{\sum_{\vec{m}} L(\vec{m})}{V_{\text{spatial}}}, \tag{3.73}$$

and the first equality follows from translation invariance.

For a theory that is confined at zero temperature, as is the case with QCD, it would cost infinite energy to remove a static quark to infinity, $F_Q = \infty$ and consequently $\langle L \rangle = 0$. If quarks are liberated at some regime, then, correspondingly, we will have $\langle L \rangle \neq 0$. In this framework, the trace of the Polyakov loop will serve as an order parameter for the deconfinement transition. The order of the transition can be obtained by integrating out all the degrees of freedom besides the Polyakov loops. The resulting three-dimensional Z_3 spin system describes the critical behavior at the transition. In particular, for $SU(3)$, this correctly predicts the first-order transition to the deconfined phase (79), which is corroborated by lattice simulations.

One can also consider the correlation function of two Polyakov loops $\langle L(\vec{m}) L^\dagger(\vec{n}) \rangle$, from which one derives the following relation (78)

$$\langle L(\vec{m}) L^\dagger(\vec{n}) \rangle = \frac{1}{Z} \sum_n e^{-\frac{E_n^{\bar{q}q}(|\vec{m}-\vec{n}|)}{T}}, \tag{3.74}$$

where the sum goes over all energy levels and $E_n^{\bar{q}q}(r)$ are the eigenvalues of the Hamiltonian of QCD in the presence of a $\bar{q}q$ pair. In the zero-temperature limit, we can calculate

$$\lim_{T\to 0} \frac{\sum_n e^{-\frac{E_n^{\bar{q}q}}{T}}}{\sum_n e^{-\frac{E_n}{T}}} = \lim_{T\to 0} e^{-\frac{(E_0^{\bar{q}q}-E_0)}{T}} \frac{1+e^{-\frac{E_1^{\bar{q}q}-E_0^{\bar{q}q}}{T}}+\dots}{1+e^{-\frac{E_1-E_0}{T}}+\dots} \to e^{\frac{-V_{\bar{q}q}(|\vec{m}-\vec{n}|)}{T}}, \tag{3.75}$$

and identify in the last equality the static potential as the energy of a $\bar{q}q$ pair above the vacuum. The sub-leading contributions are suppressed in the zero-temperature limit. At a finite temperature, one has

$$\langle L(\vec{m})L^\dagger(\vec{n})\rangle = e^{-\frac{F_{\bar{q}q}(|\vec{m}-\vec{n})|}{T}}. \tag{3.76}$$

The free-energy of a $\bar{q}q$ pair is $F_{\bar{q}q}$, which can be thought of as a temperature dependent potential and shows screening above a critical temperature. In the deconfined phase, it has the form (78)

$$\frac{F_{\bar{q}q}(r)}{T} = -\frac{c(T)e^{-m(T)r}}{(rT)^d}, \tag{3.77}$$

which is in contrast to the expected behavior in the confining phase of a Coulomb + string potential for the zero-temperature case

$$V_{\bar{q}q}(r) = \frac{B}{r} + \sigma r. \tag{3.78}$$

The susceptibility for the Polyakov loop can be defined by

$$\chi_P = N^3\left(\langle L^2\rangle - \langle L\rangle^2\right), \tag{3.79}$$

and one studies the behavior of this quantity to determine the order of the transition and the eventual critical temperature.

As with chiral symmetry, the confinement transition in the pure-gauge case is associated to the breaking of a symmetry. We first identify the corresponding symmetry of the lattice action. We begin by defining a center transformation. For a given time slice $t = t_0$, we perform the product of the temporal links for all spatial positions by an element of the center of the internal symmetry group z,

$$U_t(\vec{n}, t_0) \to z\, U_t(\vec{n}, t_0). \tag{3.80}$$

The center of the group is composed by all elements that commute with all group elements. For $SU(3)$, all elements of the center are proportional to the identity matrix with a phase $(\mathbb{1}, \mathbb{1}e^{2\pi/3}, \mathbb{1}e^{-2\pi/3})$. These elements make up a $Z(3)$ finite subgroup inside of $SU(3)$.

The center transformation is a global symmetry of the pure-gauge Wilson lattice action. It leaves all spatial plaquettes untouched, whereas the temporal plaquettes are invariant, because they include links in the positive and negative temporal directions

$$\mathrm{tr}[U_\mu(\vec{n}, t_0)U_t(\vec{n}+\hat{\mu}, t_0)U_\mu^\dagger(\vec{n}, t_0+1)U_t^\dagger(\vec{n}, t_0)] \tag{3.81}$$

$$\to \mathrm{tr}[zU_\mu(\vec{n}, t_0)U_t(\vec{n}+\hat{\mu}, t_0)U_\mu^\dagger(\vec{n}, t_0+1)U_t^\dagger(\vec{n}, t_0)z^\dagger] \tag{3.82}$$

$$= \mathrm{tr}[z^\dagger z U_\mu(\vec{n}, t_0)U_t(\vec{n}+\hat{\mu}, t_0)U_\mu^\dagger(\vec{n}, t_0+1)U_t^\dagger(\vec{n}, t_0)], \tag{3.83}$$

where we used the cyclic property of the trace and the fact that the center elements are unitary and commute with any other element of the group. The Polyakov loop, however, is not invariant with respect to center transformations, since there is only one link in the temporal direction and nothing else to cancel the center element z

$$L \to z\, L. \tag{3.84}$$

We already established that the center transformation is a symmetry of the lattice action. If the ground state is also symmetric with respect to this symmetry, then we can average over all elements of the center in the expectation value of the Polyakov loop to obtain

$$\begin{aligned}\langle L\rangle = \frac{1}{3}\langle L + zL + z^2 L\rangle = \frac{1}{3}\left(1 + e^{i2\pi/3} + e^{-i2\pi/3}\right)\langle L\rangle \\ = \frac{1}{3}\left(1 - \frac{1}{2} + \frac{\sqrt{3}}{2} - \frac{1}{2} - \frac{\sqrt{3}}{2}\right)\langle L\rangle = 0.\end{aligned} \tag{3.85}$$

This shows that the expectation value of the Polyakov loop must vanish if the ground state is symmetric with respect to center transformations. Conversely, a non-vanishing value of the Polyakov loop indicates that center symmetry is spontaneously broken. But we already linked the value of the Polyakov loop to confinement, via the static potential. We are thus led to the conclusion that the spontaneous breaking of center symmetry is connected to confinement.

As mentioned in the Introduction, the action with the inclusion of quarks is not symmetric with respect to center transformations to start with. Physically, we can interpret this as coming from a "string breaking" in the potential due to the formation of quark-antiquark pairs, which screen the confining potential. The Polyakov loop is not an order parameter in this situation and $\langle L\rangle \neq 0$ for all temperatures. However, it is still considered important, as it should still retain some information on the deconfinement transition. In practice, its value is found to increase monotonically with increasing temperature in lattice studies (80).

4 GAUGE FIXING

By their very nature, gauge theories inherently contain a large redundancy in the definitions of the fields. Since gauge transformations are symmetries in these theories, any fields related by one such transformation actually share identical physical content*. Observables measured in a laboratory are oblivious to any ambiguity caused by local gauge symmetries, because they are necessarily gauge-independent. This means that, even though the theory contains an excess of degrees of freedom, in a calculation to be compared with experimental results the redundancy present in several terms must cancel out.

The redundancy in the theoretical formulation of physical phenomena is not unique to quantum field theories. In fact, we can observe this sort of redundancy even in electrostatics, as the electrostatic potential is defined up to an overall constant. In regular classical electrodynamics, the redundancy is larger. The potentials $\vec{A}'$ and V' will carry the same physical information as two other potentials $\vec{A}$ and V, as long as they are related by

$$\vec{A}' = \vec{A} + \nabla\lambda, \tag{4.1}$$

$$V' = V - \frac{\partial\lambda}{\partial t}, \tag{4.2}$$

where $\lambda(\vec{r}, t)$ is an arbitrary scalar function. In this setting, this gauge variance of the potentials can be explored to simplify some calculations, which can become easier to perform in Coulomb or Lorenz gauge, for example.

The manifestly Lorentz-invariant formulation of gauge quantum field theories in the continuum is also defined in terms of the gauge field $A_\mu(x)$ instead of the physical electric and magnetic fields. In the case of QED, for example, one can see that a quantization of $A_\mu(x)$ will necessarily need to deal with redundancy, since it contains four real time components but the photon is known to have only two physical polarizations.

The canonical quantization of theories with gauge freedom is complicated by the impossibility of imposing commutation relations between the fields and their canonical momenta in the Lagrangian. Take the Lagrangian for electrodynamics,

$$\mathcal{L}(x) = -\frac{1}{4}F_{\mu\nu}(x)F^{\mu\nu}(x), \quad F_{\mu\nu}(x) = \partial_\mu A_\nu(x) - \partial_\nu A_\mu(x). \tag{4.3}$$

One may try to naïvely compute the associated momenta to the A_μ fields, given by

$$\pi^\mu = \frac{\partial\mathcal{L}}{\partial(\partial_0 A_\mu)} = F^{\mu 0}, \tag{4.4}$$

but $\pi^0 = F^{00} = 0$, and the field component A_0 has no canonical momentum associated. In order to fix this issue in the canonical quantization formulation, the equation $\pi^0 = 0$ has

* For this Chapter our main sources are (1, 19, 46, 50).

to be considered a constraint. A presentation of the formalism for canonical quantization with constraints by Dirac is found in (81).

The issue can also be formulated in terms of the classical equations of motion. The Lagrangian 4.3 can be rewritten, using integration by parts, as

$$\mathcal{L} = -\frac{1}{2} A_\mu(x) K_{\mu\nu} A_\nu(x), \tag{4.5}$$

where the kinetic operator is

$$K_{\mu\nu} = g_{\mu\nu}\partial^2 - \partial_\mu\partial_\nu. \tag{4.6}$$

The operator however contains pure-gauge modes with zero eigenvalue. Take an arbitrary function $\lambda(x)$, and consider $\partial^\nu\lambda(x)$. It is easy to see that this is an eigenvector with zero eigenvalue, i.e. a zero-mode of the kinetic operator, because

$$K_{\mu\nu}\,\partial^\nu\lambda(x) = (\partial_\mu\partial^2 - \partial_\mu\partial^2)\lambda(x) = 0. \tag{4.7}$$

One can derive from the Lagrangian, using Euler-Lagrange equations, the classical equations of motion,

$$K_{\mu\nu} A_\nu(x) = 0. \tag{4.8}$$

The consequence of this is that, if two fields $A_\mu(x)$ and $A'_\mu(x)$ obeying the equations of motion are related by

$$A'_\mu(x) = A_\mu(x) + \partial_\mu\lambda(x), \tag{4.9}$$

then the physical contents are the same, and the decision to use one or the other is arbitrary. This is in fact the same issue that was already discussed above for classical electrodynamics. Eq. 4.9 is simply the Abelian version of Eq. 2.8.

The gauge-freedom also has consequences for the free photon propagator, which will be needed for perturbative calculations. The propagator of the photon would be the inverse of the kinetic operator in momentum space. However, the operator, as shown above, contains pure-gauge modes with zero eigenvalue and is therefore not invertible, making the propagator ill-defined as a result.

In the path-integral formulation of gauge quantum field theories, the gauge-redundancy problem arises in the guise of infinities when calculating matrix elements or correlators. These infinities can be made to factor out and cancel away through the Fadeev-Popov method, which includes a term in the path integral to constrain the integration[†]. The constraint aims at taking only one sample for each physically distinct gauge orbit, where each orbit is defined by the set of physically nonequivalent field configurations. In other words, one is choosing a particular gauge, picking a particular A_μ to represent each

[†] This is standard content of modern quantum field theory textbooks, for example (1). For a lattice gauge-theory version of this procedure, check Sect. 3.3 of (50). The method is also shown in detail in the Chapter 2 of (82) (in Portuguese).

distinct physical configuration. The term that is included is a clever way of writing the number 1,

$$|\det\mathcal{M}[A]| \int_{\mathcal{G}} \mathcal{D}g\, \delta\left(G[A^g]\right) = 1, \quad \mathcal{M} = \left.\frac{\delta G[A^g](x)}{\delta g(y)}\right|_{G[A^g]=0}, \tag{4.10}$$

where A^g is the gauge transformed version of A by the gauge transformation g. The integral is performed over the whole space of possible gauge transformations $\mathcal{G}$ and the delta distribution implements $G[A^g] = 0$, which is the gauge condition to concretely enforce the constraint and determine which gauge configuration is being taken from the orbit. One may take, for example,

$$G[A^g] = 0 = \partial_\mu A^{g\,\mu}(x), \tag{4.11}$$

which is called Landau or Lorenz gauge condition, and is specially suitable for the Lagrangian formalism by being explicitly Lorentz invariant. A generalization of this condition is used customarily in the Fadeev-Popov method, which presents a continuous class of gauges

$$G[A^g] = \partial_\mu A^{g\,\mu}(x) = \xi, \tag{4.12}$$

where ξ is a real parameter.

The Fadeev-Popov method for non-Abelian gauge theories leaves a few traces in the final quantization. Firstly, there is the inclusion of Feynman rules for unphysical ghost particles that must be added in computations with Feynman diagrams. This ensures unitarity by canceling terms that come from non-physical polarizations of the gauge bosons. Secondly, the method also the kinetic term of the gauge boson, analogous to 4.6, in such a way that it becomes invertible. The free propagator for a gluon, for the class of ξ gauges in Minkowski continuum space, is given by

$$D_{\mu\nu,\,ab}(k) = \frac{-i}{k^2 + i\varepsilon}\left(g_{\mu\nu} - (1-\xi)\frac{k_\mu k_\nu}{k^2}\right)\delta_{ab}. \tag{4.13}$$

The parameter ξ is an arbitrary constant that disappears from the final results when calculating physical observables. In practice, one often gives it a value from the start to simplify the calculations. Common choices are $\xi = 1$, the Feynman-'t Hooft gauge, and $\xi = 0$, the Landau gauge. Choosing a particular gauge is referred to as "gauge-fixing".

In more general terms, one can say that the correlators of the fundamental fields of a gauge theory are gauge-dependent, meaning that they are not completely defined unless a gauge-fixing scheme is in place. When trying to calculate gauge-dependent quantities without gauge-fixing, the result will vanish, as a corollary of Elitzur's theorem (83), which states that local gauge symmetry cannot be broken spontaneously.

Even though we emphasize the need to perform gauge-fixing in order to study correlation functions of gauge theories, there are also other reasons to do so. In some non-perturbative renormalization schemes, for example, matrix elements are calculated in a particular gauge to renormalize composite operators (46, 84, 85).

4.1 Landau Gauge-Fixing on the Lattice

The lattice formulation presented in Chap. 3 was actually born out of the desire to explicitly maintain local gauge symmetry in the action, which means maintaining the overabundance of degrees of freedom. However, if we want to study propagators, as we do in this work, then we must provide a gauge-fixing scheme.

The matricial Landau gauge condition in Eq. 4.11 is equivalent to the extremization of the functional

$$W[A] = \sum_{\mu} \int d^4x \, \mathrm{tr}\,[A_\mu(x) A_\mu(x)] \tag{4.14}$$

with respect to gauge transformations of the non-Abelian gluon field A_μ, given by 2.8. Here we are using the Euclidean metric, so that Lorentz indices may be brought up or down without consequence.

That the quadridivergence and the functional conditions are equivalent in the continuum formulation can be shown as follows: first, we remind ourselves that $A_\mu(x)$ is in the algebra of $SU(3)$, whereas $g(x)$ is an element of the group. We can then write $g(x)$ as

$$g(x) = e^{i\varepsilon H(x)}, \tag{4.15}$$

where $H(x)$ is in the algebra, and thus is traceless and Hermitian, which implies that

$$g^\dagger(x) = e^{-i\varepsilon H(x)}. \tag{4.16}$$

In terms of $H(x)$, the gauge transformation of $A_\mu(x)$, Eq. 2.8, then becomes

$$A_\mu(x) \to A^g_\mu(x) = e^{i\varepsilon H(x)} A_\mu(x) e^{-i\varepsilon H(x)} + i(i\varepsilon)\partial_\mu H(x). \tag{4.17}$$

If we take ε to be small, we can expand the exponentials and obtain

$$\begin{aligned} A^g_\mu(x) &= [\mathbb{1} + i\varepsilon H(x)]\, A_\mu(x)\, [\mathbb{1} - i\varepsilon H(x)] - \varepsilon \partial_\mu H(x) \\ &= A_\mu(x) + i\varepsilon [H(x), A_\mu(x)] - \varepsilon \partial_\mu H(x) \\ &= A_\mu(x) + \varepsilon \left\{ i[H(x), A_\mu(x)] - \partial_\mu H(x) \right\} \end{aligned} \tag{4.18}$$

keeping only terms up to first order in ε. We can now check what is the variation of the functional in Eq. 4.14 as we do this infinitesimal gauge transformation

$$\begin{aligned} W[A] \to W[A^g] = \sum_{\mu} \int d^4x \, \mathrm{tr} \Big\{ &\left\{ A_\mu(x) + \varepsilon \left[i[H(x), A_\mu(x)] - \partial_\mu H(x) \right] \right\} \\ &\left\{ A_\mu(x) + \varepsilon \left[i[H(x), A_\mu(x)] - \partial_\mu H(x) \right] \right\} \Big\}. \end{aligned} \tag{4.19}$$

Expanding the terms we get

$$\begin{aligned} W[A^g] = W[A] + \varepsilon \sum_{\mu} \int d^4x \, \mathrm{tr} \Big\{ &i \left\{ A_\mu(x) [H(x), A_\mu(x)] + [H(x), A_\mu(x)] A_\mu(x) \right\} \\ &- A_\mu(x) \partial_\mu H(x) - \partial_\mu H(x) A_\mu(x) \Big\}. \end{aligned} \tag{4.20}$$

The terms in the commutators cancel each other, as can be seen by expanding the products

$$A_\mu(x)[H(x), A_\mu(x)] + [H(x), A_\mu(x)]A_\mu(x) =$$

$$A_\mu(x)[H(x)A_\mu(x) - A_\mu(x)H(x)] + [H(x)A_\mu(x) - A_\mu(x)H(x)]A_\mu(x) =$$

$$A_\mu(x)H(x)A_\mu(x) - A_\mu(x)A_\mu(x)H(x) + H(x)A_\mu(x)A_\mu(x) - A_\mu(x)H(x)A_\mu(x) =$$

$$H(x)A_\mu(x)A_\mu(x) - A_\mu(x)A_\mu(x)H(x),$$

and, after taking the trace, one sees that

$$\mathrm{tr}[H(x)A_\mu(x)A_\mu(x) - A_\mu(x)A_\mu(x)H(x)] = 0,$$

using the cyclic property. We are left with

$$W[A^g] = W[A] - 2\varepsilon \sum_\mu \int d^4x \,\mathrm{tr}\,[A_\mu(x)\partial_\mu H(x)]\,. \tag{4.21}$$

We now suppose that $H(x)$ goes to zero as we move far away from the origin, so that we can integrate by parts without having to worry about a surface term, in order to get

$$W[A^g] = W[A] + 2\varepsilon \int d^4x \,\mathrm{tr}\left[H(x)\sum_\mu \partial_\mu A_\mu(x)\right]. \tag{4.22}$$

But, apart from the constraint that $H(x)$ should go to a 0 as $x_\mu \to \infty$, $H(x)$ is arbitrary. If we suppose that $A_\mu(x)$ is such that $W[A]$ is at an extreme, then an infinitesimal variation around that particular field should vanish. The only way that this is true for any $H(x)$ is if $\sum_\mu \partial_\mu A_\mu(x)$ vanishes, which is the Landau gauge condition. Therefore, extremizing $W[A]$ is equivalent to fixing to Landau gauge.

For our use in this work, we need a version of the functional of Eq. 4.14 suitable for the lattice formulation, in terms of the link variables $U_\mu(n)$. We take the following expression

$$\mathcal{E}[U;g] \equiv 1 - \frac{1}{dN_c|\Lambda|}\sum_\mu \sum_{n\in\Lambda} \mathrm{Re\ tr}\left[U^g_\mu(n)\right], \tag{4.23}$$

where $U^g_\mu(n) \equiv g(n)U_\mu(n)g^\dagger(n+\hat{\mu})$, that is, a gauge-transformed link variable. The set of lattice sites is denoted by Λ, $|\Lambda|$ is the total number of sites, also called the volume on the lattice, μ is the index for the Euclidean space-time directions, $\hat{\mu}$ is the versor in the μ direction and d is the space-time dimension of the problem.

That Eq. 4.23 is a version of the continuum functional can be seen by first noting that

$$\mathrm{Re\ tr}\left[U^g_\mu(n)\right] = \frac{1}{2}\mathrm{tr}\left[U^g_\mu(n) + U^{g\,\dagger}_\mu(n)\right], \tag{4.24}$$

and then by expanding $U_\mu(n) = e^{iaA_\mu(n)}$ for small lattice spacings

$$U_\mu(n) \approx \mathbb{1} + iaA_\mu(n) - \frac{a^2}{2}A_\mu^2(n) + \mathcal{O}(a^3) \tag{4.25}$$

$$U_\mu^\dagger(n) \approx \mathbb{1} - iaA_\mu(n) - \frac{a^2}{2}A_\mu^2(n) + \mathcal{O}(a^3), \tag{4.26}$$

which results in $U_\mu(n) + U_\mu^\dagger(n) = 2\,\mathbb{1} - a^2 A_\mu^2(n)$. When plugged back into Eq. 4.23, this gives

$$\mathcal{E}[U;g] \equiv 1 - \frac{1}{2dN_c|\Lambda|}\sum_\mu \sum_{n\in\Lambda} \mathrm{tr}\left[2\,\mathbb{1} - a^2 A_\mu^2(n)\right] = \frac{a^2}{2dN_c|\Lambda|}\sum_\mu \sum_{n\in\Lambda} \mathrm{tr}\left[A_\mu^2(n)\right], \tag{4.27}$$

which is clearly a version of 4.14, apart from the irrelevant normalization constant, which will not affect the extremization (71). Thus, given a link configuration $\{U_\mu(n)\}$, in order to fix to Landau gauge in a $SU(N_c)$ gauge theory on the lattice, we must find, among all the possible gauge-transformations, one that extremizes the functional in Eq. 4.23. If we find an extremum of the functional with respect to $\mathcal{G}$, keeping $\{U(n)\}$ fixed, we have that a discretized version of the Landau gauge condition is satisfied

$$\partial_\mu A_\mu^b(n) = \sum_{\mu=1}^{d}\left[A_\mu^b(n) - A_\mu^b(n-\hat{\mu})\right] = 0, \tag{4.28}$$

for all sites n, in which b is the color index and

$$A_\mu(n) = \left[\frac{U_\mu(n) - U_\mu^\dagger(n)}{2i}\right] - \frac{1}{N_c}\mathrm{tr}\left[\frac{U_\mu(n) - U_\mu^\dagger(n)}{2i}\right] \tag{4.29}$$

is the gauge field, which can be decomposed in components

$$A_\mu^b(n) = \frac{\mathrm{tr}[A_\mu(n)T^b]}{2}, \tag{4.30}$$

where T^b are the group generators.

We stress that the procedure described for the extremization of the functional $W[A]$ presented above is completely non-perturbative. The actual algorithms used in practice for gauge-fixing on the lattice will be presented in Sect. 6.2.

4.2 Gribov copies

It can be shown that the Landau gauge condition is not ideal (19). This means that the condition is not sufficient to select a single configuration from each gauge orbit. We can rewrite 4.18 in terms of the components as

$$A_\mu^{g\,a}(x) = A_\mu^a(x) - \left[\partial_\mu H^a(x) + f^{abc}A_\mu^c(x)H^b(x)\right] = A_\mu^a(x) - D_\mu^{ab}H^b(x), \tag{4.31}$$

where $D_\mu^{ab} = \partial_\mu\delta^{ab} + f^{abc}A_\mu^c(x)$ is the adjoint covariant derivative, with f^{abc} the structure constants. If two fields $A_\mu(x)$ and $A'_\mu(x)$ related by an infinitesimal gauge-transformation obey the Landau gauge condition, then we must have that

$$\partial_\mu A_\mu^{g\,a}(x) = \partial_\mu A_\mu^a(x) - \partial_\mu D_\mu^{ab}H^b(x) = 0. \tag{4.32}$$

The question then is if there are $H^b(x)$ such that

$$-\partial_\mu D^{ab}_\mu H^b(x) = 0, \tag{4.33}$$

or, in other words, does the $-\partial_\mu D^{ab}_\mu = -\partial_\mu(\partial_\mu \delta^{ab} + f^{abc}A^c_\mu(x))$ operator have zero eigenvalues? The answer for non-abelian theories is yes (16, 19, 86). Configurations with the same physical content and which obey the same gauge condition are referred to as Gribov copies, and the resulting uncertainty in quantities evaluated for these configurations has the name of Gribov noise. In the functional approach of extremizing $W[A]$, 4.14, Gribov copies will appear as different local minima.

5 FERMIONS ON THE LATTICE

The presentation in this chapter is based on the expositions found in (25, 46, 50, 64, 87).

5.1 The doubling problem and Wilson fermions

To start, let us consider a single free Dirac fermion field without a mass term. In the continuum, the fermionic action for such a field is given simply by

$$S_{F,\text{free,massless}} = \overline{\psi}(x)\not{\partial}\psi(x) = \overline{\psi}(x)\gamma_\mu\partial_\mu\psi(x). \tag{5.1}$$

The simplest and most naïve way of adapting the fermionic action to be put on a lattice is by discretizing the derivative that appears in Eq. 5.1,

$$\partial_\mu\psi(x) \to \frac{1}{2a}(\psi(n+\hat{\mu}) - \psi(n-\hat{\mu})). \tag{5.2}$$

A symmetric discretization is used in order to try and reduce lattice artifacts, since

$$\frac{f(x+\varepsilon) - f(x)}{\varepsilon} = \frac{f(x) + \varepsilon f'(x) + \mathcal{O}(\varepsilon^2) - f(x)}{\varepsilon} = f'(x) + \mathcal{O}(\varepsilon), \tag{5.3}$$

whereas

$$\begin{aligned}
&\frac{f(x+\varepsilon) - f(x-\varepsilon)}{2\varepsilon} \\
=&\frac{1}{2\varepsilon}\left[\left(f(x) + \varepsilon f'(x) + \frac{\varepsilon^2}{2}f''(x) + \mathcal{O}(\varepsilon^3)\right) - \left(f(x) - \varepsilon f'(x) + \frac{\varepsilon^2}{2}f''(x) + \mathcal{O}(\varepsilon^3)\right)\right] \\
=&f'(x) + \mathcal{O}(\varepsilon^2).
\end{aligned}$$

We can write Eq. 5.2 as a matricial operator acting on a vector

$$\hat{\partial}_\mu\psi = \hat{\partial}_{\mu\,nm}\psi_m, \tag{5.4}$$

where

$$\hat{\partial}_{\mu\,nm} = \frac{\delta_{n+\hat{\mu},m} - \delta_{n-\hat{\mu},m}}{2a}, \tag{5.5}$$

and we notice that this is an anti-symmetric (or anti-Hermitian) matrix, since

$$\hat{\partial}_{\mu\,mn} = \frac{\delta_{m+\hat{\mu},n} - \delta_{m-\hat{\mu},n}}{2a} = \frac{\delta_{m,n-\hat{\mu}} - \delta_{m,n+\hat{\mu}}}{2a} = -\frac{\delta_{n+\hat{\mu},m} - \delta_{n-\hat{\mu},m}}{2a} = -\hat{\partial}_{\mu\,nm}. \tag{5.6}$$

Although not obvious at first sight, this discretization has one serious flaw: it introduces many more fermions species than the one we wanted to describe. To see this, we can go to

momentum space, as the Fourier transformation will diagonalize the derivative term. The Fourier-transformed fields are defined by

$$\psi(m) = \frac{1}{\sqrt{\Lambda}} \sum_{p\in\tilde{\Lambda}} \overline{\psi}(p)\, e^{ip\cdot am}, \quad \overline{\psi}(n) = \frac{1}{\sqrt{\Lambda}} \sum_{q\in\tilde{\Lambda}} \psi(q)\, e^{iq\cdot an}, \tag{5.7}$$

where, to simplify the notation, we will differentiate between the configuration-space and momentum-space ψ and $\overline{\psi}$ by their arguments only. We will not dwell on which momenta are included in $\tilde{\Lambda}$ for now, but will come back to it later in Sect. 5.3. The lattice fermionic action turns into

$$\begin{aligned}
&\sum_{n,m\in\Lambda} \overline{\psi}(n) \left[\sum_\mu \gamma_\mu \partial_{\mu\, nm}\right] \psi(m) \\
=&\sum_{n,m} \overline{\psi}(n) \left[\sum_\mu \gamma_\mu \left(\frac{\delta_{n+\hat{\mu},m} - \delta_{n-\hat{\mu},m}}{2a}\right)\right] \psi(m) \\
=&\frac{1}{\Lambda} \sum_{p,q\in\tilde{\Lambda}} \sum_{n,m} \left(\overline{\psi}(q) e^{iq\cdot an}\right) \left[\sum_\mu \gamma_\mu \left(\frac{\delta_{n+\hat{\mu},m} - \delta_{n-\hat{\mu},m}}{2a}\right)\right] \left(\psi(p) e^{ip\cdot am}\right) \\
=&\frac{1}{\Lambda} \sum_{p,q} \sum_{m} \overline{\psi}(q) \left[\sum_\mu \gamma_\mu \left(\frac{e^{iq\cdot a(m-\hat{\mu})} - e^{iq\cdot a(m+\hat{\mu})}}{2a}\right)\right] \left(\psi(p) e^{ip\cdot am}\right) \\
=&\sum_{p,q} \overline{\psi}(q) \frac{\sum_m e^{i(q+p)\cdot am}}{\Lambda} \left[\sum_\mu \gamma_\mu \left(\frac{e^{-iaq_\mu} - e^{iaq_\mu}}{2a}\right)\right] \psi(p) \\
=&\sum_{p,q} \overline{\psi}(q) \delta(p+q) \left[\sum_\mu \gamma_\mu \left(\frac{e^{-iaq_\mu} - e^{iaq_\mu}}{2a}\right)\right] \psi(p) \\
=&\sum_{p} \overline{\psi}(-p) \left[\sum_\mu \gamma_\mu \left(\frac{e^{iap_\mu} - e^{iap_\mu}}{2a}\right)\right] \psi(p) \\
=&\sum_{p} \overline{\psi}(-p) \left[\sum_\mu \frac{i\gamma_\mu \sin(ap_\mu)}{a}\right] \psi(p) \equiv \sum_p \overline{\psi}(-p) \mathcal{M}(p) \psi(p),
\end{aligned}$$

where we used properties of the Kronecker delta and its discrete Fourier representation

$$\delta(p' - p) = \frac{\sum_m e^{i(p'-p)\cdot am}}{\Lambda}. \tag{5.8}$$

The components of the momentum are $p_\mu = p \cdot \hat{\mu}$.

The inverse of $\mathcal{M}$ will give us the propagator for the fermion. This inverse is given by

$$\mathcal{M}^{-1}(p) = \frac{-\sum_\mu i\gamma_\mu \frac{\sin(ap_\mu)}{a}}{\sum_\mu \frac{\sin^2(ap_\mu)}{a^2}}. \tag{5.9}$$

In checking that this is indeed the inverse we use, in Einstein's notation,

$$\gamma_\mu K_\mu \gamma_\nu K_\nu = \frac{1}{2}\left(\{\gamma_\mu, \gamma_\nu\} + [\gamma_\mu, \gamma_\nu]\right) K_\mu K_\nu \\ = \frac{1}{2}\{\gamma_\mu, \gamma_\nu\} K_\mu K_\nu = \frac{1}{2}\left(2\delta_{\mu\nu}\right) K_\mu K_\nu = K^2 \mathbb{1}, \quad (5.10)$$

where K_μ is a generic four-vector and we used the symmetry of $K_\mu K_\nu$ to get rid of the commutator, and the anti-commutation relation for the γ-matrices, so that

$$\mathcal{M} \cdot \mathcal{M}^{-1} = \sum_\mu \frac{i\gamma_\mu \sin(ap_\mu)}{a} \cdot \frac{-\sum_\nu i\gamma_\nu \frac{\sin(ap_\nu)}{a}}{\sum_\lambda \frac{\sin^2(ap_\lambda)}{a^2}} = \frac{\mathbb{1}\sum_\mu \frac{\sin^2(ap_\mu)}{a^2}}{\sum_\lambda \frac{\sin^2(ap_\lambda)}{a^2}} = \mathbb{1}. \quad (5.11)$$

We can see that this propagator has more poles than the continuum propagator. The continuum propagator for a single massless free fermion

$$S_{\text{cont.}}(p) = \frac{-i\sum_\mu \gamma_\mu p_\mu}{p^2} \quad (5.12)$$

has a single pole when the components $p_\mu = 0$ for all μ. In Eq. 5.9, there are in fact other poles, because

$$\sin(x) = 0 \quad (5.13)$$

has solutions $x = 0$, but also $x = \pi$ in the first Brillouin zone, where the momenta are restricted to lie. This means that we have a pole for all combinations of momentum components being either 0 or π/a: 16 in total, from which 15 are spurious artifacts of the discretization.

Actually, the source of these doublers' contributions is the discretization of the derivative in Eq. 5.2. We could use a another derivative operator such as

$$\hat{\partial}^{(+)}_{\mu\, nm} = \frac{\delta_{n+\hat{\mu},m} - \delta_{n,m}}{a} \quad (5.14)$$

or

$$\hat{\partial}^{(-)}_{\mu\, nm} = \frac{\delta_{n,m} - \delta_{n-\hat{\mu},m}}{a}. \quad (5.15)$$

In fact, these are related, since

$$\left(\hat{\partial}^{(+)}_{\mu\, nm}\right)^T = \frac{\delta_{m+\hat{\mu},n} - \delta_{m,n}}{a} \\ = \frac{\delta_{m,n-\hat{\mu}} - \delta_{m,n}}{a} \\ = \frac{\delta_{n-\hat{\mu},m} - \delta_{n,m}}{a} = -\hat{\partial}^{(-)}_{\mu\, nm}. \quad (5.16)$$

We can decompose $\hat{\partial}^{(+)}_{\mu\, nm}$ into symmetric and anti-symmetric parts by

$$\hat{\partial}^{(+)}_{\mu\, nm} = \frac{1}{2}\left[\hat{\partial}^{(+)}_{\mu\, nm} + \left(\hat{\partial}^{(+)}_{\mu\, nm}\right)^T\right] + \frac{1}{2}\left[\hat{\partial}^{(+)}_{\mu\, nm} - \left(\hat{\partial}^{(+)}_{\mu\, nm}\right)^T\right]. \quad (5.17)$$

The anti-symmetric part is exactly $\hat{\partial}_{\mu\, nm}$, because

$$\frac{1}{2}\left[\hat{\partial}^{(+)}_{\mu\, nm} - \left(\hat{\partial}^{(+)}_{\mu\, nm}\right)^T\right] = \frac{1}{2}\left[\hat{\partial}^{(+)}_{\mu\, nm} + \left(\hat{\partial}^{(-)}_{\mu\, nm}\right)^T\right]$$
$$= \frac{\delta_{n+\hat{\mu},m} - \delta_{n,m}}{2a} + \frac{\delta_{n,m} - \delta_{n-\hat{\mu},m}}{2a} = \frac{\delta_{n+\hat{\mu},m} - \delta_{n-\hat{\mu},m}}{2a} = \hat{\partial}_{\mu\, nm}. \tag{5.18}$$

The symmetric part is proportional to a discretization of the Laplacian operator ∇^2

$$\frac{1}{2}\left[\hat{\partial}^{(+)}_{\mu\, nm} + \left(\hat{\partial}^{(+)}_{\mu\, nm}\right)^T\right] = \frac{1}{2}\left[\hat{\partial}^{(+)}_{\mu\, nm} - \left(\hat{\partial}^{(-)}_{\mu\, nm}\right)^T\right]$$
$$= \frac{\delta_{n+\hat{\mu},m} - \delta_{n,m}}{2a} - \frac{\delta_{n,m} - \delta_{n-\hat{\mu},m}}{2a} = \frac{\delta_{n+\hat{\mu},m} - 2\delta_{n,m} + \delta_{n-\hat{\mu},m}}{2a}.$$

We can see, by expanding

$$f(x+\varepsilon) - 2f(x) + f(x-\varepsilon) =$$
$$f(x) + \varepsilon f'(x) + \frac{\varepsilon^2}{2}f''(x) - 2f(x) + f(x) - \varepsilon f'(x) + \frac{\varepsilon^2}{2}f''(x) = \varepsilon^2 f''(x) \tag{5.19}$$

up to order $\mathcal{O}(\varepsilon^3)$, that

$$\sum_\mu \frac{1}{a}\left[\hat{\partial}^{(+)}_{\mu\, nm} + \left(\hat{\partial}^{(+)}_{\mu\, nm}\right)^T\right] = \nabla^2_{nm}. \tag{5.20}$$

Using the derivative in Eq. 5.14 causes other problems, though. For the case of QED, the authors of (88) show that this gives rise to non-covariant contributions to the fermion self-energy and vertex-function (25).

The way that Wilson chose to solve the doubler problem is by including a term in the action, instead of modifying the derivative. This term vanishes in the continuum limit and raises the doubler masses, which vanish in Eq. 5.9, to high values, so that the doublers decouple from the theory at small spacings. This extra term, moreover, should not modify the pole at $p = (0,0,0,0)$, which is the one we want to keep in place. The term Wilson proposed in momentum space is

$$\delta\mathcal{M}_{\text{Wilson}}(p) = \mathbb{1}\sum_\mu \frac{1-\cos(ap_\mu)}{a} = \mathbb{1}\sum_\mu \frac{1}{\frac{a}{2}}\sin^2\left(\frac{ap_\mu}{2}\right), \tag{5.21}$$

which is to be included in Eq. 5.9. The complete Wilson free fermion propagator can be obtained by the inversion of this extended $\mathcal{M}$ operator

$$\mathcal{M}_{\text{Wilson}}(p) = \sum_\mu \frac{i\gamma_\mu \sin(ap_\mu)}{a} + \frac{\mathbb{1}\left[\sin^2\left(\frac{ap_\mu}{2}\right)\right]}{\frac{a}{2}}. \tag{5.22}$$

The inverse is

$$\mathcal{M}^{-1}_{\text{Wilson}}(p) = \frac{\sum_\mu \frac{-i\gamma_\mu \sin(ap_\mu)}{a} + \frac{\mathbb{1}\left[\sin^2\left[\frac{ap_\mu}{2}\right]\right]}{\frac{a}{2}}}{\sum_\mu \left(\frac{\sin(ap_\mu)}{a}\right)^2 + \left[\frac{\sin^2\left(\frac{ap_\mu}{2}\right)}{\frac{a}{2}}\right]^2}, \tag{5.23}$$

which can be checked by using the same identities that were used to check Eq. 5.9. We see that, for $p = (0, 0, 0, 0)$, the Wilson term in Eq. 5.21 vanishes, because $\sin(0) = 0$. For the pole positions previously associated to the doublers, if l components of the momentum are π/a and the rest are 0, the Wilson term becomes

$$\mathbb{1}\frac{2l}{a}, \tag{5.24}$$

because $\sin(\pi/2) = 1$ for each of these components. This means that the doubler gets a contribution which acts like a mass term, since it is proportional to $\mathbb{1}$. In the continuum limit, when $a \to 0$, the extra mass contribution diverges and the doubler decouples from the theory.

We need to know what is the expression for the extra Wilson term in configuration space. In order to do this, we perform the inverse Fourier transform

$$\begin{aligned}
&\frac{1}{a\Lambda}\sum_{p\in\tilde{\Lambda}}\sum_{\mu} 1-\cos(ap_\mu)e^{iap(n-m)} = \\
&\frac{1}{a\Lambda}\sum_{p\in\tilde{\Lambda}}\sum_{\mu}\left[1-\frac{e^{iap\cdot\hat{\mu}}+e^{-iap\cdot\hat{\mu}}}{2}e^{iap(n-m)}\right] = \\
&\frac{1}{a\Lambda}\sum_{p\in\tilde{\Lambda}}\sum_{\mu}\left[e^{iap(n-m)}-\frac{e^{iap\cdot(n-m+\hat{\mu})}+e^{iap\cdot(n-m-\hat{\mu})}}{2}\right] = \\
&\sum_{\mu}\frac{2\delta(n-m)-\delta(n-m+\hat{\mu})-\delta(n-m-\hat{\mu})}{2a} = \\
&-a\sum_{\mu}\frac{\delta_{n+\hat{\mu},m}-2\delta_{n,m}+\delta_{n-\hat{\mu},m}}{2a^2}
\end{aligned}$$

and comparing to Eq. 5.19, we see that this is proportional to the Laplacian discretization, i. e. $\delta\mathcal{M}_{nm,\text{Wilson}} = -(a/2)\nabla^2_{nm}$. The Wilson Dirac operator for a free massless fermion is then given by

$$\begin{aligned}
\mathcal{M}_{nm,\text{Wilson, free, massless}} =& \sum_{\mu}\gamma_\mu\left(\frac{\delta_{n+\hat{\mu},m}-\delta_{n-\hat{\mu},m}}{2a}\right)-\mathbb{1}\frac{\delta_{n+\hat{\mu},m}-2\delta_{n,m}+\delta_{n-\hat{\mu},m}}{2a} \\
=&\frac{4}{a}\mathbb{1}\delta_{n,m}-\frac{1}{2a}\sum_{\mu}\left[(\mathbb{1}-\gamma_\mu)\delta_{n+\hat{\mu},m}+(\mathbb{1}+\gamma_\mu)\delta_{n-\hat{\mu},m}\right].
\end{aligned} \tag{5.25}$$

The addition of a mass term presents no difficulty. Since it is diagonal in both Dirac and configuration space, we can simply include it in the first term to get

$$\mathcal{M}_{nm,\text{Wilson, free}} = \left(m+\frac{4}{a}\right)\mathbb{1}\delta_{n,m}-\frac{1}{2a}\sum_{\mu}\left[(\mathbb{1}-\gamma_\mu)\delta_{n+\hat{\mu},m}+(\mathbb{1}+\gamma_\mu)\delta_{n-\hat{\mu},m}\right]. \tag{5.26}$$

Interactions can also be included, and here, again, as in the pure-gauge-theory construction of Chap. 3, the guiding principle is gauge-invariance. The terms with $\delta_{n+\hat{\mu},m}$ in $\overline{\psi}(n)\mathcal{M}\psi(m)$ will give rise to $\overline{\psi}(n)\psi(n+\hat{\mu})$, which is not invariant with respect to gauge transformations

$$\psi(n) \to \psi(n)' = g(n)\psi(n), \tag{5.27}$$

$$\overline{\psi}(n) \to \overline{\psi}'(n) = \overline{\psi}(n)g^\dagger(n). \tag{5.28}$$

In fact, a term with the product of ψ and $\overline{\psi}$ in two neighboring positions transforms as

$$\overline{\psi}(n)\psi(n+\hat{\mu}) \to \overline{\psi}(n)g^{\dagger}(n)g(n+\hat{\mu})\psi(n+\hat{\mu}). \tag{5.29}$$

What needs to be included between the fermionic fields to remove the unwanted gauge variance is something that transforms as

$$\text{something}(n,\mu) \to g(n)\,\text{something}(n,\mu)\,g^{\dagger}(n+\hat{\mu}). \tag{5.30}$$

The simplest choice is to make $something(n,\mu) = U_{\mu}(n)$, which is the link variable. Likewise, the terms with $\delta_{n-\hat{\mu}}$ will need $U_{-\mu}(n)$, defined in Eq. 3.3, to make it gauge-invariant. The interacting massive Wilson fermion is thus described by the operator

$$\begin{aligned}
\mathcal{M}_{nm,\text{Wilson}} = &\left(m+\frac{4}{a}\right)\mathbb{1}\,\mathbb{1}_c\delta_{n,m} \\
&- \frac{1}{2a}\sum_{\mu}\left[(\mathbb{1}-\gamma_{\mu})U_{\mu}(n)\delta_{n+\hat{\mu},m} + (\mathbb{1}+\gamma_{\mu})U_{-\mu}(n)\delta_{n-\hat{\mu},m}\right] && (5.31)\\
= &\left(m+\frac{4}{a}\right)\mathbb{1}\,\mathbb{1}_c\delta_{n,m} - \frac{1}{2a}\sum_{\pm\mu}(\mathbb{1}-\gamma_{\mu})U_{\mu}(n)\delta_{n+\hat{\mu},m} && (5.32)\\
= &\frac{1}{a}\left[(am+4)\,\mathbb{1}\,\mathbb{1}_c\delta_{n,m} - \frac{1}{2}\sum_{\pm\mu}(\mathbb{1}-\gamma_{\mu})U_{\mu}(n)\delta_{n+\hat{\mu},m}\right], && (5.33)
\end{aligned}$$

where the first term gets a color identity matrix $\mathbb{1}_c$, since it is also trivial in color space. Here we introduced the notation $\gamma_{-\mu} = -\gamma_{\mu}$ in order to get a more condensed expression. This lattice expression is equivalent to the minimal coupling of continuum gauge theories in the limit that the lattice spacing goes to 0. To see this, we can expand $U_{\mu}(n)$ for small a as in Eq. 4.26 and perform the Taylor expansion in the $\psi(n \pm \hat{\mu})$ fields for $\overline{\psi}\mathcal{M}_{\text{Wilson}}\psi$.

We get

$$\left(m+\frac{4}{a}\right)\mathbb{1}\,\overline{\psi}(n)\psi(n)-\frac{\overline{\psi}(n)}{2a}\sum_{\mu}\Big\{[\mathbb{1}-\gamma_\mu][\mathbb{1}_c+iaA_\mu(n)]\psi(n+\hat{\mu}) + [\mathbb{1}+\gamma_\mu][\mathbb{1}_c-iaA_\mu(n)]\psi(n-\hat{\mu})\Big\}$$

$$\approx\left(m+\frac{4}{a}\right)\mathbb{1}\,\overline{\psi}(n)\psi(n)-\frac{\overline{\psi}(n)}{2a}\sum_{\mu}\Big\{[\mathbb{1}-\gamma_\mu][\mathbb{1}_c+iaA_\mu(n)][\psi(n)+a\partial_\mu\psi(n)] + [\mathbb{1}+\gamma_\mu][\mathbb{1}_c-iaA_\mu(n)][\psi(n)-a\partial_\mu\psi(n)]\Big\}$$

$$\approx\left(m+\frac{4}{a}\right)\mathbb{1}\,\overline{\psi}(n)\psi(n)-\frac{\overline{\psi}(n)}{2a}\sum_{\mu}\Big\{\mathbb{1}\Big[\psi(n)+a\partial_\mu\psi(n)+iaA_\mu(n)\psi(n) + \psi(n)-a\partial_\mu\psi(n)-iaA_\mu(n)\psi(n)\Big] - \gamma_\mu\Big[\psi(n)+a\partial_\mu\psi(n)+iaA_\mu(n)\psi(n) - \psi(n)+a\partial_\mu\psi(n)+iaA_\mu(n)\psi(n))\Big]\Big\}$$

$$\approx\left(m+\frac{4}{a}\right)\mathbb{1}\,\overline{\psi}(n)\psi(n)-\frac{\overline{\psi}(n)}{a}\sum_{\mu}\Big\{\mathbb{1}\Big[\psi(n)\Big]-\gamma_\mu\Big[a\partial_\mu\psi(n)+iaA_\mu(n)\psi(n)\Big]\Big\}.$$

The first term in the summand cancels the $(4/a)\mathbb{1}$ after the sum over the 4 directions is performed and the last line becomes

$$\begin{aligned}&= m\,\overline{\psi}(n)\psi(n)\mathbb{1}+\overline{\psi}(n)\sum_{\mu}\gamma_\mu[\partial_\mu+iA_\mu(n)]\psi(n)\\&=\overline{\psi}(n)[m+\not{D}]\psi(n),\end{aligned}\tag{5.34}$$

where we identified the covariant derivative $D_\mu=\partial_\mu+iA_\mu(n)$. In the derivation above it is important to have in mind that we are keeping only the lowest order in a in the expressions, and each line is approximately equal to the others to this order. The expression in Eq. 5.33, shows only the space-time indices. The equivalent expression with all indices explicit is

$$\mathcal{M}_{nm\,\alpha\beta\,ab,\text{Wilson}}=\frac{1}{a}\left[(am+4)\,\delta_{\alpha,\beta}\delta_{a,b}\delta_{n,m}-\frac{1}{2}\sum_{\pm\mu}(\mathbb{1}-\gamma_\mu)_{\alpha,\beta}[U_\mu(n)]_{a,b}\,\delta_{n+\hat{\mu},m}\right].\tag{5.35}$$

5.2 γ_5-Hermiticity

There is a rather abstract symmetry that the Dirac Wilson operator obeys, called γ_5-Hermiticity. A lattice fermion operator is said to obey this symmetry if

$$(\gamma_5\mathcal{M})^\dagger=\gamma_5\mathcal{M},\quad\text{or equivalently if}\quad\mathcal{M}^\dagger=\gamma_5\mathcal{M}\gamma_5.\tag{5.36}$$

In fact, not only the Wilson operator obeys it, as will be shown in a moment, but most of the popular discretizations of lattice fermions also do (with the notable exception of twisted-mass fermions).

To prove that the Wilson operator, given in 5.33, is γ_5-Hermitian, we first note that the first term is diagonal in Dirac-space, so this part is trivial. For the term that contains the link variables, remembering that $\{\gamma_5, \gamma_\mu\} = 0$, we have that

$$\begin{aligned}
&\sum_{\pm\mu} \left[\gamma_5(\mathbb{1} - \gamma_\mu)\gamma_5\right]_{\alpha\beta} \left[U_\mu(n)\right]_{ab} \delta_{n+\hat{\mu},m} = \\
&\sum_{\pm\mu} \left(\mathbb{1} + \gamma_\mu\right)_{\alpha\beta} \left[U_\mu(n)\right]_{ab} \delta_{n+\hat{\mu},m} = \\
&\sum_{\mp\mu} \left[\mathbb{1} + (\gamma_{-\mu})\right]_{\alpha\beta} \left[U_{-\mu}(n)\right]_{ab} \delta_{n-\hat{\mu},m} = \\
&\sum_{\pm\mu} \left(\mathbb{1} - \gamma_\mu\right)_{\alpha\beta} \left[U_\mu^\dagger(n-\hat{\mu})\right]_{ab} \delta_{n-\hat{\mu},m} = \\
&\sum_{\pm\mu} \left(\mathbb{1} - \gamma_\mu\right)_{\alpha\beta} \left[U_\mu^\dagger(m)\right]_{ab} \delta_{m+\hat{\mu},n},
\end{aligned}$$

and since $\gamma_\mu^\dagger = \gamma_\mu$, in Euclidean space, this indeed corresponds to taking the Hermitian conjugate of the $\mathcal{M}$ operator: by comparing the last line with the first, we see that the positions m and n have been exchanged and U_μ has been substituted by $U_\mu^\dagger$.

One important consequence of this symmetry is that it implies that the eigenvalues are either real or come in complex-conjugate pairs. To show this, we can calculate the characteristic polynomial of such an operator

$$\begin{aligned}
P(\lambda) = \det[\mathcal{M} - \lambda\mathbb{1}] = \det[\gamma_5^2(\mathcal{M} - \lambda\mathbb{1})] = \det[\gamma_5(\mathcal{M} - \lambda\mathbb{1})\gamma_5] = \det[\gamma_5\mathcal{M}\gamma_5 - \lambda\mathbb{1}] = \\
= \det[\mathcal{M}^\dagger - \lambda\mathbb{1}] = (\det[\mathcal{M} - \lambda^*\mathbb{1}])^* = P^*(\lambda^*), \quad (5.37)
\end{aligned}$$

where we used that $\gamma_5^2 = \mathbb{1}$, the fact that the determinant of a product of matrices is the product of the determinants, and that $\det[A^\dagger] = \det[A]^*$, for $A = \mathcal{M} - \lambda\mathbb{1}$. Since the eigenvalues of the operator $\mathcal{M}$ are the roots of the characteristic polynomial, we see that, if λ is a root, so is λ^*. This means that, either both are actually the same and it is real, or at least that they come in complex-conjugate pairs, and the spectrum of the Dirac operator is mirror-symmetric about the real axis. This also implies that the determinant, as the product of the eigenvalues, is real.

The spectrum of the Wilson operator in a free theory can in fact be calculated explicitly, by diagonalizing the operator in momentum space in Eq. 5.22. The result is

$$\lambda = a^{-1}\left[\sum_\mu 2\sin^2\left(\frac{ap_\mu}{2}\right) \pm i\sqrt{\sum_\mu \sin^2(ap_\mu)}\right]. \quad (5.38)$$

5.3 Allowed momenta for the fermion on the lattice

As was the case with the gluonic fields, we must decide what to do with the fermions at the borders of the lattice. In other words, boundary conditions must be implemented.

A common choice for fermions is as following. In the spatial μ directions, we have periodic boundary conditions and, for $\mu = t$, anti-periodic conditions

$$\psi(n)|_{n_t=-1} = -\psi(n)|_{n_t=N_t-1}, \tag{5.39}$$

$$\psi(n)|_{n_t=N_t} = -\psi(n)|_{n_t=0}. \tag{5.40}$$

In fact, fermions are required to obey anti-periodic boundary conditions in the temporal direction because of the formal reconstruction of the Hilbert space by Osterwalder and Schrader (47). It appears automatically when representing the fermionic partition function in terms of a transfer operator, or calculating traces over fermionic bilinear operators using a basis of Grassmannian coherent states. In the continuum this is the usual minus sign appearing when one calculates closed fermion loops (50, 64).

For the quarks, the anti-periodic boundary condition is implemented by multiplying the *hopping* term (the second term in Eq. 5.33), which are the terms connecting different sites, by -1 when $\mu = +4$ and $n_4 = N_4$, or $\mu = -4$ and $n_4 = 0$.

The boundary conditions determine the set $\tilde{\Lambda}$ of allowed momenta. Functions on the lattice must obey

$$f(n + \hat{\mu}N_\mu) = e^{i2\pi\theta_\mu} f(n), \tag{5.41}$$

where the temporal direction corresponds to $\theta_t = 1/2$ and the spatial ones to $\theta_i = 0$. In order to have plane waves that obey the aforementioned boundary conditions, the momenta on the lattice must be

$$ap_i = \frac{2\pi}{N_i}\left(n_i - \frac{N_i}{2}\right), \quad ap_4 = \frac{2\pi}{N_4}\left(n_4 - \frac{1}{2} - \frac{N_4}{2}\right), \tag{5.42}$$

in which N_μ is the lattice extent in the direction μ and n_μ can take values between 1 and N_μ for the respective direction.

5.4 Chiral symmetry on the lattice

On the lattice, the situation with regard to chiral symmetry is more subtle than in the continuum. In fact, in lattice field theory, it is impossible to implement the continuum condition 2.19 and remove all the doublers, as stated by the fundamental Nielsen-Ninomyia no-go theorem (89). The theorem assumes very few conditions on the Hamiltonian of the system, which one would expect to hold in reasonable theories. These are

- translation invariance;
- locality, meaning that the Hamiltonian vanishes sufficiently fast for large distances, so that its Fourier transform has all derivatives;
- Hermiticity.

It is further assumed that the system has locally defined charges that are quantized (quantum numbers) and are bilinear in the fermion fields. In any lattice theory obeying the above conditions, the theorem says that the number of doublers must be even, and furthermore that they can be divided into two groups based on their chirality, such that the net chirality is 0 when all doublers are counted. A sketch of a proof of the theorem involving topology is given in (90). It is possible to obtain models with a minimal number of 2 doublers (50, 91). All known models of this kind, however, break the isotropy of the lattice by introducing different terms associated to the time and spatial directions for the Dirac operator, which complicates the tuning of the parameters in the action, the renormalization and consequently the analysis of the results in simulations (50, 90).

To clarify what is needed to overcome the consequences of this theorem in an elegant way, we follow the presentation of (46). Instead of Eq. 2.19, Ginsparg and Wilson proposed a replacement (92)

$$\{\mathcal{M}, \gamma_5\} = a\mathcal{M}\gamma_5\mathcal{M}. \tag{5.43}$$

The Ginsparg-Wilson equation is a particular case of a general theory for how to map continuum symmetries on the lattice. Suppose we have continuum fermionic fields ϕ and $\overline{\phi}$, which, for some transformation implemented by C and $\overline{C}$, behave as

$$\phi \to \phi' = e^{i\varepsilon C}\phi, \quad \overline{\phi} \to \overline{\phi}' = \overline{\phi}e^{i\varepsilon\overline{C}}, \tag{5.44}$$

and we want to know what is the corresponding transformation for the lattice version of the fields ψ and $\overline{\psi}$

$$\psi' = e^{i\varepsilon L}\psi, \quad \overline{\psi}' = \overline{\psi}e^{i\varepsilon\overline{L}}, \tag{5.45}$$

which are, moreover, suitably discretized with a lattice action

$$S_{F,\text{lattice}}[\overline{\psi}, \psi] = \overline{\psi}\,\mathcal{M}\,\psi. \tag{5.46}$$

One way to obtain the relationship between both sets of transformations is by blocking the continuum theory, in the style of real-space renormalization-group transformations (for more details, see Chapt. 9 of (46)). It can be shown that this procedure leads to the following relations

$$L = C\left(\mathbb{1} - \frac{a\mathcal{M}}{2}\right), \quad \overline{L} = \left(\mathbb{1} - \frac{a\mathcal{M}}{2}\right)\overline{C}. \tag{5.47}$$

For chiral symmetry in particular, where we have $C = \overline{C} = \gamma_5$, this means

$$L = \gamma_5\left(\mathbb{1} - \frac{a\mathcal{M}}{2}\right), \quad \overline{L} = \left(\mathbb{1} - \frac{a\mathcal{M}}{2}\right)\gamma_5. \tag{5.48}$$

The fact that the generic lattice transformation Eq. 5.45, should be a symmetry can be written as

$$\overline{\psi}'\mathcal{M}\psi' = \overline{\psi}e^{i\varepsilon\overline{L}}\mathcal{M}e^{i\varepsilon L} \stackrel{!}{=} \overline{\psi}\mathcal{M}\psi, \tag{5.49}$$

which for infinitesimal ε implies that

$$\overline{\psi}(\mathbb{1}+i\varepsilon\overline{L})\mathcal{M}(\mathbb{1}+i\varepsilon L)\psi = \overline{\psi}(\mathbb{1}+i\varepsilon\overline{L}\mathcal{M}+i\varepsilon\mathcal{M}L)\psi \stackrel{!}{=} \overline{\psi}\mathcal{M}\psi \to \overline{L}\mathcal{M}+\mathcal{M}L = 0. \quad (5.50)$$

For chiral symmetry, with L and $\overline{L}$ given in Eq. 5.48, this turns into

$$\left(\mathbb{1}-\frac{a\mathcal{M}}{2}\right)\gamma_5\mathcal{M}+\mathcal{M}\gamma_5\left(\mathbb{1}-\frac{a\mathcal{M}}{2}\right)=0, \quad (5.51)$$

i. e.

$$\gamma_5\mathcal{M}+\mathcal{M}\gamma_5 = a\mathcal{M}\gamma_5\mathcal{M} \to \{\gamma_5,\mathcal{M}\} = a\mathcal{M}\gamma_5\mathcal{M}, \quad (5.52)$$

which is the Ginsparg-Wilson equation.

Eq. 5.43 implements chiral symmetry for a discrete spacetime. In the continuum limit, when $a \to 0$, the right-hand side goes to 0 and one recovers Eq. 2.19. Another way of seeing the modification of the chiral condition with respect to the continuum can be derived by noting that, performing the product with the quark propagator, that is $\mathcal{M}^{-1} = S$, on both sides of Eq. 5.43, one has

$$\sum_{n,m}\mathcal{M}^{-1}_{rn}\mathcal{M}_{nm}\gamma_5\mathcal{M}^{-1}_{ms}+\mathcal{M}^{-1}_{rn}\gamma_5\mathcal{M}_{nm}\mathcal{M}^{-1}_{ms} = a\sum_{n,m,l}\mathcal{M}^{-1}_{rn}\mathcal{M}_{nl}\gamma_5\mathcal{M}_{lm}\mathcal{M}^{-1}_{ms} \quad (5.53)$$

$$\sum_{m}\delta_{rm}\gamma_5\mathcal{M}^{-1}_{ms}+\sum_{n}\mathcal{M}^{-1}_{rn}\gamma_5\delta_{ns} = a\sum_{l}\delta_{rl}\gamma_5\delta_{ls} \quad (5.54)$$

$$\gamma_5\mathcal{M}^{-1}_{rs}+\mathcal{M}^{-1}_{rs}\gamma_5 = a\gamma_5\delta_{rs} \quad (5.55)$$

or, renaming the indices,

$$\gamma_5 S_{nm}+S_{nm}\gamma_5 = a\gamma_5\delta(n-m), \quad (5.56)$$

which means that the anti-commutator of the fermion propagator S with γ_5 is modified by a contact term. The only fact used was the definition of the inverse $\mathcal{M}_{nl}\mathcal{M}^{-1}_{lm} = \mathcal{M}^{-1}_{nl}\mathcal{M}_{lm} = \delta_{nm} = \delta(n-m)$ and properties of the Kronecker delta.

As already stated, one needs to redefine the chiral transformations on the lattice to match the chiral symmetry condition. Instead of Eq. 2.17, one uses the lattice transformations in Eq. 5.47

$$\psi \to \psi' = \exp\left[i\alpha\gamma_5\left(\mathbb{1}-\frac{a}{2}\mathcal{M}\right)\right]\psi, \quad \psi \to \overline{\psi}' = \overline{\psi}\exp\left[i\alpha\left(\mathbb{1}-\frac{a}{2}\mathcal{M}\right)\gamma_5\right], \quad (5.57)$$

so that

$$\begin{aligned} L\left(\psi',\overline{\psi}'\right) &= \overline{\psi}'\mathcal{M}\psi' \\ &= \overline{\psi}\exp\left[i\alpha\left(\mathbb{1}-\frac{a}{2}\mathcal{M}\right)\gamma_5\right]\mathcal{M}\exp\left[i\alpha\gamma_5\left(\mathbb{1}-\frac{a}{2}\mathcal{M}\right)\right]\psi \\ &= \overline{\psi}\exp\left[i\alpha\left(\mathbb{1}-\frac{a}{2}\mathcal{M}\right)\gamma_5\right]\exp\left[-i\alpha\gamma_5\left(\mathbb{1}-\frac{a}{2}\mathcal{M}\right)\right]\mathcal{M}\psi \\ &= \overline{\psi}\mathcal{M}\psi = L\left(\psi,\overline{\psi}\right), \end{aligned}$$

where we used the alternative version of the Wilson-Ginsparg equation, given in Eq. 5.51.

Another common assumption regarding lattice fermionic operators $\mathcal{M}$ is that they obey γ_5-Hermiticity

$$\gamma_5 \mathcal{M} \gamma_5 = \mathcal{M}^\dagger, \tag{5.58}$$

as we already explored in Sect. 5.2.

The Ginsparg-Wilson equation 5.43 has a number of consequences. The first of them is that if $\mathcal{M}$ obeys it and is at the same time γ_5-Hermitian, then it commutes with its Hermitian conjugate, in other words, it is a normal operator. To see this, we can multiply the equation on either side by γ_5. In one case one gets

$$\gamma_5 \mathcal{M} \gamma_5 + \gamma_5 \gamma_5 \mathcal{M} = a \gamma_5 \mathcal{M} \gamma_5 \mathcal{M} \tag{5.59}$$

$$\mathcal{M}^\dagger + \mathcal{M} = a \mathcal{M}^\dagger \mathcal{M}, \tag{5.60}$$

and in the other

$$\gamma_5 \gamma_5 \mathcal{M} + \gamma_5 \mathcal{M} \gamma_5 = a \mathcal{M} \gamma_5 \mathcal{M} \gamma_5 \tag{5.61}$$

$$\mathcal{M} + \mathcal{M}^\dagger = a \mathcal{M} \mathcal{M}^\dagger. \tag{5.62}$$

But, since the left-hand side is equal in both cases, this means that $\mathcal{M}\mathcal{M}^\dagger = \mathcal{M}^\dagger \mathcal{M}$, which is the normal operator condition $[\mathcal{M}, \mathcal{M}^\dagger] = 0$. A normal operator has a complete set of orthonormal eigenvectors, and can thus be represented via a spectral decomposition as

$$\mathcal{M} = \sum_\lambda \lambda \, v_\lambda {v_\lambda}^\dagger, \tag{5.63}$$

where the sum runs over the eigenvalues λ. By multiplying Eq. 5.60 by a particular ${v_\lambda}^\dagger$ from the left and by ${v_\lambda}^\dagger$ from the right, we obtain, after using the spectral decomposition

$$\lambda^* + \lambda = a \lambda^* \lambda. \tag{5.64}$$

Taking $\lambda = x + iy$, we get

$$\begin{aligned}
(x - iy) + (x + iy) =& a(x^2 + y^2) \\
\left(x^2 - \frac{2x}{a}\right) + y^2 =& 0 \\
\left(x - \frac{1}{a}\right)^2 - \frac{1}{a^2} + y^2 =& 0 \\
\left(x - \frac{1}{a}\right)^2 + y^2 =& \frac{1}{a^2}.
\end{aligned} \tag{5.65}$$

This shows that the eigenvalues of a fermion operator $\mathcal{M}$ that is γ_5-Hermitian and obeys the Wilson-Ginsparg equation are located on a circumference in the complex plane centered at $x_0 = 1/a$ with radius $1/a$.

5.4.1 Overlap fermions

One solution of the Ginsparg-Wilson equation is given by the overlap operator

$$\mathcal{M}_{\text{overlap}} = \frac{1}{a}\left(\mathbb{1} + \gamma_5 \,\text{sign}[H]\right), \quad H = \gamma_5 A, \tag{5.66}$$

where A is a kernel, that is required to be γ_5-Hermitian, and can be chosen, for example, as the Wilson-Dirac operator. The γ_5-Hermiticity of A implies that H is Hermitian, because

$$H^\dagger = (\gamma_5 A)^\dagger = A^\dagger \gamma_5^\dagger = A^\dagger \gamma_5 = \gamma_5 A \gamma_5 \gamma_5 = \gamma_5 A = H, \tag{5.67}$$

where we used $\gamma_5^\dagger = \gamma_5$, and $\gamma_5^2 = \mathbb{1}$. We can now show that the overlap operator obeys Eq. 5.43, because

$$\begin{aligned} a\mathcal{M}_{\text{overlap}}\mathcal{M}^\dagger_{\text{overlap}} =& \frac{1}{a}\left(\mathbb{1} + \gamma_5 \,\text{sign}[H]\right)\left(\mathbb{1} + \text{sign}[H]\gamma_5\right) \\ =& \frac{1}{a}\left(\mathbb{1} + \gamma_5 \,\text{sign}[H] + \text{sign}[H]\gamma_5 + \mathbb{1}\right) = \mathcal{M}_{\text{overlap}} + \mathcal{M}^\dagger_{\text{overlap}} \end{aligned} \tag{5.68}$$

where we used $\text{sign}[H]^2 = \mathbb{1}$ and $\text{sign}[H]^\dagger = \text{sign}[H]$, which comes from the Hermiticity of H shown above. The sign matrix is the tricky part, even though it is well defined through the spectral representation of H

$$\text{sign}[H] = \sum_\lambda \text{sign}(\lambda) v_\lambda {v_\lambda}^\dagger, \tag{5.69}$$

where $\text{sign}(x)$ is now the usual sign function. The problem is that the explicit calculation of the spectral representation through exact diagonalization is numerically very costly, which renders this discretization impractical for full dynamical fermion calculations. With the help of a few tricks, though, one can calculate the overlap propagator for either quenched configurations or configurations generated with lattice fermions of other kinds, such as Wilson or staggered fermions (46).

5.4.2 Chirally improved fermions

Chirally improved fermions follow a different philosophy to try to obtain an approximate solution to the Ginsparg-Wilson equation (93). One considers the most general Dirac operator to have the form

$$\mathcal{M}_{\text{CI}\,xy} = \sum_{i=1}^{16} c^{(i)}_{xy}(U)\Gamma_i + m_0 \mathbb{1}, \tag{5.70}$$

with the sum running over all elements of the Clifford algebra. The constants are constructed from paths of link variables connecting the sites x and y. This Ansatz can be inserted into the Ginsparg-Wilson condition, Eq. 5.43, and one imposes also that the other symmetries expected from the lattice Dirac operator, such as γ_5-Hermiticity, are obeyed. From this results a system of coupled quadratic equations for the constants $c^{(i)}_{xy}(U)$, which can be truncated and solved numerically. The operator obtained in this way can then be inverted for the calculation of the fermion propagator.

5.4.3 Staggered fermions

Staggered fermions are a different discretization that preserves (a remnant of) chiral symmetry in a conceptually somewhat more convoluted way. One takes the naïve fermion action Eq. 5.9 and performs a staggered transformation in the fields, which mix Dirac and position indices,

$$\psi(n) = \gamma_1^{n_1}\gamma_2^{n_2}\gamma_3^{n_3}\gamma_4^{n_4}\psi'(n). \tag{5.71}$$

One then ends up with four copies of a different fermion action, which after adding interactions in the standard way (by inserting link variables to force gauge-invariance) turns into

$$S_{\text{stag.}}[\chi,\overline{\chi}] = a^4 \sum_{n,m\in\Lambda} \overline{\chi}(m)\left[\sum_\mu \eta_\mu(m)\frac{U_\mu(m)\delta_{n,m+\hat{\mu}} - U_\mu^\dagger(n)\delta_{n,m-\hat{\mu}}}{2a}\right]\chi(n). \tag{5.72}$$

The staggered sign functions $\eta_1(n) = 1$, $\eta_2(n) = (-1)^{n_1}$, $\eta_3(n) = (-1)^{n_1+n_2}$, and $\eta_4(n) = (-1)^{n_1+n_2+n_3}$ play the roles of the γ matrices in the regular fermion actions. The χ fields have no Dirac structure anymore, as it has been removed by the staggered transformation. This reduces the computational costs of inverting the fermionic operator, which is one of the characteristics that make staggered fermions attractive for simulations. Another desirable property is that the staggered operator is anti-Hermitian, as the Dirac operator in the continuum. The chiral matrix γ_5 is substituted by $\eta_5(n) = (-1)^{n_1+n_2+n_3+n_4}$, and the staggered chiral transformation is given by

$$\chi(n) \to e^{i\alpha\eta_5(n)}\chi(n), \quad \overline{\chi}(n) \to \overline{\chi}(n)e^{i\alpha\eta_5(n)}, \tag{5.73}$$

which is a symmetry of the staggered massless fermion action, Eq. 5.72, because, as the staggered action couples nearest neighbors only, the position dependent η_5 will differ between them by a minus sign, which will then be canceled among the exponentials. A mass term can be added as usual by $\delta_m S_{\text{stag}}[\chi,\overline{\chi}] = a^4\sum_{n\in\Lambda} m\overline{\chi}(n)\chi(n)$, and this will break the staggered chiral symmetry explicitly, as it should, since the sign cancellation will not happen for fields on the same site.

Another way of looking at staggered fermions is through the spectrum doubling symmetry, a symmetry of the naïve fermion discretization that exchanges the corners of the Brillouin zone (50). The fermion species associated to the doublers bring about a representation of the spectrum doubling symmetry group that is reducible. Staggered fermions are seen in this framework as the results of a particular way of reducing the representation (50, 94, 95). The Wilson discretization of fermions break the symmetry explicitly by the introduction of the Wilson term.

The doubler problem is, however, not completely solved by the staggered framework. One has four independent copies of the χ fields, each of which carry 4 of the original 16 doublers. A detailed study shows that these doubler degrees of freedom turn into tastes of

staggered fermions, which are scattered over hypercubes of side equals to two units of the lattice around the original n site.

5.5 Chiral symmetry with Wilson fermions

If one wishes to study QCD, chiral symmetry has to be taken into account. Massless Wilson fermions, however, obey neither the continuum chiral symmetry condition 2.19 nor the lattice one 5.43 (46). One of the consequences of this is that the fermion mass gets an additive renormalization (50, 90). The less elegant and more pragmatic way of enforcing chiral symmetry when using Wilson fermions is the following: one writes the Wilson operator as

$$\mathcal{M}_{nm\,\alpha\beta\,ab,\text{Wilson}} = \frac{(am_0+4)}{a}\left[\delta_{\alpha,\beta}\delta_{a,b}\delta_{n,m} - \kappa\sum_{\pm\mu}(\mathbb{1}-\gamma_\mu)_{\alpha,\beta}\left[U_\mu(n)\right]_{a,b}\delta_{n+\hat{\mu},m}\right], \quad (5.74)$$

where $\kappa = \frac{1}{2(am_0+4)}$, or equivalently

$$am_0 = \frac{1}{2\kappa} - \frac{1}{2\left(\frac{1}{8}\right)}. \quad (5.75)$$

One can then numerically calculate the pion mass for ensembles with different values of κ and extrapolate to the limit where the pion mass vanishes. This value of κ for which the pion mass vanishes is named κ_c, where the c stands for critical. In the absence of interactions, that is if $U_\mu(n) = \mathbb{1}$ for all n, the pion mass will vanish when the quark mass vanishes, which means that $\kappa_c = 1/8$ for the free theory. When the interactions are turned on, one performs the procedure described above using the pion masses. In the interacting theory, one defines the subtracted quark mass as

$$am = am_0 - am_c = \frac{1}{2\kappa} - \frac{1}{2\kappa_c}. \quad (5.76)$$

The value of the critical mass am_c can be seen as a fine-tuning correction, needed to ensure that the pion mass vanishes when the quark mass vanishes, as predicted by chiral symmetry. The values for κ_c have been computed and can be found in tables, but they depend, of course, on the action used and will vary with the value of the coupling β and other parameters.

Determinations of κ_c based on lattice perturbation theory have been tried. One calculates the perturbative estimate for κ_c that corresponds to zero renormalized quark mass, and consequently to zero pion mass. The results of this procedure are not reliable, though, as it is suspected that non-perturbative terms behaving like e^{1/g^2}, which do not have a power expansion, may contribute (50). For the quenched case, a non-perturbative determination of κ_c can be found in (96).

5.6 Improvements

In order to reduce lattice artifacts one can systematically include more terms to the action with suitable coefficients, in such a way as to eliminate contributions at some order in the lattice spacing a. This is the Symanzik improvement program. As mentioned in Chap. 3, this is particularly important for Wilson fermions. We start with an effective action

$$S_{\text{eff}} = \int d^4x \left(L^{(0)}(x) + aL^{(1)}(x) \right), \tag{5.77}$$

where $L^{(0)}(x)$ is the continuum QCD action, which contains all terms up to dimension 5 that respect the symmetries imposed by the theory. We then introduce $L^{(1)}(x)$, which contain terms of mass dimension 5 (for dimensional reasons, as we have introduced the lattice spacing in the action). These terms will necessarily contain high derivatives or powers of the quark mass. It has been shown (46) that there are 5 such operators for the fermionic Wilson action

$$L_1^{(1)} = \overline{\psi}(x)\sigma_{\mu\nu}F_{\mu\nu}\psi(x) \tag{5.78}$$

$$L_2^{(1)} = \overline{\psi}(x)\vec{D}_\mu(x)\vec{D}_\mu\psi(x) + \overline{\psi}(x)\overleftarrow{D}_\mu(x)\overleftarrow{D}_\mu\psi(x) \tag{5.79}$$

$$L_3^{(1)} = m\,\mathrm{tr}\left[F_{\mu\nu}(x)F_{\mu\nu}(x)\right] \tag{5.80}$$

$$L_4^{(1)} = m\left(\overline{\psi}(x)\gamma_\mu\vec{D}_\mu\psi(x) - \overline{\psi}(x)\gamma_\mu\overleftarrow{D}_\mu\psi(x)\right) \tag{5.81}$$

$$L_5^{(1)} = m^2\overline{\psi}(x)\psi(x), \tag{5.82}$$

where $\sigma_{\mu\nu} = [\gamma_\mu, \gamma_\nu]/2i$ and $\vec{D}_\mu(x)$ and $\overleftarrow{D}_\mu(x)$ are the covariant derivatives acting to the right and to the left respectively .

The terms $L_5^{(1)}$ and $L_5^{(3)}$ can be absorbed into a redefinition of the mass and the coupling. The improvements brought by terms proportional to $L_2^{(1)}$ and $L_4^{(1)}$ can be traded for an improvement on the fermionic fields when calculating correlators

$$\psi' = (1 + b_q am)(1 - c_q a\not{D})\psi + c_n\not{\partial}\psi, \tag{5.83}$$

where b_q, c_q and c_n are constants to be determined. These will be taken into account when we calculate the quark propagator.

Thus, we are left with the $L_1^{(1)}$ term only for the actual fermionic action improvement. The Symanzik program then postulates that we must find a suitable discretization of the continuum term that must be added to the action. For $L_1^{(1)}$, the most commonly used discretization is the so called Sheikholeslami-Wohlert term. The lattice improved action for Wilson fermions is then given by

$$S_{\text{SW-improved}} = S_{\text{Wilson}} + a^4 \sum_{n\in\Lambda} c_{SW}\,\overline{\psi}(n)\left[\frac{a\sum_{\mu<\nu}\sigma_{\mu\nu}\hat{F}_{\mu\nu}(n)}{2}\right]\psi(n). \tag{5.84}$$

The discretized field-strength tensor $\hat{F}_{\mu\nu}(n)$ is obtained using the clover discretization

$$\hat{F}_{\mu\nu}(n) = \frac{-i}{8a^2}\left(Q_{\mu\nu}(n) - Q_{\nu\mu}(n)\right), \tag{5.85}$$

where

$$Q_{\mu\nu}(n) = U_{\mu,\nu}(n) + U_{\nu,-\mu}(n) + U_{-\mu,-\nu}(n) + U_{-\nu,\mu}(n), \tag{5.86}$$

in which $U_{\mu\nu}(n)$ is the product of four link variables making up a plaquette

$$U_{\mu,\nu}(n) = U_{\mu}(n)U_{\nu}(n+\hat{\mu})U_{-\mu}(n+\hat{\mu}+\hat{\nu})U_{-\nu}(n+\hat{\nu}). \tag{5.87}$$

The lattice fermions described by the action $S_{\text{SW-improved}}$ are also called clover fermions, due to the fact that the term involves four plaquettes in a configuration which resembles a cloverleaf. With this addition, the fermionic operator now reads

$$\mathcal{M}_{nm\,\alpha\beta\,ab,\text{Clover}}[U] = \frac{1}{a}\Bigg[(am_0+4)\,\delta_{\alpha\beta}\delta_{ab}\delta_{nm} - \frac{1}{2}\sum_{\pm\mu}(\mathbb{1}-\gamma_\mu)_{\alpha\beta}(U_\mu(n))_{ab}\delta_{n+\hat{\mu}m} + c_{SW}a^2\sum_{\mu<\nu}\frac{1}{2}\sigma_{\mu\nu,\alpha\beta}\hat{F}_{\mu\nu,\,ab}(n)\delta_{n,m}\Bigg]. \tag{5.88}$$

The SW-term is diagonal in configuration space, the color indices are carried by $\hat{F}_{\mu\nu}$, and the Dirac indices are carried by $\sigma_{\mu\nu}$. Another observation is that, for free fermions, the SW-term vanishes, since, in this case, the links are all equal to $\mathbb{1}$, which implies that $Q_{\mu\nu} = Q_{\nu\mu} \to \hat{F}_{\mu\nu} = 0$. As a consequence, the free propagator for clover fermions is the same as for Wilson fermions.

One needs to determine the constant c_{SW} in order to remove $\mathcal{O}(a)$ artifacts. It can be computed through a non-perturbative procedure, where one tries to reduce the lattice corrections to the PCAC relation by tuning the values of the coefficient (70, 96) for different β. The resulting values are well approximated by a ratio polynomials on $g = \sqrt{\frac{6}{\beta}}$,

$$c_{SW} = \frac{1 - 0.656g^2 - 0.152g^4 - 0.054g^6}{1 - 0.922g^2}, \quad 0 \le g \le 1. \tag{5.89}$$

Perturbatively determined and mean-field improved formulas for c_{SW} also exist, but the non-perturbative determination has been shown to be preferable.

5.7 Free Dirac-Wilson propagator

The plain quark propagator for the interacting theory is defined in terms of the inverse of the Dirac-Wilson operator with the addition of the clover term, by

$$S_{nm,\text{Clover, plain}} \equiv \langle S_{nm,\text{Clover, plain}}[U]\rangle_U, \quad S_{nm,\text{Clover, plain}}[U] = (\mathcal{M}_{\text{Clover}})^{-1}_{nm}[U], \tag{5.90}$$

where the angle brackets $\langle\,\rangle_U$, mean the evaluation over an ensemble of generated gauge link configurations. For each gauge configuration one must invert the Dirac-Wilson-Clover

operator and then obtain the expectation value over the ensemble, together with the accompanying statistical errors, from a statistical analysis (for example, using the Statistical Bootstrap method, (46)). We will not dwell here on the techniques and algorithms to invert the $\mathcal{M}$ operator, but rather defer this exposition to Sect. 6.3. Here we simply take it for granted that somehow it has been inverted.

We can write the Dirac-Wilson operator as in Eq. 5.88 or defining $\kappa = \frac{1}{2(am_0+4)}$, as done previously, and passing the constant to the other side, so that we have an dimensionless equation,

$$\frac{a\mathcal{M}_{nm,\text{Clover}}[U]}{am_0+4} = \delta_{n,m} - \kappa \sum_{\pm\mu} (\mathbb{1} - \gamma_\mu) U_\mu(n) \delta_{n+\hat{\mu},m} + \kappa\, c_{SW} a^2 \sum_{\mu<\nu} \sigma_{\mu\nu} a^2 \hat{F}_{\mu\nu} \delta_{n,m}. \quad (5.91)$$

The bare lattice fermion mass, m_0, is given in terms of κ by Eq. 5.75. The action parameters are κ and c_{SW}. These, together with a given a configuration of link variables $\{U\}$ that was obtained for a given β, completely define the operator to be inverted. By performing the inversion of the right hand side of 5.91, we will have the inverse of $\mathcal{M}_{nm}$, by dividing the result by $(am_0+4)/a$.

It is usual to study propagators in momentum space, where they are expected to acquire a simpler form. Since we have a discretized and finite space, we perform a Discrete Fourier Transform

$$S_{p,\text{Clover, plain}}[U] = \frac{1}{\sqrt{|\Lambda|}} \sum_{n\in\Lambda} S_{n0,\text{Clover, plain}}[U] e^{-iap\cdot n}, \quad (5.92)$$

where we have fixed m to be at the origin, and used the fact that the propagator is expected to be translationally invariant and only depend on $n-m$ just to simplify, although this is strictly true only after the evaluation over an ensemble of configurations, which we will perform afterwards anyway. In practice, one can average over different positions m to increase statistics and thus reduce the error. The set of allowed momenta on the lattice $\tilde{\Lambda}$ is discussed in Sect. 5.3.

In the free case, when $U_\mu(n) = \mathbb{1}$ for all n, one can invert the clover operator in closed form in momentum space. In fact, since $\hat{F}_{\mu\nu} = 0$ for the free theory anyway, the clover propagator is the same as the Wilson propagator, given in Eq. 5.23 for the massless case. If one introduces a mass term, then the propagator becomes

$$S_{p,\text{ plain, free}} = a \frac{-ia\not{K}(p) + \mathbb{1}\left[am_0 + \frac{(aQ(p))^2}{2}\right]}{[aK(p)]^2 + \left[am_0 + \frac{(aQ(p))^2}{2}\right]^2}. \quad (5.93)$$

We have here used the notation $aK_\mu(p) \equiv \sin(ap_\mu)$ and $aQ_\mu(p) \equiv 2\sin(\frac{ap_\mu}{2})$ for the lattice momenta. We also notice that the functions $K_\mu(p)$ and $Q_\mu(p)$ become approximately p_μ

in the continuum limit as

$$K_\mu(p) = \frac{\sin(ap_\mu)}{a} = p_\mu - \frac{a^2 p_\mu^3}{6} + \mathcal{O}(a^4), \tag{5.94}$$

$$Q_\mu(p) = \frac{\sin(\frac{ap_\mu}{2})}{\frac{a}{2}} = p_\mu - \frac{a^2 p_\mu^3}{24} + \mathcal{O}(a^4). \tag{5.95}$$

One remark, which is in place here, is that the free propagator is the same independently of the choice of gauge. Since all links are set to the identity, it incidentally automatically and trivially satisfies the Landau gauge condition of $\sum_\mu \partial_\mu A_\mu(n) = 0$, because $A_\mu(n) = 0$.

Another remark is that this lattice free propagator for Wilson fermions is indeed quite different from the continuum propagator. To understand this better, we remind ourselves that, in the continuum, the most general formula for the fermion propagator that respects Lorentz and CPT symmetries is given by

$$S(p) \equiv \frac{1}{i\not{p}A(p) + \mathbb{1}B(p)} \equiv \frac{Z(p)}{i\not{p} + \mathbb{1}M(p)} = Z(p)\frac{-i\not{p} + \mathbb{1}M(p)}{p^2 + M(p)^2}, \tag{5.96}$$

or equivalently

$$(S(p))^{-1} = \frac{1}{Z(p)}[i\not{p} + M(p)\mathbb{1}], \tag{5.97}$$

where $A(p)$ and $B(p)$ are so-called form factors. One can, alternatively, use the quark renormalization function $Z(p) = \frac{1}{A(p)}$ and the mass function $M(p) = B(p)/A(p)$ to describe the propagator. In particular, for a free fermion theory in the continuum $Z_{\text{free}}(p) = 1$ and $M_{\text{free}}(p) = m_0$, where m_0 is the bare mass present in the Lagrangian.

When comparing Eq. 5.96 with Eq. 5.93, one notices that instead of $\not{p}$ one has $\not{K}$ in the lattice formula. This is not new to fermion propagators, and indeed is a lattice artifact that appears for the gluon and ghost propagators as well: the lattice momenta is not the Fourier-momentum variable. In light of Eqs. 5.95, we see that the difference between p_μ and K_μ is of $\mathcal{O}(a^2)$ and thus decreases as one decreases the lattice spacing. More concerning, though, is the mass function. On the lattice, for Wilson fermions it has the form

$$M_{\text{p, plain, free}} = \frac{am_0 + \frac{(aQ(p))^2}{2}}{a} = m_0 + a\frac{Q^2(p)}{2}, \tag{5.98}$$

which differs from the continuum value in $\mathcal{O}(a)$. The source of this discrepancy is the Wilson term, Eq. 5.21, which was added to get rid of the doublers: so this is a feature of Wilson and clover fermions. In momentum space these differences will manifest themselves in the high-momentum region, which probes the microscopic structure of the lattice.

As mentioned in Sect. 5.5, since the discretized Dirac-Wilson operator does not respect chiral symmetry as the Dirac continuum operator does, it is necessary to introduce a κ critical, which forces the pion mass to be zero when the quark mass is zero in the interacting theory. This subtracted mass is the correct quark mass that must be considered in the interacting theory.

The functions $A(p)$ e $B(p)$ can be obtained from traces of the propagator, as follows. First, we define

$$\mathcal{A}(p) = \frac{i}{4N_c(aK)^2}\mathrm{tr}\left(a\not{k}\frac{S(p)}{a}\right), \tag{5.99}$$

$$\mathcal{B}(p) = \frac{1}{4N_c}\mathrm{tr}\left(\frac{S(p)}{a}\right), \tag{5.100}$$

with traces taken in color and Dirac-space. From these functions, we get

$$A(p) = \frac{\mathcal{A}(p)}{(aK)^2\mathcal{A}^2(p) + \mathcal{B}^2(p)} \tag{5.101}$$

$$B(p) = \frac{\mathcal{B}(p)}{(aK)^2\mathcal{A}^2(p) + \mathcal{B}^2(p)}, \tag{5.102}$$

and from these the $M(p)$ and $Z(p)$ form factors.

5.8 Improved propagator

The improved propagator, used to reduce the lattice artifacts, is defined by using the improved fields as in 5.83. The coefficients used here are those used in (87, 97), which are $b'_q = c'_q = 1/4$ e $c_n = 0$. We get

$$\begin{aligned} S_I(x,y) &\equiv \left\langle \psi'(x)\overline{\psi}'(y)\right\rangle \\ &= \left\langle (1+b_q am)^2(1 - c_q a\not{D}(x,w))S_{\mathrm{plain}}(w,z;U)(1 + c_q a\overleftarrow{\not{D}}(z,y))\right\rangle, \end{aligned} \tag{5.103}$$

in which $\not{D}$ is defined by

$$a\not{D}(x,y) = \frac{1}{2}\sum_\mu \gamma_\mu\left(U_\mu(x)\delta_{x+\hat{\mu},y} - U^\dagger_\mu(y)\delta_{x-\hat{\mu},y}\right) \tag{5.104}$$

and $\overleftarrow{\not{D}}$ is given by

$$a\overleftarrow{\not{D}}_{xy} = \frac{1}{2}\sum_\mu \gamma_\mu\left(U^\dagger_\mu(y)\delta_{x-\hat{\mu},y} - U_\mu(x)\delta_{x+\hat{\mu},y}\right) = -a\not{D}(x,y). \tag{5.105}$$

In the free theory, we can also obtain analytic expressions for the improved propagator, Eq. 5.103. In momentum space, its expression becomes

$$S^{\mathrm{free}}_I(ap) = \mathbb{1}_c\left(1 + \frac{am}{2}\right)\left(\mathbb{1}_s - \frac{ia\not{K}(ap)}{4}\right)S^{\mathrm{free}}_{\mathrm{plain}}(ap)\left(\mathbb{1}_s - \frac{ia\not{K}(ap)}{4}\right). \tag{5.106}$$

Expanding the product of the terms we arrive at the expression

$$S^{\mathrm{free}}_I(ap) = \mathbb{1}_c\frac{1 + \frac{am}{2}}{\mathrm{Den}(ap)}\left(-ia\not{K}(ap)A'_I(ap) + \mathbb{1}_s B'_I(ap)\right), \tag{5.107}$$

where

$$A'_I(ap) = 1 + \frac{am}{2} + \frac{3}{16}(aK)^2 + \frac{(aQ)^2 - (aK)^2}{4}, \tag{5.108}$$

$$B'_I(ap) = am\left[1 - \frac{(aK)^2}{16}\right] + \frac{(aQ)^2 - (aK)^2}{2} - \frac{(aK)^2\,(aQ)^2}{32}, \tag{5.109}$$

$$\mathrm{Den}(ap) = (aK)^2 + \left[am + \frac{(aQ)^2}{2}\right]^2. \tag{5.110}$$

The traces of the propagator give

$$\mathrm{tr}\left[S_I^{\mathrm{free}}(ap)\frac{iaK\!\!\!/}{(ak)^2}\right] = 4N_c\frac{(1+\frac{am}{2})}{\mathrm{Den}(ap)}A'_I(ap), \tag{5.111}$$

$$\mathrm{tr}\left[S_I^{\mathrm{free}}(ap)\right] = 4N_c\frac{(1+\frac{am}{2})}{\mathrm{Den}(ap)}B'_I(ap). \tag{5.112}$$

Inverting Eq. 5.107, we arrive at

$$(S_I^{\mathrm{free}}(ap))^{-1} = \mathbb{1}_c\frac{\mathrm{Den}(ap)}{(1+am/2)\mathrm{Den}_I(ap)}\left[iaK\!\!\!/A'_I(ap) + B'_I(ap)\mathbb{1}_s\right], \tag{5.113}$$

where $\mathrm{Den}_I(ap) = (ak(ap))^2A'_I(ap)^2 + B'_I(ap)^2$. Comparing with Eq. 5.97, with the substitution $p\!\!\!/ \to K\!\!\!/$, which was already discussed for the unimproved propagator, we get that the form factors are

$$Z_I^{\mathrm{free}}(ap) = \frac{1}{A_I^{\mathrm{free}}(ap)}, \tag{5.114}$$

$$M_I^{\mathrm{free}}(ap) = \frac{B_I^{\mathrm{free}}(ap)}{A_I^{\mathrm{free}}(ap)}, \tag{5.115}$$

with

$$A_I^{\mathrm{free}}(ap) = \frac{\mathrm{Den}(ap)}{\mathrm{Den}_I(ap)(1+\frac{am}{2})}A'_I(ap), \tag{5.116}$$

$$B_I^{\mathrm{free}}(ap) = \frac{\mathrm{Den}(ap)}{\mathrm{Den}_I(ap)(1+\frac{am}{2})}B'_I(ap). \tag{5.117}$$

5.9 Renormalization of the quark propagator

From symmetry arguments, the renormalized Euclidean-space quark propagator in the continuum must have the form

$$S(\mu;p) = \frac{Z(\mu;p^2)}{ip\!\!\!/ + M(\mu;p^2)} \equiv \frac{1}{ip\!\!\!/A(\mu;p^2) + B(\mu;p^2)}, \tag{5.118}$$

where μ is the renormalization point.

The renormalizability of QCD implies a relationship between a regularized quark propagator and the renormalized quark propagator (87),

$$S_{\mathrm{regularized}}(a;p) = Z_2(\mu;a)S(\mu;p), \tag{5.119}$$

where $Z_2(\mu, a)$ is the quark wave-function renormalization. The regularized propagator may be, for example, the quark propagator calculated on the lattice for finite spacing a, which is what we are most interested in. This relationship between regularized and renormalized propagators will only be verified if the regularized theory is, in some sense, close to the continuum theory. For a lattice regularization, this means that we have small spacings and are in the scaling region, discussed in Sect. 3.2. When the relationship holds, we may derive how renormalized propagators for two distinct renormalization points. Since 5.119 is independent of μ on the left hand side, the product of Z_2 by S must also be independent on the right-hand side. So

$$Z_2(\mu'; a)S(\mu'; p) = Z_2(\mu; a)S(\mu; p) \rightarrow S(\mu'; p) = \frac{Z_2(\mu; a)}{Z_2(\mu'; a)}S(\mu; p), \tag{5.120}$$

that is, two renormalized propagators are related by a multiplicative constant that is independent of the momentum. In particular, from the structure of the quark propagator in 5.118, it follows that

$$Z(\mu'; p^2) = \frac{Z_2(\mu; a)}{Z_2(\mu'; a)}Z(\mu; p^2), \quad M(\mu'; p^2) = M(\mu; p^2) \equiv M(p^2), \tag{5.121}$$

which means that a change in renormalization is just a rescaling of Z by a momentum-independent constant and the mass function is renormalization point independent.

The non-perturbative renormalization scheme that we use here, called "momentum subtraction scheme" (46, 50, 87, 98), or MOM in short, is defined by the following renormalization conditions for the Landau-gauge quark propagator form factors

$$Z(\mu; \mu^2) = 1, \quad M(\mu; \mu^2) = m(\mu). \tag{5.122}$$

For sufficiently high values of μ, we can argue from the asymptotic freedom of QCD that $m(\mu)$ is the usual running mass calculated in perturbation theory.

The regularized form factors coming from the lattice, are

$$Z_{\text{regularized}}(a, p^2) \equiv Z_2(\mu; a)Z(\mu; p^2), \quad M_{\text{regularized}}(a, p^2) \equiv M(p^2). \tag{5.123}$$

The constant $Z_2(\mu; a)$ is determined from the lattice data by imposing the renormalization condition $Z(\mu; \mu^2) = 1$ at a specified normalization point μ,

$$Z_2(\mu; a) = Z_{\text{regularized}}(a, \mu^2), \tag{5.124}$$

and the mass form factor should be independent of a for small enough a, as discussed previously.

Evaluating the left equation in 5.121 for $p^2 = \mu'^2$, we obtain the scaling constant that relates Z at two renormalization points

$$Z(\mu'; \mu'^2) = \frac{Z_2(\mu; a)}{Z_2(\mu'; a)}Z(\mu; \mu'^2) \rightarrow \frac{Z_2(\mu; a)}{Z_2(\mu'; a)} = \frac{Z(\mu'; \mu'^2)}{Z(\mu; \mu'^2)}. \tag{5.125}$$

The MOM renormalization scheme, sometimes called RI-MOM (46) or simply RI scheme, has been related to the modified minimal subtraction $\overline{MS}$ scheme, more commonly used in the particle physics community (99, 100), via continuum perturbation theory.

6 ALGORITHMS

6.1 Pure-gauge configuration generation

When performing quenched simulations, most often the goal is to calculate expectation values of quantities on the euclidean lattice by

$$\langle \mathcal{O} \rangle = \int \mathcal{D}U \, \mathcal{O}[U] e^{-S_E[U]}. \tag{6.1}$$

The configurations U are collections of the link variables $\{U_\mu(n)\}$, introduced in Chap. 3 that represents the gluon field on the lattice. We remark here that the number of degrees of freedom, even for modest lattice sizes, is very large. Take, for example a four-dimensional lattice of size 32^4. This will contain $32^4 \times 4$ links. Each link can be parametrized by 8 real values $A^a_\mu(n)$ as

$$U_\mu(n) = \exp\left(i \sum_{a=1}^{8} A^a_\mu(n) T^a \right), \tag{6.2}$$

where a is the adjunt color index and T^a are the generators of the $SU(3)$ algebra, for example, the Gell-Mann matrices. This corresponds to approximately 33.5 million continuous real values which need to be integrated over. The functional form, which involves an exponential of a sum of plaquettes, which are themselves sums over products of links, is also not particularly encouraging for an analytical evaluation in general. Analytical integration is sometimes possible in some limits, though, such as when the inverse coupling β is small. This is called a strong coupling expansion. Then, a calculation of some quantities, such as the Wilson loop, for example, can be performed. This is done via the expansion of the exponential in powers of the β and the use of integration identities which can be derived from properties of the Haar measure (46).

Another approach, known as lattice perturbation theory, is possible when β is large, which implies that the coupling g is small (25, 50). One can then expand the links in terms of the quadrivector potential in the Lagrangian, go to momentum space and obtain Feynman rules for the lattice theory. As in the continuum limit, one needs to worry about gauge-fixing and the Fadeev-Popov determinants at some point. The Feynman rules of lattice perturbation theory are also rather clumsy and involve vertices with no continuum analog such as the 2 gluon - 2 quark vertex and the 2 gluon - 2 ghost vertices, and their expressions contain trigonometric functions of the momenta involved, which come about due to the subjacent lattice structure. This approach has been rather important in the understanding of renormalization on the lattice and also quantum anomalies and scaling violations, but its awkward nature, together with a restricted range of validity makes it impractical for several applications.

These expansions break down for values of β which correspond to moderately small a, which are usually in the range $5.8 < \beta < 6.3$ for pure gauge theory, and/or cannot be performed if $\mathcal{O}$ does not have a suitable form. We need to substitute these expansions by something more pragmatic and which has a more general scope.

The solution used most frequently in numeric lattice studies is to evaluate Eq. 6.1 numerically by Monte Carlo importance sampling from the space of all possible gauge field configurations (46). Of course, in practice, this ensemble of samples will contain a finite number of configurations, which gives rise to a statistical error associated with the procedure. The error from virtually all Monte Carlo sampling techniques goes as $\mathcal{O}(1/\sqrt{N})$, which is a consequence of the central limit theorem (101). The number of samples can be increased to reduce this error, which is referred to as "increasing the statistics", and although this is rather inefficient, we are stuck with this method for the large number of degrees of freedom which characterizes lattice QCD simulations.

In the Monte Carlo approach, one choose (pseudo)random configurations based on the probability distribution

$$dP[U] = \frac{\mathcal{D}U\, e^{-S_E[U]}}{\int \mathcal{D}U\, e^{-S_E[U]}}, \tag{6.3}$$

and approximate Eq. 6.1 by

$$\langle \mathcal{O} \rangle \approx \frac{\sum_{i=1}^{N} O[U_i]}{N} \tag{6.4}$$

where the configurations U_i are chosen randomly following the probability distribution in Eq. 6.3. Configurations with lower values for the action will contribute with a higher probability, since the exponential with a minus sign implies that they have a higher weight. In fact, we can intuitively guess that most configurations will have a rather rough "shape" which will cause them to contribute less by having a low statistical weight. Configurations with the highest possible weights are the ones with the lowest action values, which should correspond to solutions of the classical equations of motion. Quantum fluctuations are naturally generated by allowing other configurations to give some contribution to the evaluation of the expectation values.

We therefore need algorithms that are capable of generating random configurations that follow the probability distribution of Eq. 6.3. These were available before the advent of lattice field theory and were used to study statistical mechanics models, such as the Ising model. The Metropolis algorithm is one such method. It is based on the idea of a particular kind of stochsatic process called a Markov chain. We want to use the markovian stochastic process to generate the probability distribution in Eq. 6.3 in the equilibrium. In order to do this, we need to place some restrictions on the transition probabilities. To see how this goes, we must first characterize the Markov process more rigorously.

A Markov chain is a stochastic process characterized by a space of different states, an initial probability distribution of being in any of the possible states, and a conditional

probability to transition between them (102). The transition probability for a Markov process can depend only on the two states that are involved in the transition and not on which step we are on the chain: the process has no memory. The transition probability $T(S', S)$ of transitioning to state S' from the state S has to obey restrictions, stemming from the mere fact that it is a probability

$$0 \leq T(S', S) \leq 1, \quad \sum_{S'} T(S', S) = 1. \tag{6.5}$$

We may also interpret $T(S', S)$ as a transition matrix. We define the probability of being in a given state S at step t by

$$P_t(S) = \sum_{S'} T(S, S') P_{t-1}(S'), \tag{6.6}$$

or in matrix notation

$$P_t = T P_{t-1}, \tag{6.7}$$

where we are associating each entry of the probability vector P_t with a particular state. We can iterate this equation to get that

$$P_t = T^t P_0, \tag{6.8}$$

where P_0 is the initial probability vector of being in any particular state at the start of the chain. What we want is that

$$\lim_{t \to \infty} P_t = P, \tag{6.9}$$

where P is the equilibrium probability of Eq. 6.3. Furthermore, we must have that

$$TP = P, \tag{6.10}$$

which means that P is a stationary distribution and is the one that the chain converges to as the number of steps increases. We may see this as stating that P is an eigenvector of T with eigenvalue $\lambda = 1$. We also want to make sure that all states are reachable in principle, which, in the language of the importance sampling that we are after, means that each configuration will have a chance of contributing to the sum. In the matrix language, this is equivalent to requiring that T must be irreducible: if it is reducible, it will get trapped into some absorbing subset of states with no chance of getting out. A matrix is called reducible if it can be put in the form

$$\begin{pmatrix} X & Z \\ \mathbb{0} & Y \end{pmatrix}, \tag{6.11}$$

by a permutation of indices, where $\mathbb{0}$ is a null rectangular matrix. Among the irreducible matrices, we restrict ourselves to the acyclic ones: some stochastic matrices produce systems that alternate between states in a periodic fashion, which is not what is required

for our application. Matrices which are irreducible and acyclic are called regular. The regularity condition is guaranteed if, for some power l, T^l has all entries being strictly positive.

The Perron-Frobenius theorem guarantees that for irreducible matrices the eigenvalue $\lambda = 1$ is non-degenerate and P is thus the unique equilibrium probability distribution, with all its entries being strictly positive real numbers. Moreover, if T is acyclic, as we require, then $|\lambda| < 1$ for all other eigenvectors. We thus have that P is reached independently of the initial distribution P_0.

Eq. 6.10 for the stationary solution can be written as

$$P(S) = \sum_{S'} T(S, S')P(S'), \tag{6.12}$$

but using the fact that $\sum_{S'} T(S', S) = 1$ from the normalization of the transition probability, we may write

$$\sum_{S'} T(S', S)P(S) = \sum_{S'} T(S, S')P(S'), \tag{6.13}$$

which is called the global balance equation and is equivalent to the stationary solution equation for T. The right-hand side is the probability of getting into state S if we were previously in state S', summed over all possible states S': this is the probability of jumping into state S, regardless of the previous state. The left-hand side contains the probability of jumping out of S, which is the probability of being in the state S to start with and then the transition probability of jumping out of it regardless of the final state. In conclusion, the global balance equation indicates that these two probabilities are the same: the probability of hopping into and out of a given state must be the same at equilibrium. But we know P already, which is the distribution we want to generate states with. We basically need to reverse engineer T such that the condition given by Eq. 6.13 is obeyed. The most straightforward way of doing this is by requiring a more restrictive sufficient condition called detailed balance

$$T(S', S)P(S) = T(S, S')P(S'), \tag{6.14}$$

or in other words, requiring that the balance equation holds term by term in the sum of Eq. 6.13.

6.1.1 Metropolis Algorithm

The Metropolis algorithm uses detailed balance to generate configurations with probability

$$P[U] = \frac{e^{-S[U]}}{Z}, \quad Z = \int \mathcal{D}U e^{-S[U]}. \tag{6.15}$$

First, we must define a neighborhood for the states. This neighborhood is such that all states within the neighborhood are reachable within one step of the algorithm. The states out of the neighborhood will be reachable only within multiple steps. We also must make

sure that if U' is in the neighborhood of U, then the reverse must also be true. More precisely, when transitioning from a configuration U to U'

$$T(U',U) = 0 \,\text{if}\, U \notin \text{neighborhood of U},$$
$$T(U',U) \neq 0 \,\text{if}\, U \in \text{neighborhood of U}.$$

We call N the number of configurations in the neighborhood of a given state, and to simplify we have chosen all neighborhoods to have the same number of states. The Metropolis transition probability for two states in the same neighborhood is given by

$$\begin{aligned} T(U',U) &= \frac{1}{N} e^{-(S[U']-S[U])}, \,\text{if}\, S[U'] > S[U], \\ T(U',U) &= \frac{1}{N}, \,\text{if}\, S[U'] \leq S[U], \\ T(U,U) &= 1 - \sum_{U' \neq U} T(U',U). \end{aligned} \tag{6.16}$$

That detailed balance is obeyed can be seen by taking two states U_1 and U_2. For definiteness we take $S[U_1] > S[U_2]$, then

$$T(U_1,U_2) = \frac{1}{N} \exp\left(-(S[U_1] - S[U_2])\right), \quad T(U_2,U_1) = \frac{1}{N}, \tag{6.17}$$

so that

$$\frac{T(U_1,U_2)}{T(U_2,U_1)} = \exp\left(-(S[U_1] - S[U_2])\right) = \frac{\exp\left(-S[U_1]\right)}{\exp\left(-S[U_2]\right)} = \frac{P[U_1]}{P[U_2]}, \tag{6.18}$$

which is the detailed balance equation. We notice that the normalization factor Z does not need to be known.

The algorithm that implements the transition probability in Eqs. 6.16 is the following: We start with any configuration. We then randomly choose a configuration in the neighborhood of the previous one with uniform probability. If the action change $\Delta S \leq 0$, we accept the new configuration. If, however $\Delta S > 0$, we accept it with probability $\exp(-\Delta S)$, that is, we generate a random number ξ in the interval $[0,1]$. If ξ is less or equal than $\exp(-\Delta S)$, we accept the new configuration, otherwise we keep the same configuration as before. We iterate this over and over again. Eventually we reach the equilibrium and we can start using the sampled configurations to evaluate expectation values. It is remarkable that this rather simple procedure, in the equilibrium, samples the configurations with the exactly correct distribution.

In practice the Metropolis algorithm is used in a link per link basis. That is, we sweep through the lattice for all sites n and spacetime directions μ and update the link variable $U_\mu(n)$ by

$$U'_\mu(n) = X U_\mu(n), \tag{6.19}$$

where X is a $SU(3)$ group element close to the identity, so that $U'_\mu(n)$ is in the neighborhood of $U_\mu(n)$. The spread around the identity can be controlled in order to have an acceptance

around 50%, which ensures that one is walking in the space of all possible configurations quickly while also reducing the correlation between subsequent configurations, which we will deal with later. A variation is called multihit Metropolis: one takes advantage of the fact that the numerically costly action change is already calculated to perform more updates on the same site. The number of hits can also be tuned for efficiency.

Some remarks are in place here. Firstly, the generation of pseudo-random numbers is a highly sensitive matter in lattice gauge theory simulations. This is because the amount of pseudo-random numbers needed is huge, which means that one needs a generator with a likewise huge orbit. The ranlux generator (103), is a rather renowned high-quality generator that is commonly used in lattice QCD simulations and is part of the GNU scientific library.

As we already stated, the algorithms based on Markov chains need some steps until the distribution reaches a state of equilibrium. In order to monitor this, one can begin a simulation with different starting points and check when some observable converges to the same region, which should eventually happen independent of the initial start. One can choose all links to be the identity matrix, for example, which is referred to as a cold start, or all random matrices, which is called a hot start. Considering, for definiteness, the value of the action, we can mark the first step that the values for the observable cross for different starts and, just to be on the safe side, take 10 times that step as the number of steps to reach equilibrium.

6.1.2 Heat Bath algorithm

Another Monte Carlo algorithm is the heat bath. Instead of looking at the probability for the whole configuration, one looks at what is the probability density for a single link variable in the heat bath of all other links kept fixed. The Wilson gauge action is given by Eq. 3.21. From the point of view of a single link, its contribution to the action is given by

$$S_{\text{local}}[U_\mu(n)] = \frac{\beta}{N_c}\sum_{i=1}^{6}\text{Re tr}[\mathbb{1} - U_\mu(n)\text{Staple}_i(n,\mu)] = \frac{\beta}{N_c}\text{Re tr}[\mathbb{1} - U_\mu(n)A(n,\mu)], \quad (6.20)$$

where $A(n,\mu)$ is the sum of staples, which are simply the plaquettes with the $U_\mu(n)$ link that is under consideration removed, and which have the format of a paper staple

$$A(n,\mu) = \sum_{i=1}^{6}\text{Staple}_i(n,\mu) = \sum_{\nu\neq\mu}\Big(U_\nu(n+\hat{\mu})U_{-\mu}(n+\hat{\mu}+\hat{\nu})U_{-\nu}(n+\hat{\nu}) + U_{-\nu}(n+\hat{\mu})U_{-\mu}(n+\hat{\mu}-\hat{\nu})U_\nu(n-\hat{\nu})\Big). \quad (6.21)$$

The probability distribution for the whole configuration can be written as

$$dP[U] = \frac{1}{Z}\exp\left\{-\frac{\beta}{N_c}\sum_{n,\mu}\text{Re tr}[\mathbb{1} - U_\mu(n)A(n,\mu)]\right\}\mathcal{D}U \tag{6.22}$$

$$= \frac{1}{Z'}\exp\left\{\frac{\beta}{N_c}\sum_{n,\mu}\text{Re tr}[U_\mu(n)A(n,\mu)]\right\}\mathcal{D}U. \tag{6.23}$$

The local probability for a single link is given thus by

$$dP[U_\mu(n)] = \frac{1}{Z''}\exp\left\{\frac{\beta}{N_c}\text{Re tr}[U_\mu(n)A(n,\mu)]\right\}dU_\mu(n), \tag{6.24}$$

and the Z'' constant is irrelevant in what follows, so we might as well set it to 1.

6.1.2.1 Heat Bath Algorithm for SU(2)

We will first show the Heat Bath algorithm for $SU(2)$ gauge theory, which is a building block for $SU(3)$. The important mathematical fact for $SU(2)$ is that the matrix A, which is a sum of group elements, is proportional to an $SU(2)$ group element. The most general $SU(2)$ group element u can be written as

$$u = \begin{pmatrix} u_0 + iu_3 & u_2 + iu_1 \\ -u_2 + iu_1 & u_0 - iu_3 \end{pmatrix} \tag{6.25}$$

or more succinctly

$$u = u_0\mathbb{1} + i\vec{u}\cdot\vec{\sigma}, \tag{6.26}$$

where σ are the Pauli sigma matrices, u_0 and u_i are real parameters. It is easy to see that $\det[u] = \sum_{i=0}^{3} u_i^2$. In order for this to be an $SU(2)$, element we need to add the condition that the sum of the squares of the real parameters have to add up to 1.

When we add $SU(2)$ elements u and v, we get

$$u + v = (u_0 + v_0)\mathbb{1} + i(\vec{u} + \vec{v})\cdot\vec{\sigma}. \tag{6.27}$$

We want to show that $u + v$ is proportional to an $SU(2)$ element. For a $SU(2)$ element, one should have that its Hermitian conjugate is equal to the inverse. Let us calculate the Hermitian conjugate of the sum

$$(u + v)^\dagger = (u_0 + v_0)\mathbb{1} - i(\vec{u} + \vec{v})\cdot\vec{\sigma}, \tag{6.28}$$

where we have used that the identity and the Pauli σ matrices are Hermitian. Here we note that the determinant is real, and thus $\det[(u + v)^\dagger] = \det[u + v]$, since it is the sum of the square of the real components and the inverted sign does not change the result of this calculation. We can then perform the product

$$(u + v)(u + v)^\dagger = (u_0 + v_0)\mathbb{1} + \sum_{j,k}(u_j + v_j)(u_k + v_k)\sigma_j\sigma_k, \tag{6.29}$$

where the cross terms cancel. But we know that $\sigma_j\sigma_k = \frac{1}{2}(\{\sigma_j,\sigma_k\}+[\sigma_j,\sigma_k])$. The commutator part will not contribute, as it is contracted with a symmetric term, and $\{\sigma_j,\sigma_k\} = 2\delta_{jk}\mathbb{1}$, so

$$(u+v)(u+v)^\dagger = ((u_0+v_0)^2+(\vec{u}+\vec{v})^2)\mathbb{1} = \det[u+v]\mathbb{1}. \tag{6.30}$$

From this we claim that $(u+v)/\sqrt{\det[u+v]}$ is an $SU(2)$ element, since

$$\frac{u+v}{\sqrt{\det[u+v]}}\frac{(u+v)^\dagger}{\sqrt{\det[(u+v)^\dagger]}} = \mathbb{1} \tag{6.31}$$

and

$$\det\left[\frac{u+v}{\sqrt{\det[u+v]}}\right] = \frac{(u_0+v_0)^2+(\vec{u}+\vec{v})^2}{\det[u+v]} = 1. \tag{6.32}$$

The sum of staples can then be written as $A = a\,A_{SU(2)}$, where $A_{SU(2)}$ is an $SU(2)$ element and $a = \sqrt{\det[A]}$. We rewrite Eq. 6.24 for $SU(2)$ as

$$dP[U] = \exp\left[\frac{a\beta}{2}\text{Re tr}[UA_{SU(2)}]\right]dU, \tag{6.33}$$

or writing $X = UA_{SU(2)}$, and using the property of the Haar measure that $dU = dX$, since X and U are related by the constant matrix $A_{SU(2)}$,

$$dP[X] = \exp\left[\frac{a\beta}{2}\text{Re tr}[X]\right]dX. \tag{6.34}$$

We will need to express the abstract Haar measure in terms of the parametrization of Eq. 6.26. The Haar measure must be normalized

$$\int dX = 1. \tag{6.35}$$

We can express it as

$$dX = \mathcal{X}\,d^4x\,\delta(x_0^2+|\vec{x}|^2-1), \tag{6.36}$$

where we are explicitly enforcing that the determinant of X has to be 1 with the delta function, and $\mathcal{X}$ is a normalization constant, which can be calculated to normalize the Haar measure

$$\mathcal{X}\int d^4x\,\delta(x_0^2+|\vec{x}|^2-1) = \mathcal{X}\int dx_0\,d^2\Omega\,d|\vec{x}|\,|\vec{x}|^2\frac{\delta\left(|\vec{x}|-\sqrt{1-x_0^2}\right)+\delta\left(|\vec{x}|+\sqrt{1-x_0^2}\right)}{2\sqrt{1-x_0^2}} \tag{6.37}$$

where we used that

$$\delta(f(s)) = \sum_{s_0}\frac{\delta(s-s_0)}{|f'(s)|_{s_0}}. \tag{6.38}$$

The value of x_0 is restricted to the $[-1,1]$ interval, where the square root in the delta function is real. The second delta function in fact does not contribute, as $|\vec{x}|$ is positive, so we are left with

$$4\pi\mathcal{X}\int dx_0\,\frac{\left(\sqrt{1-x_0^2}\right)^2}{2\sqrt{1-x_0^2}} = 2\pi\mathcal{X}\int_{-1}^{1} dx_0\,\sqrt{1-x_0^2}, \tag{6.39}$$

and the integral can be solved by elementary methods

$$\int_{-1}^{1} dx_0\,\sqrt{1-x_0^2} = \int_0^{\pi} dy\,\sin(y)\sqrt{1-\cos^2(y)} = \int_0^{\pi} dy\,\sin^2(y) = \int_0^{\pi} dy\,\frac{1-\cos(2y)}{2} = \frac{\pi}{2}. \tag{6.40}$$

The integral of the Haar measure $\int dX = \mathcal{X}\pi^2$, and so, to normalize it, $\mathcal{X} = 1/\pi^2$. In terms of the parameters x_i the differential probability in Eq. 6.34 is then

$$dP[X] = \frac{\sqrt{1-x_0^2}}{2\pi^2}\exp\left[a\,\beta\,x_0\right]\,d^2\Omega\,dx_0, \tag{6.41}$$

where we have used that $\mathrm{tr}[X] = 2x_0$, which can be deduced from the parametrization in Eq. 6.26, and we fixed that $|\vec{x}| = \sqrt{1-x_0^2}$. We need to choose x_0 randomly respecting the distribution 6.41 and the x_i uniformly on the surface of a sphere. Following (104), we define a variable $\lambda^2 = \frac{1-x_0}{2}$ with the range $\lambda \in [0,1]$, so that

$$dx_0\sqrt{1-x_0^2}\exp(a\,\beta\,x_0) \propto d\lambda\,\lambda^2\,\sqrt{1-\lambda^2}\,\exp(-2\,a\,\beta\,\lambda^2). \tag{6.42}$$

We proceed in the generation of numbers following this distribution in two steps. Firstly we generate λ with the distribution

$$p_1(\lambda) = \lambda^2\,\exp(-2\,a\,\beta\,\lambda^2). \tag{6.43}$$

Since random number generators usually produce numbers uniformly in the interval $[0,1)$, we need to express the new distribution in terms of such numbers instead. This can be accomplished by choosing a triplet of random numbers uniformly distributed in the aforementioned interval and combining them as

$$\lambda^2 = -\frac{1}{2\,a\,\beta}\left(\ln(1-r_1) + \cos^2(2\pi(1-r_2))\ln(1-r_3)\right), \tag{6.44}$$

and we will have that λ follows distribution 6.43. To correct for the square root in 6.42, we take one more uniformly distributed random number r and accept λ only if it obeys

$$r^2 \leq 1-\lambda^2. \tag{6.45}$$

If this inequality does not hold, one starts over again by repeting the procedure of drawing numbers r_1, r_2 and r_3 from the random number generator and calculating λ. Having λ, we calculate $x_0 = 1-2\lambda^2$. For the x_i, which need to be uniformly distributed on the surface of a sphere of radius $\sqrt{1-x_0^2}$, we simply draw three uniformly distributed random numbers

in the interval $[0,1)$, and make them be in the interval $[-1,1)$ by multiplying by 2 and subtracting 1. We accept the numbers if the sum of their squares is less than 1. We then normalize $\vec{x}$ to the desired length. Finally, having now $X = x_0\mathbb{1} + i\vec{\sigma}\cdot\vec{x} = UA_{SU(2)}$, we obtain the link variable U by

$$U = XA^{\dagger}_{SU(2)} = X\frac{A^{\dagger}}{\sqrt{\det[A]}}, \tag{6.46}$$

where A is the sum of staples and we have used the unitarity of $A_{SU(2)}$.

6.1.2.2 (Pseudo) Heat Bath Algorithm for SU(3)

The local probability density for a link U in the heat bath of the fixed surrounding links for $SU(3)$, similarly as for $SU(2)$, is

$$dP(U) = \exp\left(\frac{\beta}{3}\text{Re tr}[UA]\right)dU. \tag{6.47}$$

For $SU(3)$ the sum of staples is not proportional to an element of $SU(3)$ as was the case for $SU(2)$. Because of this, we need a few tricks to make the heat bath scheme work for $SU(3)$ (105, 106).

We may rewrite the heat bath step in terms of an update to the link which is already in place currently. Let us say we have a link U^{old} an we want to find what is the update V given by the heat bath, so that afterwards we will end up with $U^{\text{new}} = VU^{\text{old}}$. The probability distribution for V is given by

$$dP(V) = \exp\left(\frac{\beta}{3}\text{Re tr}[VU^{\text{old}}A]\right)d(VU^{\text{old}}) = \exp\left(\frac{\beta}{3}\text{Re tr}[VW]\right)dV, \tag{6.48}$$

where we have used the property of the Haar measure that it is invariant under products by group elements $dV = d(VU^{\text{old}})$, and defined $W = U^{\text{old}}A$. We will use now the Cabbibo-Marinari trick (107) and write the update matrix as $V = R$, where R is a $SU(2)$ matrix embedded in a $SU(3)$ matrix

$$R = \begin{pmatrix} r_0 + ir_3 & r_2 + ir_1 & 0 \\ -r_2 + ir_1 & r_0 - ir_3 & 0 \\ 0 & 0 & 1 \end{pmatrix}. \tag{6.49}$$

In this way, we are finding the heat bath update corresponding to this $SU(2)$ subgroup of $SU(3)$. We can now calculate the expression in the exponent of the probability distribution

$$\begin{aligned}\text{Re tr}[RW] = r_0\text{Re}\,(w_{11}+w_{22}) - r_1\text{Im}\,(w_{12}+w_{21}) - \\ r_2\text{Re}\,(w_{12}-w_{21}) - r_3\text{Im}\,(w_{11}-w_{22}) + \text{Re}\,(w_{33})\end{aligned} \tag{6.50}$$

where w_{ij} corresponds to the entry of the W matrix at the i-th row and j-th column. The last term in this expression has no dependence on r and can thus be absorbed in

the normalization of the probability distribution. The other terms are what would have been obtained if we had taken the real part of the trace of the product of the 2×2 $SU(2)$ submatrix of R, which we call $R_{SU(2)}$, by a 2×2 matrix $W_{2\times 2}$ in the format of Eq. 6.25 with

$$(w_{2\times 2})_0 = \frac{\mathrm{Re}(w_{11} + w_{22})}{2}, \tag{6.51}$$

$$(w_{2\times 2})_1 = \frac{\mathrm{Im}\,(w_{12} + w_{21})}{2}, \tag{6.52}$$

$$(w_{2\times 2})_2 = \frac{\mathrm{Re}\,(w_{12} - w_{21})}{2}, \tag{6.53}$$

$$(w_{2\times 2})_3 = \frac{\mathrm{Im}(w_{11} - w_{22})}{2}. \tag{6.54}$$

We have thus established that Re tr$[RW]$ = Re tr$[R_{SU(2)}W_{2\times 2}]$ + irrelevant constant. The matrix $W_{2\times 2}$ by virtue of being written in the form of Eq. 6.25 is proportional to an $SU(2)$ matrix. We have thus arrived at a problem analogous to the $SU(2)$ heat bath, with a probability density given by

$$dP(R_{SU(2)}) = \exp\left(\frac{\beta}{3}\mathrm{Re\ tr}[R_{SU(2)}W_{2\times 2}]\right) dR_{SU(2)}. \tag{6.55}$$

After determining $R_{SU(2)}$, we need to update $W' = RU^{\mathrm{old}}A = RW$, and repeat the procedure with an update matrix

$$S = \begin{pmatrix} s_0 + is_3 & 0 & s_2 + is_1 \\ 0 & 1 & 0 \\ -s_2 + is_1 & 0 & s_0 - is_3 \end{pmatrix}, \tag{6.56}$$

all steps will be analogous, with $W'_{2\times 2}$ given by

$$(w'_{2\times 2})_0 = \frac{\mathrm{Re}(w_{11} + w_{33})}{2}, \tag{6.57}$$

$$(w'_{2\times 2})_1 = \frac{\mathrm{Im}\,(w_{13} + w_{31})}{2}, \tag{6.58}$$

$$(w'_{2\times 2})_2 = \frac{\mathrm{Re}\,(w_{13} - w_{31})}{2}, \tag{6.59}$$

$$(w'_{2\times 2})_3 = \frac{\mathrm{Im}(w_{11} - w_{33})}{2}. \tag{6.60}$$

Updating again $W'' = SW'$, and repeating the procedure with the update matrix

$$T = \begin{pmatrix} 1 & 0 & 0 \\ 0 & t_0 + it_3 & t_2 + it_1 \\ 0 & -t_2 + it_1 & t_0 - it_3 \end{pmatrix}, \tag{6.61}$$

we will have that $W''_{2\times 2}$ will be

$$(w''_{2\times 2})_0 = \frac{\mathrm{Re}(w_{22}+w_{33})}{2}, \tag{6.62}$$

$$(w''_{2\times 2})_1 = \frac{\mathrm{Im}\,(w_{23}+w_{32})}{2}, \tag{6.63}$$

$$(w''_{2\times 2})_2 = \frac{\mathrm{Re}\,(w_{23}-w_{32})}{2}, \tag{6.64}$$

$$(w''_{2\times 2})_3 = \frac{\mathrm{Im}(w_{22}-w_{33})}{2}. \tag{6.65}$$

After calculating R, S and T in this fashion, one gets the new updated link as $U^{\mathrm{new}} = TSRU^{\mathrm{old}}$. One must then iterate the algorithm for all links on the lattice.

Due to the accumulation of numerical errors in the matrix products needed to update the configurations, one needs to project the links periodically to $SU(3)$ when generating the configurations. In the case of $SU(3)$ this can be done in the following manner (46): We write the link U as

$$U = \begin{pmatrix} \boldsymbol{u} \\ \boldsymbol{v} \\ \boldsymbol{z} \end{pmatrix}$$

where $\boldsymbol{u}, \boldsymbol{v}$ and $\boldsymbol{z}$ are complex vectors with three components. In order to perform the projection we take

$$U_{\mathrm{SU(3)}} = \begin{pmatrix} \boldsymbol{u}_{\mathrm{new}} \\ \boldsymbol{v}_{\mathrm{new}} \\ \boldsymbol{u}^*_{\mathrm{new}} \times \boldsymbol{v}^*_{\mathrm{new}} \end{pmatrix} \tag{6.66}$$

where $\boldsymbol{u}_{\mathrm{new}} = \boldsymbol{u}/|\boldsymbol{u}|$ and $\boldsymbol{v}_{\mathrm{new}} = \boldsymbol{v}'/|\boldsymbol{v}'|$ and $\boldsymbol{v}'$ is obtained using Gram-Schmidt orthogonalization from $\boldsymbol{v}$, that is, $\boldsymbol{v'} = \boldsymbol{v} - \boldsymbol{u}_{\mathrm{new}}(\boldsymbol{v}\cdot\boldsymbol{u}^*_{\mathrm{new}})$. That this form indeed describes an $SU(3)$ matrix can be seen by calculating $\det[U_{\mathrm{SU(3)}}]$ and $U_{\mathrm{SU(3)}}\cdot U^\dagger_{\mathrm{SU(3)}}$. For the determinant we can use the formula in terms of the Levi-Civita symbol

$$\begin{aligned} \det[U_{\mathrm{SU(3)}}] &= \sum_{ijk} \varepsilon_{ijk} u_i v_j (\boldsymbol{u}^* \times \boldsymbol{v}^*)_k \\ &= \sum_{ijklm} \varepsilon_{ijk}\varepsilon_{lmk} u_i v_j u^*_l v^*_m \\ &= \sum_{ijlm} (\delta_{il}\delta_{jm} - \delta_{im}\delta_{jl}) u_i v_j u^*_l v^*_m \\ &= (\boldsymbol{u}\cdot\boldsymbol{u}^*)(\boldsymbol{v}\cdot\boldsymbol{v}^*) - (\boldsymbol{u}\cdot\boldsymbol{v}^*)(\boldsymbol{v}\cdot\boldsymbol{u}^*) = 1, \end{aligned} \tag{6.67}$$

where the last equality follows by noting that $\boldsymbol{u}$ and $\boldsymbol{v}$ are normalized and orthogonal by construction and from the second to the third line, we used the property of Levi-Civita symbols that $\sum_k \varepsilon_{ijk}\varepsilon_{lmk} = (\delta_{il}\delta_{jm} - \delta_{im}\delta_{jl})$. We dropped the subscript "new" to reduce cluttering.

The Hermitian conjugate is given by

$$U^{\dagger}_{\mathrm{SU(3)}} = \begin{pmatrix} (\boldsymbol{u}^*)^T & (\boldsymbol{v}^*)^T & (\boldsymbol{u}\times\boldsymbol{v})^T \end{pmatrix}, \tag{6.68}$$

so that $U_{\mathrm{SU(3)}} \cdot U^{\dagger}_{\mathrm{SU(3)}}$ is

$$\begin{pmatrix} \boldsymbol{u} \\ \boldsymbol{v} \\ \boldsymbol{u}^* \times \boldsymbol{v}^* \end{pmatrix} \cdot \begin{pmatrix} (\boldsymbol{u}^*)^T & (\boldsymbol{v}^*)^T & (\boldsymbol{u}\times\boldsymbol{v})^T \end{pmatrix} = \tag{6.69}$$

$$= \begin{pmatrix} \boldsymbol{u}\cdot\boldsymbol{u}^* & \boldsymbol{u}\cdot\boldsymbol{v}^* & \boldsymbol{u}\cdot(\boldsymbol{u}\times\boldsymbol{v}) \\ \boldsymbol{v}.\boldsymbol{u}^* & \boldsymbol{v}\cdot\boldsymbol{v}^* & \boldsymbol{v}\cdot(\boldsymbol{u}\times\boldsymbol{v}) \\ (\boldsymbol{u}^*\times\boldsymbol{v}^*)\cdot\boldsymbol{u}^* & (\boldsymbol{u}^*\times\boldsymbol{v}^*)\cdot\boldsymbol{v}^* & (\boldsymbol{u}^*\times\boldsymbol{v}^*)\cdot(\boldsymbol{u}\times\boldsymbol{v}) \end{pmatrix} = \mathbb{1}, \tag{6.70}$$

which is evident if one notices again that $\boldsymbol{u}$ and $\boldsymbol{v}$ are normalized and orthogonal to each other and that $x\cdot(x\times y) = y\cdot(x\times y) = (x\times y)\cdot x = (x\times y)\cdot y = 0$ for any x and y. The term $(\boldsymbol{u}^*\times\boldsymbol{v}^*)\cdot(\boldsymbol{u}\times\boldsymbol{v})$ actually calculates the determinant, which is 1 as we have already shown, because

$$(\boldsymbol{u}^*\times\boldsymbol{v}^*)\cdot(\boldsymbol{u}\times\boldsymbol{v}) = \sum_{ijklm} \varepsilon_{ijk}\varepsilon_{lmk} u_i v_j u_l^* v_m^* = \det[U_{\mathrm{SU(3)}}] = 1, \tag{6.71}$$

as a comparison with the second line of 6.67 shows.

6.1.3 Statistical treatment of the data

Some quantities are not costly to calculate, such as the average plaquette or the Polyakov loop, and they can be evaluated "on the fly" for every single sweep of the configuration generation algorithm. Others quantities, like the quark propagator are very expensive and have to be evaluated for a fraction of the total number of configurations generated on the simulation. Another reason for not evaluating quantities for all generated configurations is that subsequent sweeps produce configurations which are very close to each other, i. e. they are highly correlated. Performing calculations on correlated configurations is wasteful, since they will contain mostly redundant information.

Correlation also complicates the error determination, because the naïve formulas for the standard deviation of the mean for an observable $\mathcal{O}$ with mean $\hat{\mathcal{O}}$ with N samples, for example,

$$\sigma^2_{\mathcal{O}} = \sum_{i=1}^{N} \frac{(\mathcal{O}_i - \bar{\mathcal{O}})^2}{N(N-1)}, \tag{6.72}$$

presuppose that the data points are independent. The correct formula for correlated data would be (46)

$$\sigma^2_{\mathcal{O}} = \sum_{i=1}^{N} \frac{(\mathcal{O}_i - \bar{\mathcal{O}})^2}{N(N-1)} 2\tau_{\mathcal{O},\mathrm{int}}, \tag{6.73}$$

where $\tau_{\mathcal{O},\text{int}}$ is the integrated autocorrelation time, given by

$$\tau_{\mathcal{O},\text{int}} = \frac{1}{2} \sum_{t=-\infty}^{\infty} \Gamma_{\mathcal{O}}(t), \tag{6.74}$$

in which $\Gamma_{\mathcal{O}}(t)$ is the normalized autocorrelation function, defined by

$$\Gamma_{\mathcal{O}}(t) \equiv \frac{C_{\mathcal{O}}(t)}{C_{\mathcal{O}}(0)}, \tag{6.75}$$

and the correlation function is $C_{\mathcal{O}}(t) = \langle \mathcal{O}_i \mathcal{O}_{i+t} \rangle - \langle \mathcal{O}_i \rangle \langle \mathcal{O}_{i+t} \rangle$ (101).

Although this calculation is certainly possible for numerically cheap observables, it is not worth it to evaluate the errors like this for the quark propagators or quantities derived from it. In particular, one notices that all quantities related to autocorrelation depend on the quantity that is under consideration. Moreover, a high number of measurements is needed in order to estimate the autocorrelation realiably.

The usual practice is to create an ensemble of uncorrelated configurations by saving configurations spaced by a number of sweeps. The spacing between uncorrelated configurations can be estimated from the autocorrelation length for Polyakov loops or the average plaquette, and one multiplies this by 10 to be on the safe side. By proceeding in this way, one is effectively decoupling the configuration generation from the numerical measurement process: one makes an effort to generate several uncorrelated configurations which can then be stored and used to calculate quantities later. In fact, another advantage of this approach is that one does not need to know beforehand what are the quantities one is interested, as would be the case if all evaluations were made "on the fly". Most collaborations nowadays, if not all, generate ensembles which are then kept for years, while the members decide which quantities of interest they want to extract from them. This is specially true when dealing with configurations with dynamical fermions, which are considerably more expensive to generate than quenched, as discussed in 3.1. Our approach is to proceed this way and evaluate quark propagators only on uncorrelated configurations.

Another issue related to correlation arises when one tries to evaluate quantities which depend on the various degrees of freedom of the configuration in complicated ways. We will use the quark propagator again as an example. The procedure employed here is to obtain the propagator in configuration space by inverting the Dirac operator, which is already a non-trivial function of the configurations, then transform the propagator to momentum space and extract the form factors by taking traces. These form factors are then combined to obtain more easily interpretable mass and quark renormalization functions, which can then be fitted or further manipulated. It is hopeless to try to perform any sort of error propagation to reliably obtain the uncertainties associated to the final figures. There are however techniques to determine the errors reliably. We will rely and present one specific resampling technique called "statistical boostrap".

Suppose we have a set of N data and we want to estimate a quantity θ, which is a complicated function of this data. The statistical bootstrap prescribes that we can resample the original set by taking N randomly chosen data from the original set K times. Since they are chosen randomly, the same data will sometimes be drawn more than once. At this point we will have K sets each with N data. For each of the sets, one computes the quantity θ_k. The estimates for the expectation value and the errors are given by

$$\bar{\theta} = \frac{1}{K}\sum_{k=1}^{K}\theta_k, \quad \sigma_{\bar{\theta}}^2 = \frac{1}{K}\sum_{k=1}^{K}(\theta_k - \bar{\theta})^2, \tag{6.76}$$

and one quotes $\langle\theta\rangle = \bar{\theta} \pm \sigma_{\bar{\theta}}$.

6.2 Gauge-fixing

The gauge-fixing procedure is, in practice, done in an iterative fashion through the use of numeric algorithms, which implies that for a configuration to be considered gauge-fixed to Landau gauge, the quadridivergence of $A(n)$ (or some proxy of it) must be less than a given level of tolerance.

6.2.1 The Los Alamos algorithm for SU(2)

The Los Alamos algorithm is a local algorithm. In order to explain its principle, we can define a local version of the functional $\mathcal{E}$ of Eq. 4.23, which exhibits the local dependence of a specific site n

$$\mathcal{E}[g(n)] \equiv \frac{1}{dN_c|\Lambda|}\mathrm{tr}[g(n)h(n)] \equiv -\frac{1}{dN_c|\Lambda|}\mathrm{tr}[w(n)], \tag{6.77}$$

with

$$h(n) = \sum_{\mu=1}^{d}\left[U_\mu(n)g^\dagger(n+\hat{\mu}) + U_\mu^\dagger(n-\hat{\mu})g^\dagger(n-\hat{\mu})\right]. \tag{6.78}$$

In the Los Alamos algorithm for SU(2), we do "sweeps" over all sites of the lattice and at each site extremize the expression of Eq. 6.77. To achieve this, we take advantage of the fact that, for this group, $h(n)$, being the sum of a product of $SU(2)$ matrices, is proportional to an element of the group, with a proportionality constant given by $\sqrt{\det h(n)}$. We can then define a projection to the $SU(2)$ group by

$$\mathcal{P}_{\mathrm{SU(2)}}\left[h(n)\right] = \frac{h(n)}{\sqrt{\det h(n)}}. \tag{6.79}$$

The matrix $g(n)$ which extremizes Eq. 6.77 is $\mathcal{P}_{\mathrm{SU(2)}}\left[h^\dagger(n)\right]$, as will be shown in the next section by using Lagrange multipliers.

Another way of writing this, is as an update to the previous gauge-transformation

$$g^{\mathrm{new}}(n) = A(n)g^{\mathrm{old}}(n), \tag{6.80}$$

which for the $SU(2)$ Los Alamos algorithm is

$$A^{\mathrm{LA}}(n) = \mathcal{P}_{\mathrm{SU(2)}}\left[h^{\dagger}(n) g^{\mathrm{old}^{\dagger}}(n)\right] = \mathcal{P}_{\mathrm{SU(2)}}\left[w^{\mathrm{old}^{\dagger}}(n)\right], \tag{6.81}$$

with $w(n)$ defined by Eq. 6.77.

We sweep the lattice then, multiple times, updating the values of $g(n)$ by the ones which extremizes the local functional, and at the end of each sweep, we measure a quantity indicative of how close we are to the gauge-fixing condition. One possible indicator of this is

$$e_2 = \frac{1}{V} \sum_{n \in \Lambda} \sum_{b=1}^{N_c^2 - 1} \left(\partial_\mu A_\mu^b(n)\right)^2, \tag{6.82}$$

and we consider a configuration to be gauge-fixed when this quantity is below 10^{-16}.

6.2.2 (Pseudo) Los Alamos algorithm for SU(3)

Ideally, we would like to put $\mathcal{E}[g(n)]$ at an extreme at each update of $g(n)$, just like we do with $SU(2)$, i. e. we want to find an update of $g^{\mathrm{old}}(n)$ in such a way that Re tr$[g^{\mathrm{new}}(n)h(n)]$ = Re tr$[w^{\mathrm{new}}(n)]$ was extremized.

By using the procedure described below, based on the Cabbibo-Marinari (107) trick, we will only have that Re tr$[w^{\mathrm{new}}(n)] >$ Re tr$[w^{\mathrm{old}}(n)]$, in principle, a less effective update. However, since the final goal is not the local extremization but the global one, and the global maximum will not respect the local individual maxima, we hope this will not be as big of an issue.

The limiting property of the $SU(3)$ Los Alamos algorithm is that $w(n)$ is not proportional to a group element, as was the case for $SU(2)$. In our current understanding, the best one can do is, taking advantage of the logic of the $SU(2)$ algorithm, subdivide the $h(n)$ matrix into submatrices, as in the Cabbibo-Marinari trick for the heatbath algorithm for configuration generation, and perform an update

$$g^{(\mathrm{new})}(n) = A(n) g^{(\mathrm{old})}(n), \tag{6.83}$$

in which $A(n) = T(n)S(n)R(n)$, and R, S and T are $SU(2)$ matrices embedded in a $SU(3)$ matrix:

$$R(n) = \begin{pmatrix} r_0 + ir_3 & r_2 + ir_1 & 0 \\ -r_2 + ir_1 & r_0 - ir_3 & 0 \\ 0 & 0 & 1 \end{pmatrix}, \tag{6.84}$$

$$S(n) = \begin{pmatrix} s_0 + is_3 & 0 & s_2 + is_1 \\ 0 & 1 & 0 \\ -s_2 + is_1 & 0 & s_0 - is_3 \end{pmatrix}, \tag{6.85}$$

$$T(n) = \begin{pmatrix} 1 & 0 & 0 \\ 0 & t_0 + it_3 & t_2 + it_1 \\ 0 & -t_2 + it_1 & t_0 - it_3 \end{pmatrix}, \tag{6.86}$$

where $\sum_{i=0}^{3} r_i^2 = \sum_{i=0}^{3} s_i^2 = \sum_{i=0}^{3} t_i^2 = 1$. The matrices R, S and T will be calculated from $w(n)$. In general, we have for $w(n)$

$$w(n) = \begin{pmatrix} w_{00} & w_{01} & w_{02} \\ w_{10} & w_{11} & w_{12} \\ w_{20} & w_{21} & w_{22} \end{pmatrix}, \tag{6.87}$$

where w_{ij} is a complex number. Firstly, we can set $S(n) = T(n) = \mathbb{1}$ and update $g(n)$ with the $R(n)$ matrix. In this case, we can ask ourselves what is the values that r_0, r_1, r_2 and r_3 need to have for $\mathrm{Re\ tr}[R(n)w(n)]$ to be extremized, given a fixed $w(n)$, with the constraint that $\sum_i r_i^2 = 1$. This is a extremization with constraints problem, which can be solve, for example, with the method of Lagrange multipliers. This results in

$$\begin{aligned} r_0 &= \frac{\mathrm{Re}[w_{00} + w_{11}]}{\lambda_R} \\ r_1 &= -\frac{\mathrm{Im}[w_{01} + w_{10}]}{\lambda_R} \\ r_2 &= -\frac{\mathrm{Re}[w_{01} - w_{10}]}{\lambda_R} \\ r_3 &= -\frac{\mathrm{Im}[w_{00} - w_{11}]}{\lambda_R}, \end{aligned} \tag{6.88}$$

with $\lambda_R = \sqrt{\mathrm{Re}\left[w_{00} + w_{11}\right]^2 + \mathrm{Im}\left[w_{01} + w_{10}\right]^2 + \mathrm{Re}\left[w_{01} - w_{10}\right]^2 + \mathrm{Im}\left[w_{00} - w_{11}\right]^2}$. This is equivalent to an $SU(2)$ update, Eq. 6.81, in the case that the submatrix of $w(n)$ relevant to the calculation is proportional to a $SU(2)$ matrix. In an iterative fashion, we can then use the matrix $w'(n) = R(n)w(n)$, with the $R(n)$ update as calculated above, and use this for the following update with the submatrix associated to $S(n)$. The result for the s_i is

$$\begin{aligned} s_0 &= \frac{\mathrm{Re}[w'_{00} + w'_{22}]}{\lambda_S} \\ s_1 &= -\frac{\mathrm{Im}[w'_{02} + w'_{20}]}{\lambda_S} \\ s_2 &= -\frac{\mathrm{Re}[w'_{02} - w'_{20}]}{\lambda_S} \\ s_3 &= -\frac{\mathrm{Im}[w'_{00} - w'_{22}]}{\lambda_S}, \end{aligned} \tag{6.89}$$

and as with the R update, λ_S needs to obey $\sum_i^4 s_i^2 = 1$. Analogously, for $T(n)$

$$\begin{aligned} t_0 &= \frac{\mathrm{Re}[w''_{11} + w''_{22}]}{\lambda_T} \\ t_1 &= -\frac{\mathrm{Im}[w''_{12} + w''_{21}]}{\lambda_T} \\ t_2 &= -\frac{\mathrm{Re}[w''_{12} - w''_{21}]}{\lambda_T} \\ t_3 &= -\frac{\mathrm{Im}[w''_{11} - w''_{22}]}{\lambda_T}, \end{aligned} \tag{6.90}$$

where $w''(n) = S(n)w'(n)$. In the end we have the complete update $A(n) = T(n)S(n)R(n)$.

We emphasize here once more the fact that the $A(n)$ matrix build this way is not the matrix which extremizes Re tr$[A(n)w^{\rm old}(n)]$. But since each step is guaranteed to increase the real part of the trace of $w(n)$, as the number of "hits" of this algorithm grows, we asymptotically approach the maximum. However, the extra work (and time to perform it) may not translate into an actual time improvement to attain the gauge-fixing condition, so that an efficiency study is needed to find out how much is it worth it to go the extra mile. This is presented in sections 8.1.1 and 8.1.2.

In order to obtain the $SU(3)$ matrix which extremizes $E[g(n)] =$ Re tr$[A(n)w^{\rm old}(n)]$ in an analytical closed form, one can, in principle, try also a procedure of extremization with constraints. Parametryzing again $A(n) = T(n)S(n)R(n)$, with the T, S and R matrices given by Eqs. 6.84-6.86 and a fixed $w(n)$, we can treat $E[g(n)]$ as a function of the r_i, s_i and t_i, under the constraint that $\sum_i r_i^2 = \sum_i s_i^2 = \sum_i t_i^2 = 1$. However, when one tries to apply the Langrange multiplier method in this case one generates an intricate system of non-linear coupled equations between the variables and the multipliers. Unfortunately we could not find the solution to this system, even with the help of symbolic manipulation software.

6.2.3 Stochastic overrelaxation

Inspired also by $SU(2)$ methods (71), we can propose stochastic updates, with the aim of avoiding regions with little variation in the global functional, Eq. 4.23. In SU(2), what one does is update the gauge transformation as

$$A^{\rm SOR}(n) = \begin{cases} A^{\rm LA}(n) & \text{with probability } 1-p, \\ \left(A^{\rm LA}(n)\right)^2 & \text{with probability } p, \end{cases} \tag{6.91}$$

in which $A^{\rm LA}(n)$ is the Los Alamos update, given by Eq. 6.81. What this does is that with probability $1-p$ the functional goes to its maximum and with probability p the value of the functional does not change, but we do jump to another region in the space of gauge-transformations, improving our exploration and reducing the chance of getting trapped in regions where the functional does not change significantly. In order to show that the functional does not change if we perform the $\left(A^{\rm LA}(n)\right)^2$ update in the $SU(2)$ case, we can notice that, since $h(n)$ is proportional to an $SU(2)$ matrix,

$$\begin{aligned} \text{Re tr}[(A^{\rm LA})^2 g^{\rm old} h] &= \text{Re tr}[\mathcal{P}_{\rm SU(2)}(h^\dagger g^{\rm old\dagger} h^\dagger g^{\rm old\dagger}) g^{\rm old} h] \\ &= \text{Re tr}\left[\frac{h^\dagger}{\sqrt{\det(h)}} g^{\rm old\dagger} \frac{h^\dagger}{\sqrt{\det(h)}} g^{\rm old\dagger} g^{\rm old} h\right] \\ &= \text{Re tr}[g^{\rm old\dagger} h^\dagger] \\ &= \text{Re tr}[g^{\rm old} h], \end{aligned}$$

where we have used the cyclic property of the trace, the unitarity of $g(n)$ and that $h^\dagger h = \det(h)$. The last equality follows if we remember that, also for SU(2), $g(n) = g_0 \mathbb{1} + i\vec{g}.\vec{\sigma}$ and similarly for $h(n)$.

In SU(3), since h is not proportional to an element of the group, we do not have that $\text{Re tr}[(A^{\text{LA}})^2 g^{\text{old}} h] = \text{Re tr}[g^{\text{old}} h]$. In fact, we can verify that this equality is not satisfied when performing the updates during the gauge-fixing. However, we also verified that, in practice, the fixing with the same scheme as in Eq. 6.91 for $SU(3)$ is still considerably more efficient: occasional increases in the value of the global functional are more than compensated by the higher mobility in the space of gauge transformations, as will be demonstrated in section 8.1.1.

6.2.4 Overrelaxation

Another way of accelerating the process of convergence for the Landau gauge condition is using the usual overrelaxation method (108). It turns out, that for $SU(3)$ this was the fastest option, as will be seen in Sect. 8.1.1. In this method, one uses a fixed power ω of the update matrix, $A^{\text{LA}}(n)^\omega$, instead of $A^{\text{LA}}(n)$. The exponent must be such that $1 \leq \omega \leq 2$, where, of course for $\omega = 1$ we have the usual Los Alamos algorithm, which corresponded to $p = 0$ for the stochastic overrelaxation and $\omega = 2$ corresponds to $p = 1$. The update $A^{\text{LA}}(n)$ is calculated with the iterative procedure described in 6.2.2, and here the optimal amount of hits is also a parameter to be fixed, besides the optimal ω. We verified, however, that just like for the stochastic overrelaxation method, here the best value for the amount of hits is 2, taking into account the number of sweeps and the time of execution of the algorithm, and due to this we will concentrate on showing the results for the optimization of ω only.

To evaluate the ω power of the matrix $A^{\text{LA}}(n)$, we use the following formula

$$A^\omega = \sum_{m=0}^{\infty} \frac{a_m(\omega)}{m!} (A - \mathbb{1})^m, \tag{6.92}$$

where

$$a_m(\omega) = \frac{\Gamma(\omega + 1)}{\Gamma(\omega + 1 - m)}. \tag{6.93}$$

In practice we truncate the series in its second term and project to SU(3), since as the gauge-fixing proceeds, the updates quickly get closer to the unity matrix, which justifies this approximation. The projection to $SU(3)$ is done via the formula 6.66.

6.3 Fermion operator inversion

The inversion of fermionic operators is a major problem in lattice gauge-theories, and algorithmic developments in this field have been very important in the last decades, and vital to ensure that unquenched simulations with low pion masses are now feasible with relatively moderate computational resources.

In principle the inversion is a linear algebra problem of trying to find the vector x, which solves

$$A\mathbf{x} = \mathbf{b} \tag{6.94}$$

for a particular source $\mathbf{b}$, where A is a matricial operator. We can obtain the j-th column of the inverse matrix A^{-1} by setting $b_i = \delta_{ij}$ and solving the system. If we want multiple columns of the matrix, we just need to vary j.

In order to invert the fermionic matrix numerically, we use the BiConjugate Gradient - Stabilized, in short Bi-CGSTAB (46,109). It is part of a family of Krylov solver conjugate gradient algorithms (50, 110, 111). The idea behind these algorithms is to firstly transform the linear algebra problem in 6.94 into an extremization problem. The algorithm then goes on to create search vectors $\mathbf{p}_i$ at each iteration. These vectors are perpendicular to all previous $A\mathbf{p}_j$, thus creating a vector space called a Krylov subspace. The solution is given as a linear combination of an initial guess vector and the search direction vectors. For these algorithms, one does not need to store the A matrix in memory, but only vectors. The algorithm involves matrix-vector products and vector-vector products only.

For the case of the Dirac operator inversion, A is a sparse matrix having entries which correspond to the diagonal elements and the nearest neighbors in position space. The matrix-vector product is performed by having a function or procedure which implements the action of the matrix on the vector, without actually performing the product row by row, since this would be wasteful, as most of the time we would be calculating products with 0.

At the moment of the convergence, the $\mathbf{x}$ vector will contain an approximation to

$$\mathbf{x} = A^{-1}\mathbf{b}, \tag{6.95}$$

which is a column of A^{-1} if $\mathbf{b}$ is the point source. Thus, if we perform the product with a matrix R to the point source $b_i\delta_{ij}$ before the inversion, and use this transformed source $R\mathbf{b}$ instead, $\mathbf{x}$ will turn out to be

$$\mathbf{x} = A^{-1}R\mathbf{b} = (A^{-1}R)\mathbf{b}, \tag{6.96}$$

which is a column of $(A^{-1}R)$.

The pseudocode for the BiConjugate Gradient algorithm is presented in the Algorithm Table 1.

Algorithm 1 BiCG-Stab

$\mathbf{r}^{(0)} = \mathbf{b} - A\,\mathbf{x}^{(0)}$
$\tilde{\mathbf{r}} = \mathbf{r}^{(0)}$
$i = 1$
while converged=False **do**:
    $\rho_{i-1} = \tilde{\mathbf{r}}^{\dagger} \cdot \mathbf{r}^{(i-1)}$
    if $\rho_{i-1} == 0$ **then**
        Method fails.
        break
    if $i == 1$ **then**
        $\mathbf{p}^{(1)} = \mathbf{r}^{(0)}$
    else
        $\beta_{i-1} = \alpha_{i-1}\,\rho_{i-1}/(\omega_{i-1}\,\rho_{i-2})$
        $\mathbf{p}^{(i)} = \mathbf{r}^{(i-1)} + \beta_{i-1}\left(\mathbf{p}^{(i-1)} - \omega_{i-1}\,\mathbf{v}^{(i-1)}\right)$
    $\mathbf{v}^{(i)} = A\mathbf{p}^{(i)}$
    $\alpha_i = \rho_{i-1}/(\tilde{\mathbf{r}}^{\dagger} \cdot \mathbf{v}^{(i)})$
    $\mathbf{s} = \mathbf{r}^{(i-1)} - \alpha_i\,\mathbf{v}^{(i)}$
    if $\mathbf{s}^{\dagger} \cdot \mathbf{s} <$ tolerance **then**
        $\mathbf{x}^{(i)} = \mathbf{x}^{(i-1)} + \alpha_i\,\mathbf{p}^{(i)}$
        converged=true
        break
    else
        $\mathbf{t} = A\,\mathbf{s}$
        $\omega_i = \mathbf{t}^{\dagger} \cdot \mathbf{s}/(\mathbf{t}^{\dagger} \cdot \mathbf{t})$
        $\mathbf{r}^{(i)} = \mathbf{s} - \omega_i\,\mathbf{t}$
        $\mathbf{x}^{(i)} = \mathbf{x}^{(i-1)} + \alpha_i\,\mathbf{p}^{(i)} + \omega_i\,\mathbf{s}$
        $i = i + 1$

6.3.1 Tests on the inversion of Dirac operator

The most obvious test to an implementation of the inversion algorithm is to test if the resulting $\mathbf{x}$ is indeed a column of the inverse. This can be done by performing the operation $A\mathbf{x}$ and checking the result to see if it is approximately equal to the point source. By reducing the tolerance both should get closer. Another test can be performed by noticing that the initial guess vector $\mathbf{x}^{(0)}$ is not specified. Different $x^{(0)}$ should converge to the same $\mathbf{x}$ within numeric precision.

If the inverse matrix is known analytically in some limit, this can also be used to test the algorithm. This is the case for the Wilson-Dirac operator. For the free case, an analytical formula is available in momentum space. One can then obtain the inverse of A through the algorithm, perform a Fourier transformation and compare with the analytical formulas.

For the interacting case, when the Dirac operator is not known analytically in closed form, one can also perform a few tests. One of them is to calculate hadronic correlators,

which are gauge-invariant. For the pion, the hadronic correlator is given by

$$C_{\pi^{\pm}}(n_t) = \sum_{\vec{n}\in\Lambda_3} \sum_{\alpha,\beta,a,b} \left| \left(\mathcal{M}^{-1}\right)_{\alpha\beta,\, ab} (n|0) \right|^2 . \tag{6.97}$$

One calculates the pion correlator for the same configuration with different random gauge transformations and compare the results. A difference between hadronic correlators would signal a bug in the code.

For a small enough lattice, say a lattice with $4^4 = 256$ lattice points, some more explicit tests can be performed. One can check that the implementation of the matrix A as the operator that acts on a vector v and returns Av gives the same result as the explicit matrix form of A. This can be done, for example in a symbolic manipulation software, such as Mathematica. Also, for small lattices, the interacting A can be inverted in Mathematica for a few configurations, and the result can be compared with the inversion performed by the production C code.

All the tests described above were performed on the program used to invert the Wilson-Dirac fermion operator numerically.

6.4 Code

The latest version of the code used for the configuration generation, gauge fixing and operator inversion can be found in the Github repository (112) under a GPLv3 license.

For the transformation to momentum space, we use the fast Fourier transform implementation of the fftw3 library (113).

7 LITERATURE REVIEW OF QUARK PROPAGATORS ON THE LATTICE

There has been a considerable progress in obtaining and analyzing data from lattice quark propagators. Much of this is motivated by the desire to understand the confinement and dynamic chiral symmetry breaking mechanisms of QCD. These studies are usually part of programs of obtaining other Green's functions of QCD, such as the gluon and ghost propagators, and sometimes vertices.

We can divide the articles published on this subject in many different ways. One of them is by groups and collaborations. We decided to give an overview of the studies based on this criterion, although this is not so clear cut sometimes, because it allows us to follow the methodologies as they developed over the years.

We have focus solely on quark propagator studies with the $SU(3)$ gauge group on the lattice.

7.1 American collaboration

The first paper on the literature on the quark propagator on the lattice is by Professors Claude W. Bernard and Amarjit Soni, and by Drs. Kenton K. Yee and Daniel Murphy (114). There, they study the quark propagator for Coulomb and Landau gauge for quenched configurations, and Wilson fermions are used. The paper shows form factors in configuration space and from those a dynamical quark effective mass of $\approx 350\,\mathrm{MeV}$ is extracted. Following up on this first article, they have explored the quark propagator further in (115), specially the gauge variance of the effective mass, showing a small, albeit statistically significant, dependence in the class of λ-gauges, which comprise the Landau ($\lambda = 1$) and Coulomb ($\lambda = 0$) gauges as limiting cases.

In (116), a value of $350(40)\,\mathrm{MeV}$ is cited for the infrared quark mass in Landau gauge and the researchers reaffirm a gauge-dependence for the effective quark mass.

7.2 Adelaide group

The group that has published most papers on the subject is the Adelaide University CSSM Lattice group. The studies of the group were initiated in the mid-nineties by professors Jon-Ivar Skullerud and Anthony G. Williams and are now centered around Prof. Derek Leinweber and Dr. Waseem Kamleh. Other people based in this center who contributed significantly along the way are Dr. Patrick O. Bowman, Prof. Urs M. Heller, Prof. Jianbo Zhang, Dr. Frédéric D. R. Bonnet, Dr. Maria B. Parappilly, Dr. Peter J. Moran, Dr. Amalie Trewartha, and Adam Virgili.

Although the seminal works of this group used Wilson-Clover fermions (87,117–121), they have moved since the early 2000s to other discretizations. Several studies were produced between 2001 and 2010 using Kogut-Susskind and Asqtad fermions (122–128), which are types of staggered fermions. Since 2002, however, most studies were produced with overlap fermions (120, 124, 129–146), which offer better chiral properties as explained in Chap. 5.

One caveat of the overlap propagator studies, that might be worth mentioning, is that, due to the high cost of calculating overlap propagators, the gauge configurations cannot currently be generated from them. Therefore, their results with overlap fermions have been calculated with configurations which are either quenched or generated with less demanding fermion discretizations, such as the ones produced by the PACS-CS collaboration which uses Wilson-Clover or the ones by the MILC collaboration using staggered fermions. Regarding the overlap propagators, they have implemented many improvements to the overlap kernel along the way, such as introducing the FLIC (fat-link irrelevant clover) kernel in (134) and adding stout-link smearing to the fermion actions in (136). Among the explorations of the overlap quark propagator, they produced studies of unquenching effects (125, 127, 145) and scaling behavior (126, 130–132), showing how the form factors that characterize the propagator change with a change in the lattice spacing and, sometimes, extrapolating to the $a \to 0$ limit.

Even though, just like the rest of the community, their default gauge of choice is Landau gauge, they have also produced interesting results in the Laplacian gauge, which is free of the Gribov ambiguity (122, 123, 133, 147).

The first paper considered in this section, by Professor Skullerud, (117) was actually produced at the time of his PhD at Edinburgh University, but we include it here because we find that it naturally gave rise to the ones that follow. In it, using clover improved quarks, he introduced the study of momentum space form factors and observed that the Landau gauge quark propagator seems to present a clear signal, which allows its determination with relatively small errors even with modest statistics. The quark wave-function improvement and the "tree-level correction", which are necessary for Wilson fermions and were presented in Sect. 5.6, were first implemented in (87, 118). The form factors found in these studies show roughly the same shape that was later obtained in all subsequent studies, including the characteristic infrared behavior showcasing dynamical mass generation for $M(p)$, with a chiral limit extrapolation of $M(0) \approx 300\,\mathrm{MeV}$, and suppression of the quark renormalization function $Z(p)$. A hybrid tree-level correction was introduced in (119), where non-perturbatively determined coefficients were used in place of the mean-field values employed previously.

Results for the plain and improved staggered quark propagators are displayed in (122, 123), where a comparison is made between Landau gauge and Laplacian gauge. The mass function shows no gauge dependence, although the infrared supression of $Z(p)$ is

larger in the Laplacian case. A chiral extrapolation is tried, obtaining a $M_{\text{chiral}}(p)$ slightly below 300 MeV. In (121) the researchers model the tail of the quark propagator mass function with two Ansätze, and are able to extract values for the chiral condensate from the data. In the same study, stronger finite volume effects are seen for $Z(p)$ than for $M(p)$. Unquenching of the staggered propagator was studied in (125), where it was shown that dynamical sea quarks have a rather small effect on the resulting form factors, thus displaying the importance of gluons for the dynamical generation of mass. In the theme of unquenching, it was also verified that the mass of the sea quarks matters very little in the form factor results (126, 127), at least in the range explored in the paper. These studies also show that a lattice spacing of 0.12 fm seems to be enough for the staggered form factors to be insensitive to the cutoff.

In (120, 129), the overlap quark propagator was calculated. A relevant property of overlap quarks is that their propagators need no tree-level correction. Form factors were extracted for several bare quark masses and although they disagree quantitatively with the previous clover improved Wilson quark results, the authors claim that an agreement was obtained with the staggered formalism. The qualitative shape of the curves is similar in the infrared for all discretizations. A linear chiral extrapolation gives, again, a value of around 300 MeV.

A study of the scaling of the overlap form factors was performed in (130–132), where the authors concluded that they were close to the continuum limit, although a finer lattice would be desirable and also larger volumes would allow them to establish the behavior of the quark wave-function renormalization with more precision, as this form factor seems to be more sensible to finite volume effects (124). A mass dependence of $Z(p)$ is seen in the infrared. A comparison with staggered fermions is given in (124), where both are shown to agree over a wide range of momenta. The overlap quark propagator in Laplacian gauge is compared to the Landau gauge one in (133) and, like in the staggered case, the mass function generally agrees in both gauges, with the wave-function renormalization showing some gauge-dependence with a stronger supression in the infrared. A scaling analysis of the overlap fermion with the improved FLIC (fat-link irrelevant-clover) kernel is performed in (134), where the authors conclude that the improved kernel scales better than the simple one they used previously.

Unquenching of overlap quark propagators was studied in (135). As was the case for staggered fermion unquenching, the mass function is mostly insensitive to the sea-quark mass, at least for values in the range considered. The $Z(p)$ has a slightly more pronounced dependence on the mass of the sea-quarks, especially in the infrared. The effect of smearing in the form factors was also found to be very small (136, 137). Partly in response to the Maynooth-Coimbra study with Wilson fermions (97), to be discussed in the next section, the Australians produced (144), with dynamical quarks close to the physical pion mass.

The main point of divergence with the earlier study was that the $Z(p)$ found by the Europeans showed a week non-monotonic dependence on the momentum, whereas the most recent study has found an absolutely monotonic growth in the quark renormalization function as the absolute value of the momentum increases.

One of their major lines of investigation from 2010 onward has been analyzing what mechanism drives the chiral symmetry breaking in QCD. The importance of instantons and the associated center vortices in the QCD vacuum and their effect on the mass and renormalization functions of the quark propagator have been explored in (128, 138–143, 145, 146).

Using a smearing technique designed to retain and isolate the instanton content of the QCD vacuum, the authors of (138, 139) obtained that, after many levels of smearing were performed, they could still reproduce most of the non-perturbative mass function from overlap quarks in a background of configurations dominated by instantons, thus providing a possible link between these topological objects and the spontaneous breaking of chiral symmetry. The infrared suppression of the $Z(p)$ function is shown to become milder in the instanton background.

In (128), using staggered fermions, it was found that removing center vortices from the configurations, although drastically reducing the string tension of the quark-antiquark potential, did little to reduce dynamical chiral symmetry breaking, as measured by the mass function. However, the authors of (140–142), using overlap quarks, found that vortex removed configurations showed an elimination of dynamical mass generation. The vortex-only ensembles also showed little mass generation in the infrared, however, after cooling (a technique to reduce the roughness of the configuration) was implemented, the authors were able to reproduce the behavior of untouched configurations, with regards to the propagator form factors. The authors claim that smoothing, be it through cooling or smearing, exposes a connection between the vortices and instanton objects, being a step necessary to the manifestation of chiral symmetry breaking in vortex-only configurations. It was also found in (143), done with dynamical quarks close to the physical point, that the removal of center-vortices suppressed dynamical chiral symmetry breaking. In the wave-function renormalization function, a stronger suppression is seen in the infrared on vortex-removed configurations in comparison with the untouched ones. In (145), it was found that a clearer picture can be established with respect to the role of center vortices as drivers of QCD low-energy dynamics when dynamical fermion configurations are used. In particular, as pertaining to the quark propagator, the suppression of dynamical mass is stronger for unquenched configurations. Finally, (146) presents even stronger evidence of the role of center vortices to the low-energy dynamics of QCD, specially the chiral symmetry breaking mechanism, also using dynamical configurations close to the physical point.

7.3 Maynooth-Coimbra-Adelaide collaboration

After publishing a few seminal papers during his time in Adelaide in the 90s and early 2000s, already discussed in the previous section, Prof. Jon-Ivar Skullerud, has published articles in collaboration with professors Orlando Oliveira, Ayşe Kızılersü, Paulo Silva and Dr. André Sternbeck. Their articles have focused on Wilson-Clover fermions in Landau gauge for unquenched configurations (97, 148) and a range of quark masses, with their smallest corresponding to physical pion masses. They obtained a mass function with the same qualitative shape as previous lattice studies, with $M(0) \approx 320\,\mathrm{MeV}$. The dependence of the $Z(p)$ with respect to quark masses is small in the ultraviolet, and some dependence is detected for small momenta: the quark renormalization function $Z(p)$ is suppressed as the mass is reduced, although some suppression is shown to be due to the finite volume of the lattice. In order to try to reduce lattice artifacts, they perform a $H4$ extrapolation (97, 149), which takes into consideration the fact that the lattice has a hypercubic symmetry, and extrapolate to the limit where the hyperspherical symmetry is recovered. The results of the $H4$-extrapolation were mixed, as they also increase the uncertainties, specially for the mass function.

The Coimbra components of this collaboration, together with Alexandre Falcão have explored the analytical structure of propagators in (150, 151). Regarding quark propagators in particular, they report to have detected no complex poles, predicted by some Dyson-Schwinger studies. They also report a possible pole for Minkowski-like momenta at $p^2 \approx -0.2\mathrm{GeV}^2$, which is interpreted as an effective quark mass. However the value obtained $\approx 450\,\mathrm{MeV}$ is larger than what is usually associated for constituent quark masses $\approx 300\,\mathrm{MeV}$. The technique they used to extend the lattice data collected for Euclidean momenta to the rest of the complex plane is based on Padé approximants. At least preliminarily, the position of the pole was observed to correlate with the square of the pion mass as required by the PCAC relation if this is to be identified with a quark mass.

A Coulomb gauge study in which we were involved in collaboration with some members of this group has been tried recently (152), but results were not easily reconciled with previous work and the situation for this gauge choice seems to be more subtle. This was produced using anisotropic lattices with Wilson quarks improved with a clover term.

7.4 Japanese collaboration

In the mid 2000s Professors Sadataka Furui and Hideo Nakajima produced some results for the quark propagators using staggered fermions. In (153), even though their primary goal was to perform a study to verify the Kugo-Ojima confinement criterion and the effect that unquenching has on the said criterion, they incidentally mention that the

quark renormalization function is suppressed in the infrared, in accordance with what was found in many other studies of the quark propagator. In their article (154), they find results for form factors with a behavior that agrees with the previous literature, with an infrared suppressed Z function largely independent on the bare mass and a M function showing dynamical mass generation in the infrared, with the amount of generated mass being smaller for heavier quarks. They then go on to calculate condensates from the quark propagator, via a relationship presented in (155, 156) and link the behavior of the renormalization function to the Kugo-Ojima confinement criterion.

In (157), Professor Furui calculated the quark mass function for a few lattice momenta close to the diagonal and using the domain wall fermion discretization. Results showed a rough compatibility to previous ones using the staggered fermion discretization.

7.5 Tübingen-Graz collaboration

Starting in 2010 in Tübingen and then continuining in Graz, Dr. Mario Schröck with his collaborators Professors Giuseppe Burgio, Hugo Reinhardt and Markus Quandt and later Dr. Markus Pak and Dr. Hannes Vogt, produced results on the quark propagator using chirally improved, overlap and Asqtad fermions, a type of staggered fermion. In their work, besides Landau gauge, they also explored Coulomb gauge and the maximally Abelian gauge.

In the context of studying the gluon and ghost propagators and comparing results for Coulomb and Landau gauge, members of the collaboration report some results for the quark propagator in (158). These are quenched results using staggered fermions. For the Coulomb gauge quark propagator, the study finds that a term proportional to $p_0 \not{\vec{p}}$, that is in principle allowed in the quark propagator, vanishes. Thus the number of non-trivial form factors is reduced to 3. They integrate over p_0 to get the static quark propagator $S(\vec{p})$. The form factors of the static quark propagator seems to indicate a vanishing value for $Z(\vec{p})$ in the infrared, and dynamically generated mass in the form of an enhancement of $M(\vec{p})$ in the infrared, as is typical for quark propagator studies.

The studies (159,160) present a method for artificially restoring chiral symmetry by removing low-lying eigenmodes of the valence Dirac operator. They showcase the method in an unquenched ensemble. Their choice for the fermion discretization is the chirally improved propagator, which they use as sea quarks as well as valence quarks. It is shown what is the effect in the form factors Z and M in Landau gauge. The typical Landau gauge finite value for the Z form factor in the infrared is completely suppressed until vanishing in the infrared after removing a large number of eigenmodes, although its ultraviolet behavior is unaltered. For M a supression is also seen after a severe removal of eigenmodes, even though the chiral partners ρ and a_1 become degenerate after a moderate removal. This indicates that chiral symmetry is already restored for a less aggressive removal than what

is needed to completely supress the mass function M. This is puzzling, as it seems to indicate that dynamical mass is still being generated even in a chiral symmetric vacuum.

This collaboration has also obtained results quark propagator in Coulomb gauge (161). The interest in Coulomb gauge arises from continuum analyses in the context of studying the dispersion relations of gluons and ghosts in the Gribov-Zwanziger framework (162). They aim at extending this to the quark sector. Quenched and unquenched ensembles are utilized, where staggered fermions are chosen for the sea (in the unquenched case) and valence quarks. The results show that a possible form factor A_d allowed in Coulomb gauge for the inverse propagator, associated with a $p_j\sigma_{j4}$ Dirac structure vanishes. They also show that the form factors have no energy dependence, depending solely on the spatial momentum. The mass form factor M is shown to coincide with the Landau gauge result, giving a chiral mass of $M(0) = m_\chi = 310(10)\,\mathrm{MeV}$ in the deep infrared. The Z form factor shows gauge dependence, with a behavior that indicates $Z \to 0$ as $|\vec{p}| \to 0$, different from Landau gauge, where a finite value is achieved in the infrared. The form factor α associated to $\gamma_t p_t$ in the quark propagator is shown to vanish unless one fixes the residual gauge freedom between different time slices, which the Coulomb gauge condition does not constrain. When this residual gauge freedom is fixed, using the Integrated Polyakov Gauge, α is non-zero, allowing for the obtainment of the quark dispersion relation, which displays a divergent behavior in the IR. The authors claim that this extends the Gribov-Zwanziger scenario of gluons and ghosts to the quark sector, in which a divergent dispersion relation indicates confinement, (162). They also perform a scaling analysis of the Coulomb gauge quark propagator, concluding that it is multiplicatively renormalizable, and that their results are close to the continuum limit. By comparing the unquenched and quenched results, it is checked that the effects of unquenching are rather mild.

In (163, 164), Dr. Schröck and collaborators have further explored the connection between confinement and chiral symmetry breaking in Coulomb gauge, using the chiral symmetric overlap fermions and a quenched ensemble this time. Again, their use of Coulomb gauge is motivated by some earlier works in the continuum, which predicted that the quark renormalization function Z goes to 0 in the deep infrared and which linked this behavior to confinement. Conversely their A_S and B dressing functions should diverge for small momenta. They indeed get indications that Z vanishes in the infrared, confirming the continuum predictions and in consonance to their staggered fermion results. In harmony with most studies, Z seems not to depend on the valence quark masses. For the M form factor, the authors obtain the usual enhancement at low momenta, and even though they cannot get too deep in the infrared, an estimate gives a value of around 300 MeV for vanishing momentum in a chiral extrapolation. Once more the shape of the M form factor is similar to the one obtained in Landau gauge in other studies. In the second part of (164), the researchers restore chiral symmetry artificially by removing the low-lying Dirac eigenmodes of the valence propagator. With this, they see a suppression of $M = B/A$,

as expected, but A and thus Z, which is its inverse, remain roughly the same. This is interpreted as chiral symmetry being restored, but confinement staying intact.

In (165) the authors explore the gluon and quark propagator in maximally Abelian gauge (MAG). The motivation for this choice of gauge comes from the dual-superconductor picture of confinement, which states that the Abelian parts of the gauge fields should dominate the infrared dynamics. In maximally Abelian gauge the Abelian parts of the gauge fields are enhanced, which should presumably expose the dynamics more clearly. Like Coulomb gauge, this is considered an incomplete gauge, meaning that a residual gauge redundancy remains. This is fixed in their paper by applying the Landau gauge condition supplementary with respect to subset of Abelian gauge transformations. The ensembles considered in this study are composed by quenched and dynamical configurations using staggered fermions. The quark propagator is calculated using staggered fermions in all cases and the authors compare results for a background of gluon fields in Landau gauge, MAG, only diagonal MAG (that is, only the components associated to the Gell-Mann generators λ_3 and λ_8), only off-diagonal MAG. The MAG results show a mass function which is slightly higher than the Landau gauge one, but the data points generally agree within error bars (MAG error bars are larger, denoting a larger noise in comparison to Landau). The quark renormalization function shows gauge dependence when comparing both gauge choices, as was observed with Coulomb gauge before, with a stronger IR supression in the MAG case, although not as severe as the Coulomb supression. Diagonal only MAG results show dynamical generation of mass in the same order of magnitude as Landau gauge, even slightly higher, whereas off-diagonal MAG results show no dynamical mass generation and a value for the quark renormalization function which is close to its tree level value of 1. From this the authors claim that indeed the Abelian dominance hypothesis is justified when explaining QCD infrared dynamics.

7.6 Scattered studies

Some studies seem to not have established a long-living tradition of quark propagator calculations and/or have focused on the extraction of QCD constants such as the renormalized quark masses. We include references to them here, with a brief description of the relevant content for the sake of completeness.

In (166, 167) quark masses are extracted from fits to the tail of the momentum dependent mass form factor of the propagator. They use quenched configurations and Wilson quarks.

The European Twisted Mass Collaboration has also produced studies which show quark propagators form factors in Landau gauge. In (168), although the study is focusing on the determination of renormalization constants, some plots for the inverses of the form factors are shown. In (169), they used dynamical twisted mass configurations. By

comparing the Landau gauge quark propagator lattice data to a perturbation series, they are able to estimate the quark mass and chiral condensate, getting values that agree with other estimates, but with larger error bars. Although presented in lattice units, the plots seem to have the general shape found in Landau gauge propagator studies, with a mass function presenting dynamical mass generation in the infrared and the quark renormalization function attaining a finite value for low momenta and saturating at high momenta.

Gauge dependence was detected in a study comparing the Landau gauge quark propagator form factors with covariant-gauge ones (170).

In (171), plots are shown of the quark propagator form factors. The Landau gauge mass function shows the usual shape and the renormalization function has a dip in the infrared, but has a non-monotonic behavior as the absolute value of the momentum grows, as was also found latter in (97), discussed in Sect. 7.3. They use domain-wall fermions, which is an alternative chiral fermionic discretization on the lattice.

A technique to reduce lattice artifacts is applied to the quark propagator in (149). Incidentally, the authors conclude that overlap propagators have larger hypercubic artifacts than the ones calculated with clover improved quarks.

7.7 Finite temperature studies

The first study of quark propagators on the lattice at finite temperature was produced by Masatoshi Hamada, Hiroaki Kouno, Atsushi Nakamura, Takuya Saito, and Masanobu Yahiro, (172). They were based on several research centers in Japan. They performed a study on quenched configurations using plain and clover improved Wilson fermions in Landau gauge. Firstly, a different behavior is shown before and after the confinement phase transition: for low temperatures the mass function of the quark propagator increase quickly, whereas for high temperatures, they still see an increase albeit slower (the temperature dependence is further explored in a follow-up paper (173)). The researchers have obtained a linear relation between the thermal quark mass and the temperature, as predicted by a perturbative calculation (74). Their definition of the quark thermal mass is given by the mass function at 0 momentum. When comparing the plain Wilson fermions with the clover ones, they obtain that Wilson quarks present a mass function which is about 20% larger than the clover counterparts.

In (174), Dr. Paulo Silva and Prof. Orlando Oliveira of Coimbra University, reported results for quark propagators at finite temperature using Wilson fermions non-perturbatively improved with the clover action using quenched configurations in Landau gauge. They show that as the theory passes the transition temperature, the mass function, for the lowest momentum and Matsubara frequency available, decreases to about half of

its value in comparison to the low temperature case. The mass function, however, remains large in comparison to the bare quark masses, which should signal that chiral symmetry is not completely restored at the highest temperature of 275 MeV used in the study. Reference (175) complements this initial study by going to higher temperatures (up to 324 MeV) and presenting more detailed plots for all form factors. For these higher temperatures, the mass function shows a flattening for small momenta, beginning at 290 MeV.

As was explained in Sect. 3.3, as the temperature increases the absolute value of the Polyakov loop becomes non-zero and for each configuration, one may associate a particular sector corresponding to a center element of $SU(3)$, which is determined from the argument of the complex value of Polyakov loop. In (176), the authors explored what happens to propagators obtained from configurations in different sectors of the Polyakov loop. They found that the thermal behavior of the quark propagators in the infrared is extremely sensitive to the gauge sector, even though the configurations are quenched and, therefore, center transformations are a symmetry of the action. For high-temperatures, the quark propagator from the $0\pi/3$ sector indeed tends to a free particle behavior. However, for the $2\pi/3$ and $4\pi/3$ sectors, the form factors strongly deviate from a trivial behavior, with the mass function showing a greater amount of dynamical mass generation, for example.

8 RESULTS

8.1 Gauge-fixing optimization results

8.1.1 Analysis of the stochastic overrelaxation parameters

We still need to discuss the value of p in Eq. 6.91 and the numbers of hits, as indicated at the end of section 6.2.2. A efficiency study is needed in order to fix the value of these two parameters. We also need to notice that, in principle, p can vary with all other parameters of the simulation: the inverse coupling β, the lattice size and number of hits of the gauge-fixing update.

The Los Alamos algorithm can be thought as a the $p = 0$ version of the stochastic overrelaxation algorithm. We can then study the gains offered by the stochastic overrelaxation together with the search for the optimal value of p, and have the Los Alamos algorithm as a particular case. For the study of the efficiency as a function of p, we will first hold $\beta = 5.9$, and will vary the lattice size (N^4, with $N = 4, 8, 10, 16$) and, for each lattice size, vary the number of local hits in the update (1, 2, 3 or 8).

An important aspect of the efficiency is that the typical number of sweeps needed to gauge-fix should be the smallest possible, when comparing different versions of the algorithm. In order to analyse this, we can establish what is the distribution of the number of sweeps needed to gauge-fix for a sufficiently big sample of configurations to have their gauges fixed. From these distributions we can obtain the typical number of sweeps needed and their dispersion. In this study, we analyzed the fixing for the same 200 configurations with size 4^4, 8^4 and 10^4 and 100 configurations of size 16^4, with different parameters, as explained in the paragraph above.

Some statistical indices for the 4^4 lattice are shown in Table 1. To obtain what is the typical number of sweeps, we prefer to look at the medians. This is because we noticed that a few configurations demand an exceptionally large number of sweeps to be fixed, which raises the mean and makes this indicator unsuitable, because it does not represent a value that is common for the number of sweeps. In any case, we present the values for the median, mean and standard deviation in the table, so that a few conclusions can be taken independently of what statistical index one may choose.

The first conclusion is that, very clearly, the Los Alamos algorithm, or $p = 0$, is worse than overrelaxation for a sufficiently high p, whatever the number of local hits one chooses to perform. Another result is that by performing 2 hits, the median (or mean) decreases, if p is adjusted accordingly. In other words, the minimal median, as a function of p, is lower for 2 hits in comparison with 1. We also observe that increasing the number of hits beyond 2 does not decrease the median significantly, so that one has little reason

to go beyond 2, since the extra work does not pay.

It is worth noting that for $1 > p > 0.78$, we observed that the algorithm does not converge in the 1 hit variant, which means that for these parameters, the movement in the space of possible gauge transformations does not compensate the low precision in the determination of $g(n)$. By performing 2 or more hits, the convergence occurs even for high values of p, such as 0.9999.

Moreover, the table shows that for the same p, here $p = 0.67$, the median is lower for a higher number of hits. We also see that the optimal value of p is lower for 1 hit ($p \approx 0.5$) and then increases for 2 hits ($p \approx 0.62$), however, as the number of hits goes beyond 2, the optimal value stabilizes.

Table 1 – Values for the median, mean and standard deviation for the distribution of the number of sweeps to attain the Landau gauge-fixing for different parameters, with $\beta = 5.9$ and lattice size 4^4. The sample size for these results was 200 configurations.

hits	p	median	mean	std. deviation
1	0	250	314.9	226.3
1	0.45	102.5	134.4	84.3
1	0.5	94.5	131.3	73.8
1	0.55	108	135.3	67.2
1	0.67	231	240.9	46.6
1	0.78	∞	∞	-
2	0	257	331.4	257.2
2	0.58	82	105.8	72.3
2	0.6	79.5	105.8	69.0
2	0.62	77	99.0	51.6
2	0.65	81	102.7	49.8
2	0.67	85	99.2	34.4
3	0	259	314.1	221.0
3	0.58	82	103.1	62.0
3	0.62	76	103.6	59.6
3	0.67	86	104.7	48.7
8	0	262	325.0	263.5
8	0.58	78.5	100.1	53.9
8	0.62	78	100.3	47.3
8	0.67	87	100.8	37.8

Source: By the author.

Observing the table for a lattice of size 8^4, we see that the general trends are the same as for the 4^4 one. We still have that $p = 0$ is a bad choice; 2 hits instead of 1 decreases the typical number of sweeps for gauge-fixing and going beyond this does not bring more benefits; and, lastly, the optimal p for 1 hit is lower than for 2 hits, and after that, the value remains constant. However, we also observe that the optimal p increases be it for 1

hit (from $p \approx 0.5$ to $p \approx 0.63$) or for 2 or more (from $p \approx 0.62$ to $p \approx 0.8$), in comparison with the 4^4 lattice. Thus, we can conclude that the optimal p depends on the size of the lattice considered, being larger for larger lattices.

Table 2 – Values for the median, mean and standard deviation for the distribution of the number of sweeps to attain the Landau gauge-fixing for different parameters, with $\beta = 5.9$ and lattice size 8^4. The sample size for these results was 200 configurations.

hits	p	median	mean	std. deviation
1	0	882	1158.4	1248.1
1	0.58	283	337.0	266.9
1	0.63	246	308.7	196.2
1	0.67	325	376.4	220.0
1	0.75	∞	∞	-
2	0	867.5	1173.1	1278.4
2	0.67	207	248.2	148.6
2	0.75	163.5	209.4	174.0
2	0.8	158.5	190.8	104.9
2	0.82	171	207.7	129.7
3	0.67	210.5	261.1	220.6
3	0.8	158	199.5	130.1

Source: By the author.

For the 10^4 lattice, whose results are presented in Table 3, we abandoned the Los Alamos algorithm ($p = 0$), given the results for smaller lattices, as well as the act of performing 3 or more hits, given the fact that no significant gain was seen. We can observe that the optimal value for p keeps growing with the lattice size, and that, now, it is $p \approx 0.67$ for 1 hit and $p \approx 0.82$ for 2 hits. This shows that as we continue increasing the lattice size, the "squared" step of the stochastic overrelaxation algorithm grows in importance, which is the step that is responsible for a higher motion in the space of possible gauge transformations and does not necessarily decrease the value of the functional. Doing this the algorithm does not get trapped in "flat" regions with low variation of the functional Eq. 4.23. The region of non-convergence for the 1 hit version continue being $p > 0.75$, as for the 8^4 lattice.

For the 16^4 lattice, the optimal p for 1 hit is approximately 0.67, and for 2 hits it is 0.89.

Lastly, for 2 hits and a 24^4 lattice, we have the results presented in Table 5. The 1 hit variation was not tried, as it became clear from the previous results that it is less efficient.

Table 3 – Values for the median, mean and standard deviation for the distribution of the number of sweeps to attain the Landau gauge-fixing for different parameters, with $\beta = 5.9$ and lattice size 10^4. The sample size for these results was 200 configurations.

hits ou sub	p	mediana	média	desvio padrão
1	0.60	420.5	530.2	390.1
1	0.63	400	463.7	246.7
1	0.67	372	458.9	206.0
1	0.69	468.5	537.2	249.7
1	0.75	∞	∞	-
2	0.67	349	446.4	356.3
2	0.8	218.5	264.1	136.8
2	0.82	201.5	245.2	114.0
2	0.84	210.5	268.8	151.9
2	0.87	239	268.3	166.5

Source: By the author.

Table 4 – Values for the median, mean and standard deviation for the distribution of the number of sweeps to attain the Landau gauge-fixing for different parameters, with $\beta = 5.9$ and lattice size 16^4. The sample size for these results was 100 configurations.

hits	p	median	mean	std. deviation
1	0.65	1200	1445.4	888.8
1	0.67	1170	1318.0	567.0
1	0.71	1190	1421.2	803.4
2	0.67	1192.5	1347.4	597.9
2	0.88	440	494.2	262.1
2	0.9	440	559.6	443.8

Source: By the author.

Table 5 – Values for the median, mean and standard deviation for the distribution of the number of sweeps to attain the Landau gauge-fixing for different parameters, with $\beta = 5.9$ and lattice size 24^4. The sample size for these results was 20 configurations.

hits	p	median	mean	std. deviation
2	0.67	3310.0	3954.0	1901.6
2	0.90	1260	1368.0	713.6
2	0.92	780	813.0	193.9
2	0.95	720	771.0	150.9
2	0.97	1020	1053.0	72.2

Source: By the author.

8.1.2 Execution time

As pointed out in Section 6.2.2, there is a balance between gains and losses when performing several update hits in the gauge-transformation at each site: one the one hand,

if we make many hits, we get closer to the local maximum, which should presumably have a positive influence on the extremization of the global functional; on the other hand, each hit takes some time to be performed, in such a way that performing multiple hits may not be compensated. Since we do not know *a priori*, what is the ideal number of hits, we are forced to turn to an empirical study.

The results of last section show that in practice it makes no sense to do more than 2 hits. It remains to be checked whether making 1 or 2 hits is best, when time is taken into account.

In order to measure what is the ratio between the characteric times for each variant, we can take a large number of sweeps in one configuration using the three algorithms and record the time it took for each of them. In the computer we used in this study, 100 thousand sweeps for a 4^4 lattice take 41.2 seconds for the 1 hit variant and 47.5 seconds for the 2 hits variant, with the ratio of the two being 1.153. We can then compare if the gain in sweeps shown in the previous sections compensates the extra time to perform the 2 hits in that variant. The results are presented in Table 6 in arbitrary time units, which should not be compared among different lattice sizes.

Table 6 – Optimal p, medians and approximate execution time in arbitrary units for the variants of the considered algorithms, with $\beta = 5.9$.

lattice size	hits	optimal p	median	aprox. execution time
4^4	1	0.5	94.5	1
4^4	2	0.62	77	0.94
8^4	1	0.63	246	1
8^4	2	0.8	158.5	0.74
10^4	1	0.67	372	1
10^4	2	0.82	201.5	0.62
16^4	1	0.67	1170	1
16^4	2	0.88	440	0.43

Source: By the author.

We see that, in each of the cases considered, performing 2 hits always brings a considerable gain in the time to process the gauge-fixing in comparison to the 1 hit alternative. We can also observe that as the lattice grows, this is even more the case.

8.1.3 Optimal p dependence with inverse coupling

Having estabilished that the best variant is the 2 hits one, we can ask ourselves how the optimal p value varies with β. The results we obtained for lattice sizes 8^4 and 10^4 for $\beta = 6.1$ and 8^4 for $\beta = 6.3$, are shown in Table 7.

As we see in the data, the optimal value for p in a 8^4 lattice with $beta = 6.1$ is $p \approx 0.78$, and for $\beta = 6.3$ one has $p \approx 0.77$, to be compared with the value for $\beta = 5.9$

Table 7 – Median, mean and standard deviation of the distribution of the number of sweeps needed for gauge-fixing for 2 hits, using the stochastic overrelaxation algorithm for different β, varying p.

β	lattice size	p	meadian	mean	std. deviation
6.1	8^4	0.60	234	343.71	385.47
6.1	8^4	0.75	169.5	207.69	109.11
6.1	8^4	0.77	165	204	121.8
6.1	8^4	0.775	162	198.3	96.2
6.1	8^4	0.78	162	203.1	111.1
6.1	8^4	0.785	164.5	211.7	180.5
6.1	8^4	0.79	168	204.0	87.9
6.1	8^4	0.795	165	210.4	183.7
6.1	8^4	0.80	165	207.9	141.3
6.1	8^4	0.82	175.5	209.7	104.7
6.1	8^4	0.85	207	225.3	43.2
6.1	8^4	0.9	309	315	21
6.1	10^4	0.80	216	308.8	357.3
6.1	10^4	0.81	211.5	299.0	266.3
6.1	10^4	0.82	216	272.8	171.7
6.3	8^4	0.75	178.5	227.5	163.3
6.3	8^4	0.76	182.5	226.1	150.1
6.3	8^4	0.765	179	233.8	162.7
6.3	8^4	0.77	172.5	219.7	134.4
6.3	8^4	0.775	173	228.0	157.9
6.3	8^4	0.78	178.5	215.6	111.2
6.3	8^4	0.79	174	227.3	143.6
6.3	8^4	0.8	178	222.0	133.0
6.3	8^4	0.81	174	215.7	96.8

Source: By the author.

which was 0.8. We see a slight decrease in the value for the optimal p in this β interval, however, it is rather mild and even using $p = 0.8$ we keep approximately the same number of sweeps. The typical number of sweeps also increases mildly as β grows, being 158.5 for $\beta = 5.9$, 162 for $\beta = 6.1$ and 172.5 for $\beta = 6.3$.

For the 10^4 lattice, we see a variation of the optimal p of approximately 0.82 with $\beta = 5.9$ to $p \approx 0.81$ for $\beta = 6.1$, following the decreasing that was also observed for lattices with 8^4 sites. The typical number of sweeps growns from 201.5 to 211.5 with this variation of β, which represents an increase of about 5%.

The results for the overrelaxation method are presented in Table 8, for several lattice sizes with $\beta = 5.9$. We notice here that when the lattice grows the optimal ω value gets close to 2, an analogous behavior to the stochastic overrelaxation, where p approaches 1. Comparing with the stochastic overrelaxation algorithm, we see that overrelaxation is more efficient. For example, for a 16^4 lattice, we obtain a median in the optimal case

of, 580 sweeps for the fixing whereas for the stochastic overrelaxation the number is 720 sweeps.

Table 8 – Values for the median, mean and standard deviation of the distribution of sweeps necessary to gauge-fix for different ω, with $\beta = 5.9$ and several lattice sizes. The sample size was 200 configurations for 4^4, 8^4 and 10^4, 100 configurations for 16^4 and 20 configurations for 24^4.

lattice size	ω	median	mean	std. deviation
4^4	1.0	257	331.4	257.2
4^4	1.62	65	86.4	55.8
4^4	1.63	64	85.3	53.7
4^4	1.64	63.5	84.1	51.6
4^4	1.65	64	83.1	49.6
4^4	1.66	64	81.9	47.6
8^4	1.65	206	258.4	246.2
8^4	1.70	173	225.0	213.2
8^4	1.82	124	81.9	47.6
8^4	1.85	126.5	151.8	76.4
10^4	1.83	165	198.5	112.9
10^4	1.84	155	190.9	104.8
10^4	1.85	152	184.3	94.4
10^4	1.86	151.5	177.2	80.4
10^4	1.87	152.5	178.5	76.5
16^4	1.92	320	352.6	120.6
16^4	1.925	300	339.8	120.8
16^4	1.93	300	332.0	97.4
16^4	1.935	320	341.6	95.9
16^4	1.94	320	356.6	107.0
24^4	1.94	630	676.0	219.2
24^4	1.95	580	642.0	250.4
24^4	1.96	620	620.0	132.5

Source: By the author.

We can also study the behavior when varying β, as we did for the stochastic algorithm. The results are in Table 9. We observe that there is a slight increase for the median, as in the stochastic case, but the optimal ω changes very little.

Table 9 – Values for the median, mean and standard deviation for the distribution of sweeps needed to gauge-fix for 2 hits of the overrelaxation algorithm with changing βs, in the region around the optimal ω.

β	lattice size	ω	median	mean	std. deviation
6.1	8^4	1.79	135.5	160.7	84.4
6.1	8^4	1.80	134	158.7	80.7
6.1	8^4	1.81	132	157.4	75.7
6.1	8^4	1.82	134	156.4	70.5
6.1	8^4	1.83	135.5	155.7	64.6
6.1	10^4	1.84	177	212.9	135.4
6.1	10^4	1.85	173.5	210.1	128.5
6.1	10^4	1.86	174	205.8	114.4
6.3	8^4	1.78	151.5	182.0	102.6
6.3	8^4	1.79	151	178.8	97.5
6.3	8^4	1.80	151	175.6	91.0
6.3	8^4	1.81	147.5	174.5	89.3
6.3	8^4	1.82	147.5	173.6	84.8
6.3	8^4	1.83	149	175.0	85.1

Source: By the author.

Analysis with constant physics In order to obtain a critical exponent from the data, we need configuration obtained with constant physics. This means that we need to change the physical lattice spacing a, at the same time that we change the number of sites N for each side of the four-dimensional hypercube where the configurations are obtained, in order to have $N \times a$ constant. Following (46, 73), the physical spacing can parameterized, for $5.7 < \beta < 6.92$, by

$$a = r_0 \exp(f(\beta)), \tag{8.1}$$

with

$$f(\beta) \equiv -1.6804 - 1.7331(\beta - 6.0) + 0.7849(\beta - 6.0)^2 - 0.4428(\beta - 6.0)^3, \tag{8.2}$$

for the pure gauge Wilson action, in which $r_0 \approx 0.5$ fm is the Sommer parameter. In order to have $N \times a$ constant, we need to change β as we change N, following the equation

$$Na = N'a', \tag{8.3}$$

which brings us to

$$f(\beta') = f(\beta) + \log\left(\frac{N}{N'}\right). \tag{8.4}$$

This equation should be solved for β'. The statistical values for the gauge-fixing using configurations with β obtained from this procedure are shown in Tables 10 and 11, for the stochastic overrelaxation and overrelaxation respectively.

A more detailed and rigorous analysis was performed by a former member of our group, Dr. Matheus Cerqueira, in parallel to the presented above. The results are in (82).

Table 10 – Median, mean and standard deviation for the distribution of the number of necessary sweeps for gauge-fix using 2 hits of the stochastic overrelaxation algorithm and different lattice sizes, changing β to obtain a constant physical size, and varying p around its optimal value.

β	lattice size	p	median	mean	std. deviation
5.84572	6^4	0.67	123	168.6	144.5
5.84572	6^4	0.68	120	158.9	105.5
5.84572	6^4	0.69	115.5	155.0	115.5
5.84572	6^4	0.70	117	155.3	111.4
5.84572	6^4	0.71	116.5	158.1	103.5
6.00000	8^4	0.77	158.5	197.1	93.9
6.00000	8^4	0.78	152.5	200.5	129.5
6.00000	8^4	0.79	158	201.0	118.9
6.13655	10^4	0.79	217.5	287.9	283.8
6.13655	10^4	0.80	197.0	274.5	264.6
6.13655	10^4	0.81	201.5	286.2	290.25
6.26010	12^4	0.80	290	363.1	233.6
6.26010	12^4	0.81	267.5	334.7	175.7
6.26010	12^4	0.82	268.5	330.0	183.8
6.26010	12^4	0.83	260	326.8	185.3
6.26010	12^4	0.84	248	307.1	165.4
6.26010	12^4	0.85	262.5	326.6	174.7
6.47466	16^4	0.85	380	475.4	376.2
6.47466	16^4	0.86	340	415.2	197.1
6.47466	16^4	0.87	340	402.4	165.7

Source: By the author.

The program used to produce the results presented here was developed independently from Dr. Cerqueira's and were shown to produce congruent results. A variant was latter developed to study Coulomb gauge for an anisotropic lattice study (152). This variant was tested independently by Dr. Benjamin Page of Swansea University and was found to fulfill their requirements. The results from the Coulomb version were also compared to the results using a different implementation (177), and were also found to be the same within statistical errors.

8.2 Quark form factors

The ensembles we produced for the study of the quark propagator were meant to access different temperatures, finite size effects and finite lattice spacing effects. They were quenched ensembles and a summary of their characteristics is presented in Table 12.

According to the Necco-Somer formula 3.63, the lattice spacing for $\beta = 6.0$ is $a = 0.093\,\text{fm}$, which corresponds to $a^{-1} = 2.11\,\text{GeV}$. For $\beta = 6.13655$, one has $a = 0.0745\,\text{fm}$ and $a^{-1} = 2.65\,\text{GeV}$.

Table 11 – Median, mean and standard deviation for the distribution of the number of necessary sweeps for gauge-fix using 2 hits of the overrelaxation algorithm and different lattice sizes, changing β to obtain a constant physical size, and varying ω around its optimal value.

β	lattice size	ω	median	mean	std. deviation
5.84572	6^4	1.75	93	120.2	89.0
5.84572	6^4	1.76	92	119.2	85.2
5.84572	6^4	1.77	93	119.0	81.4
5.84572	6^4	1.78	94	118.4	77.7
5.84572	6^4	1.79	95	118.2	74.2
6.00000	8^4	1.81	137.5	166.5	111.9
6.00000	8^4	1.82	133.5	162.7	103.3
6.00000	8^4	1.83	133.5	161.1	97.1
6.00000	8^4	1.84	134	162.1	92.3
6.13655	10^4	1.85	166	215.2	184.2
6.13655	10^4	1.86	163	211.6	170.7
6.13655	10^4	1.87	169.5	211.4	158.6
6.13655	10^4	1.88	170.5	213.5	153.1
6.26010	12^4	1.87	211.5	250.9	137.8
6.26010	12^4	1.88	210.5	253.4	134.3
6.26010	12^4	1.89	214.5	253.9	122.4
6.26010	12^4	1.90	223.5	253.3	107.7
6.47466	16^4	1.89	280	328.0	176.1
6.47466	16^4	1.90	270	323.4	169.4
6.47466	16^4	1.91	280	315.0	134.1

Source: By the author.

Table 12 – Ensembles produced to study the quark propagator

N_s	N_t	β	temperature (MeV)	spatial volume (fm^3)	# configurations
16	4	6.0	530.60	3.31	100
32	4	6.0	530.60	26.48	50
16	6	6.0	353.06	3.31	100
32	6	6.0	353.06	26.48	20
16	48	6.0	44.13	3.31	40
20	48	6.0	44.13	6.466	40
20	60	6.13655	44.13	3.31	30

Source: By the author.

For the propagator inversion we used the improvement coefficient $c_{SW}(\beta = 6.0) = 1.76923$ and $\kappa_c(\beta = 6.0) = 0.135196$ for the coarser lattice and $c_{SW}(\beta = 6.13655) = 1.76923$ with $\kappa_c(\beta = 6.13655) = 0.135605$ for the finer lattice, following the formulas in (96), as explained in 5.6.

The critical transition temperature in quenched $SU(3)$ gauge theory is around $T_c = 270\,\text{MeV}$ (175). We have produced our ensembles trying to stay away from the

transitional region and focusing on temperatures which are undoubtedly within the confined or the deconfined phase, as can be seen in Table 12. We will refer to the lattices at $T = 44.13\,\mathrm{MeV}$ as the zero-temperature lattices, as this temperature is expected to be too low to show any thermal effects.

The quark propagator at finite temperature is expected to have the following form

$$S(\omega, \vec{p}) = \frac{Z(\omega, \vec{p})}{i\gamma_4\omega + i\vec{\not{p}}\, R(\omega, \vec{p}) + \mathbb{1}\, M(\omega, \vec{p})}, \tag{8.5}$$

where ω is the Matsubara frequency. The fermionic Matsubara frequencies allowed on the discretized lattice are

$$\omega_{n_t} = \frac{2\pi}{aN_t}\left(n_t + \frac{1}{2}\right), \tag{8.6}$$

with $n_t = -N_t/2 + 1, \ldots, N_t/2$. In the zero-temperature limit, the R function should be unity and the dependence on the momentum should be on the variable $p = \sqrt{p_\mu p^\mu} = \sqrt{\omega^2 + \vec{p}\cdot\vec{p}}$ only, as demanded by Lorentz symmetry.

On the lattice, for Wilson fermions, we expect, instead of Eq. 8.5,

$$S(\omega, \vec{p}) = \frac{Z(\omega, \vec{p})}{i\gamma_4 a K_4(p) + ia\vec{\gamma}\cdot\vec{K}\, R(\omega, \vec{p}) + \mathbb{1}\, M(\omega, \vec{p})}, \tag{8.7}$$

due to our discussion around Eq. 5.93, where $aK_\mu(p) = \sin(ap_\mu)$. The form factors Z, M and R can be obtained by taking traces of the propagator, similarly to what was shown in Sect. 5.7 for the zero temperature case.

8.2.1 Zero temperature results

The Wilson quark propagator is known to present large lattice artifacts, even with improvement in place. In Fig. 1, the interacting form factors are shown plotted against the norm of different kinds of 4-momenta for $\kappa = 0.1335$: the Fourier momentum p, the lattice sine momentum K and the $Q_\mu(p) = 2\sin(p_\mu/2)$ momentum. Above 0.5 units of momentum measured in lattice units, we see strong lattice artifacts related to the breaking of rotational symmetry. In the infrared, the data agree with each other no matter the momentum used.

The plots in Fig. 1 are uncorrected plots. We had anticipated in Sect. 5.7 that a characteristic of the Wilson propagator, even in the free case, is that its form factors do not correspond to the continuum ones. The mass form factor, for example, contains a term quadratic in Q_μ (see Eq. 5.98). This shows in the plot for the uncorrected mass form factor as a momentum dependent mas that grows in the ultraviolet, which is a non-physical discretization phenomenon.

The free improved propagator, Eq. 5.103, depends on the K_μ and Q_μ in an intricate way. This complicates the choice of variable to plot the form factors against. We have

chosen to stick to the p momentum for all subsequent plots, as using the other momentum variables do not show great improvements to the readability of the figures anyway.

We notice that the plot for the $R(p)$ form factor, which we expected to be 1 for zero temperature, as is the case here, actually shows some deviations from unity. These may be due to finite-size effects, as our lattice is asymmetric. Another source of asymmetry between the imaginary time and spatial directions is the anti-periodic boundary condition that the fermion fields are required to obey. We have used a multiplicative correction for the quark wave-function renormalization Z form factor, in order to try to cancel the lattice artifacts (87) for medium and high-momenta. The Z form factor is expected to be 1 at tree-level, so we force this value by dividing the data by $Z_I^{\text{free}}(p)$ of Eq. 5.114.

$$Z_I^{\text{mult. corr.}}(p) = \frac{Z_I^{\text{uncorr.}}(p)}{Z_I^{\text{free}}(p)}. \tag{8.8}$$

We have tried three possible corrections for the mass form factor. The mass function in lattice units should be equal to am at tree level. We can define a multiplicative correction for the $M(p)$ form factor, as was done for $Z(p)$ by

$$aM_I^{\text{mult. corr.}}(p) = am\,\frac{M_I^{\text{uncorr.}}(p)}{M_I^{\text{free}}(p)}, \tag{8.9}$$

where $M_I^{\text{free}}(p)$ is given in Eq. 5.115. A subtractive correction was also tried,

$$aM_I^{\text{subt. corr.}}(p) = am + a(M_I^{\text{uncorr.}}(p) - M_I^{\text{free}}(p)), \tag{8.10}$$

which would also result in a corrected form factor with the value am at tree-level.

A third scheme for the mass form factor is provided by a hybrid correction (119). It is a mixture of the subtractive and multiplicative corrections, tuned to reduce the lattice artifacts

$$aM_I^{\text{hyb. corr.}}(p) = \frac{aM_I^{\text{uncorr.}}(p) - \Delta M_I^{(-)}(p)}{\Delta M_I^{(\times)}(p)}, \tag{8.11}$$

with

$$\Delta M_I^{(-)}(p) = -\frac{1}{16A_I'(p)}\left[am\,(aK)^2 + \frac{1}{2}(aK)^2(aQ)^2\right] \tag{8.12}$$

$$\Delta M_I^{(\times)}(p) = \frac{1}{amA_I'(p)}\left\{am\, + \frac{1}{2}\left[(aQ)^2 - (aK)^2\right]\right\}, \tag{8.13}$$

where the p dependence of $K_\mu(p)$ and $Q_\mu(p)$ was suppressed and $A_I'(p)$ is given by Eq. 5.108. We plot a comparison of the correction schemes in Fig. 2. In the infrared the uncorrected data agrees with all corrections, which shows that the artifacts are associated to a finite spacing effect, as expected. The hybrid correction seems to perform best of the three to remove the lattice artifacts of the $M(p)$ form factor, although some effects associated to the breaking of the rotational symmetry are still displayed. The mass form

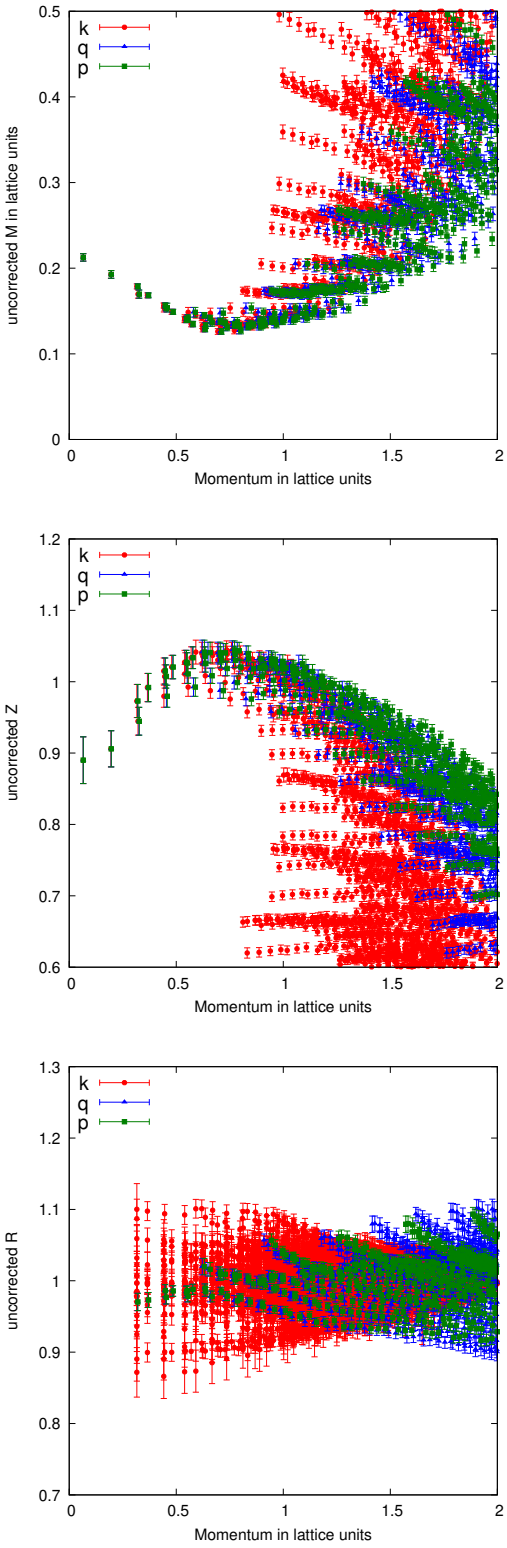

Figure 1 – The three form factors of the propagator plotted against different momentum variables for a $20^3 \times 48$ lattice at $\beta = 6.0$ and $\kappa = 0.1335$.

Source: By the author..

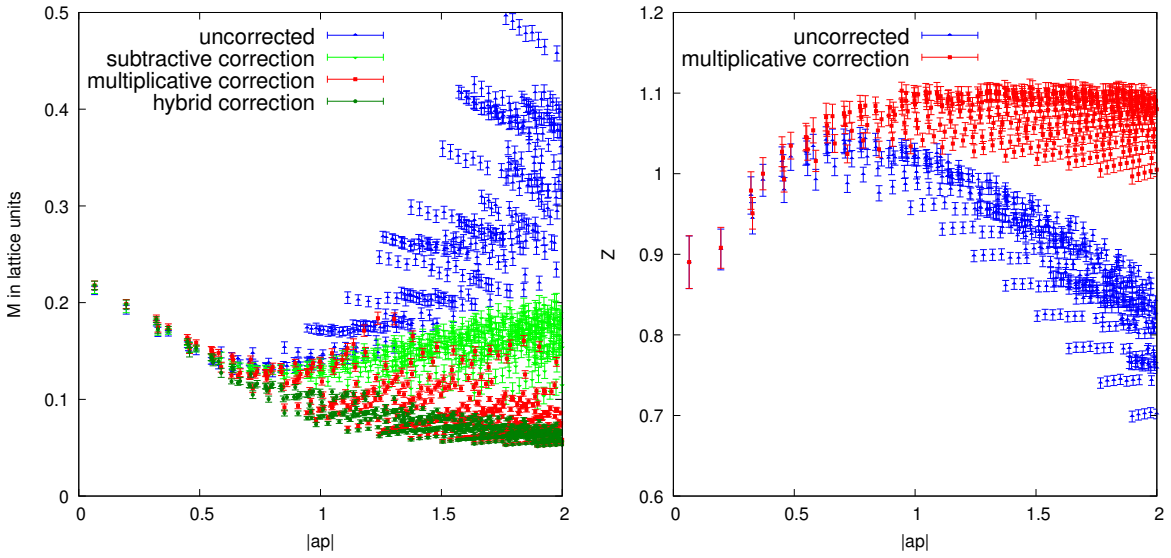

Figure 2 – Corrections to the $M(p)$ and $Z(p)$ form factors for a $20^3 \times 48$ lattice at $\beta = 6.0$ and $\kappa = 0.1335$.

Source: By the author..

factor indeed shows dynamical mass generation in the infrared, just like all previous studies cited in Chap. 7. The value for $M(p)$ for the lowest momentum available is $aM \approx 0.22$, which corresponds to $M \approx 460\,\text{MeV}$.

The corrected quark wave-function renormalization shown in the right-hand side of Fig. 2, the value seems to saturate, in accordance with most studies of the quark propagator in the vacuum. The characteristic dip in the infrared of the Landau gauge quark propagator is also clearly seen in the plot.

When inverting the quark propagator, the value of κ determines the bare quark mass that is being used. The equation relating both is Eq. 5.75. Table 13 shows the conversion of κ to corrected bare quark mass for the values used here.

Table 13 – Corrected bare quark mass used in the propagator calculations.

κ	am	m(MeV)
0.1335	0.0470	99.5
0.13392	0.0352	74.6
0.1342	0.0266	56.4

Source: By the author.

The plot in Fig. 3 shows the mass dependence of the propagator form factors for the uncorrected data and Fig.4 for the corrected data.

The mass dependence is stronger for the mass form factor $M(p)$, with larger κ, corresponding to smaller bare masses, laying lower in the plot, as expected. The $Z(p)$ and

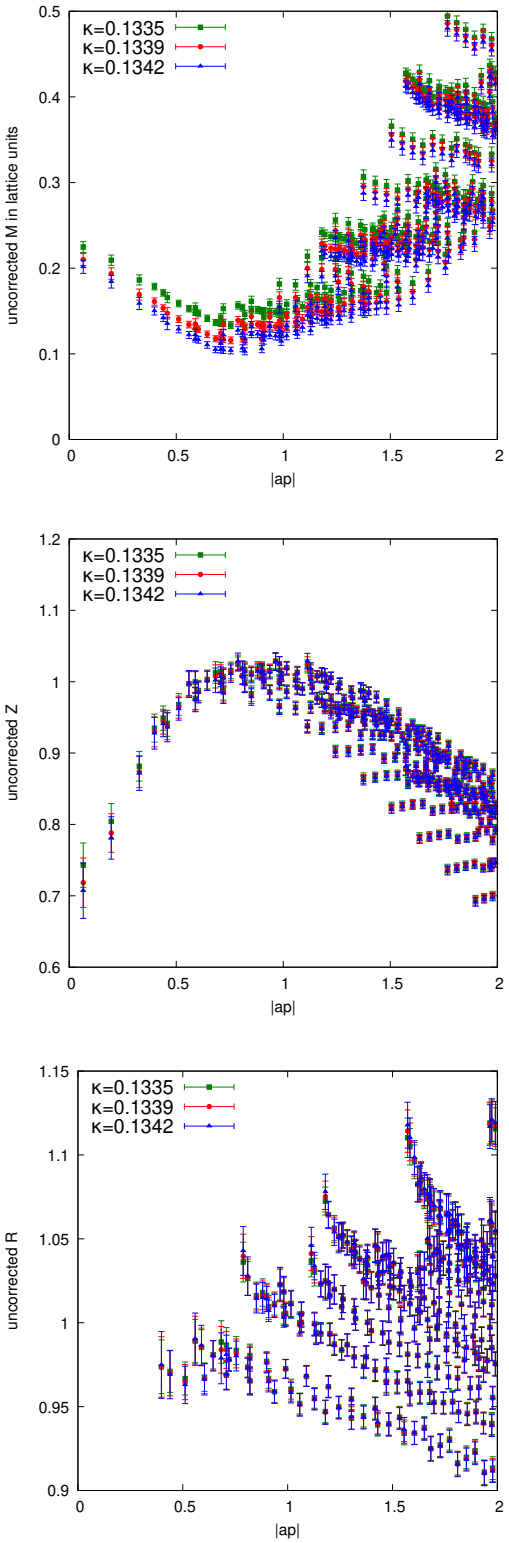

Figure 3 – The mass dependence of the quark propagator uncorrected form factors for a $16^3 \times 48$ lattice at $\beta = 6.0$ for several κ.

Source: By the author..

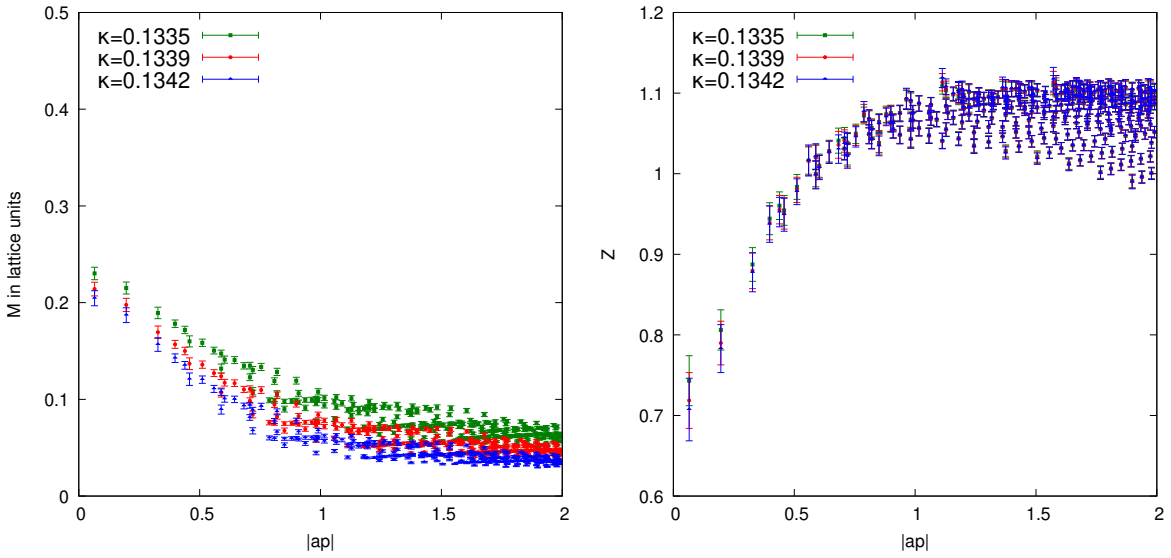

Figure 4 – The mass dependence of the quark propagator corrected form factors, with our preferred corrections, for a $16^3 \times 48$ lattice at $\beta = 6.0$ for several κ.

Source: By the author..

$R(p)$ form factors have no discernible mass dependence, as far as the uncertainties allow us to probe.

We have inverted the propagator for $\kappa = 0.1335$ on lattices with two spatial volumes, keeping all else constant. The comparison between the two volumes is presented in Fig.5.

When looking at Table 12, we see that the physical spatial volume almost doubles between the two lattices. In the plot, one sees that finite volumes are definitely present for data in the infrared, although both form factors still retain their qualitative form. The dip in in the infrared of the quark renormalization is smaller for larger volume lattices, indicating that the suppression may be, at least partially, a finite volume effect.

Keeping the physical volume, as well as the bare quark mass in physical units, we have calculated the form factors for two different lattice spacings. The results for the $M(p)$ and $Z(p)$ form factors is presented in Fig. 6. For the $16^3 \times 48$ lattice with $\beta = 6.0$, $\kappa = 0.1335$, whereas for the $20^3 \times 60$ lattice with $\beta = 6.13655$, $\kappa = 0.13423$, in order to maintain the value of the bare quark mass in physical units.

Differently from the volume dependence, the plot shows that the mass function is more sensitive to a change in the lattice spacing than the quark renormalization function. The finer lattice shows a smaller degree of dynamical mass generation, although the qualitative features of the plot are still present.

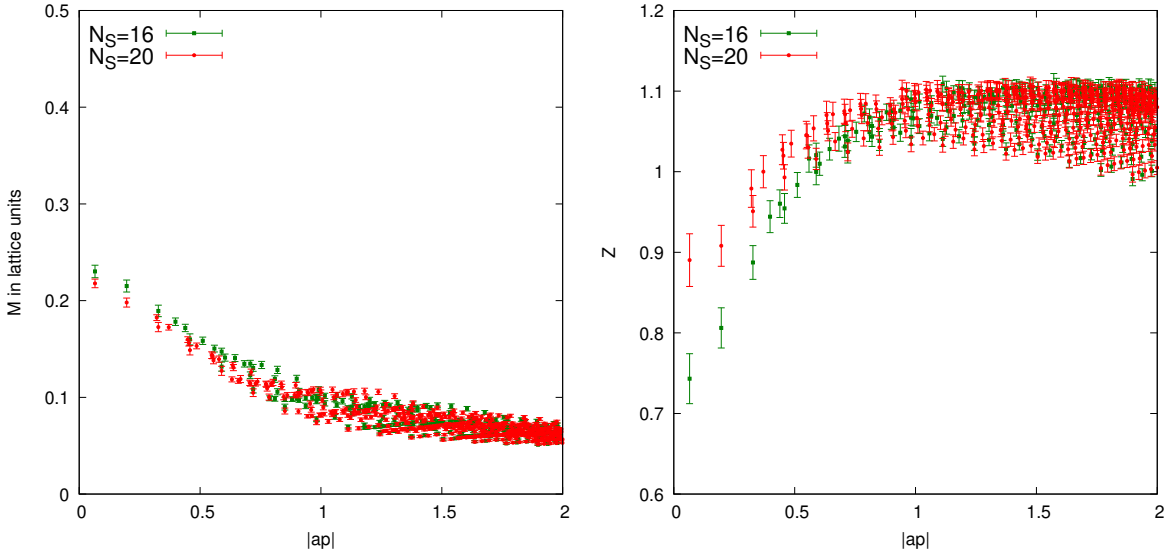

Figure 5 – The volume dependence of the quark propagator corrected form factors $M(p)$ and $Z(p)$, with our preferred corrections, for an Euclidean temporal extent of $N_t = 48$ at $\beta = 6.0$ with $\kappa = 0.1335$.

Source: By the author..

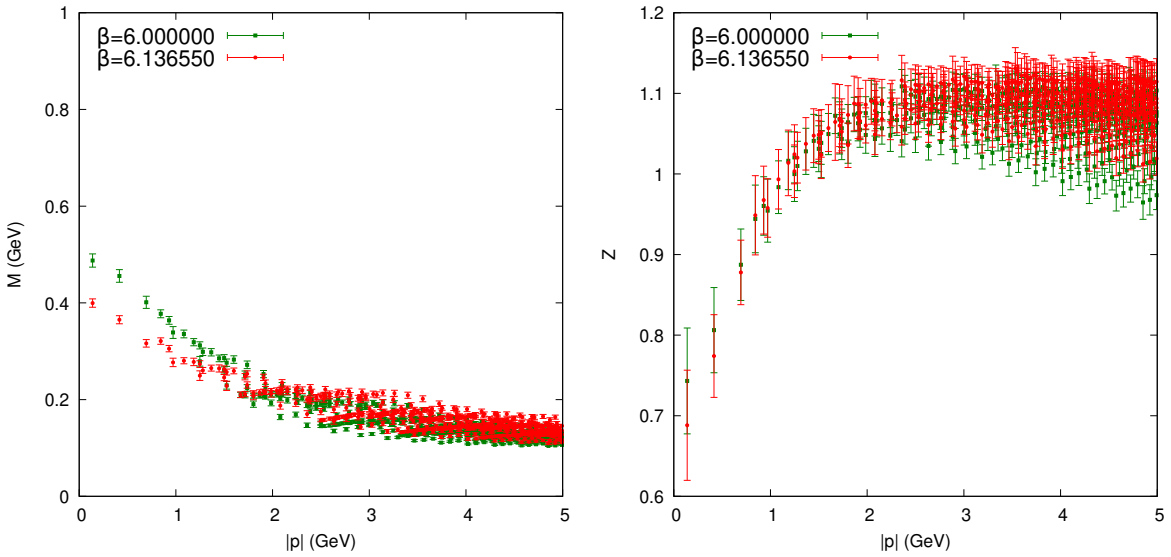

Figure 6 – The spacing dependence of the quark propagator corrected form factors $M(p)$ and $Z(p)$, with our preferred corrections with the same physical volume and bare mass parameter in physical units.

Source: By the author..

8.2.2 Finite-temperature results

At high temperatures, as discussed in Sect. 3.3, QCD undergoes a phase transition. For the quenched theory, the order parameters for this transition is the Polyakov loop. Its value vanishes for small temperatures, in the confining phase of the theory, and develops a finite value at high temperatures, signaling deconfinement. For $SU(3)$, the expectation value of the Polyakov loop is a complex number and, as such, can be written as

$$P = \langle P[U] \rangle = |P| e^{i\varphi}. \tag{8.14}$$

The angle φ is known to gather around the three phases of the center elements: $\varphi = 0,\ 2\pi/3$ and $4\pi/3$. This is similar to what happens in Ising model simulations, where the broken phase can have magnetization in one of two $M = \pm 1$ phases. The pure-gauge action is symmetric under center transformations, however these transformations change the values of the Polyakov loops as explained around Eq. 3.80. The action being symmetric under these transformations mean that two configurations related to one another by a center transformation actually have the same statistical weight and thus have, in principle, the same probability of being drawn in the Monte Carlo sampling. However, due to the local nature of the updates of the Heat-Bath or Metropolis algorithm, a tunneling between different sectors of the Polyakov loop is actually very unlikely, as the volume of the lattice grows. This is also true in the Ising example, where tunneling between the two phases gets more unlikely as the size of the system is increased.

What one can do is generate all configurations in one sector and then apply a center transformation to each of them to get to the other sectors. We can then calculate the propagator in these different sectors and see if we detect any change in them. There is no reason, in the quenched theory, why any sector may be preferred, so we show our results for all of them on equal footing. This analysis is similar to the one presented in (176).

Figs. 7, 8 and 9 show how the uncorrected form factors behave at finite temperature for the different sector and separate Matsubara frequencies as a function of $|\vec{p}|$. The corrected form factors are presented in Fig. 10 for the highest temperature available in our ensembles. We show here only the results for our lightest quark, with $\kappa = 0.1342$.

Comparing the form factors for different sectors, we see that, indeed they have quite a different behavior. The $0\pi/3$ sector shows a suppression of the mass generation in the infrared, whereas the $2\pi/3$ and $4\pi/3$ sectors show dynamical mass generation for one of the lowest Matsubara frequencies associated to $n_t = 0$ and $n_t = -1$ respectively. When calculating the Matsubara frequency for these values of n_t from the formula in Eq. 8.6, we get

$$\omega_{-1} = \frac{2\pi}{aN_t}\left(-1 + \frac{1}{2}\right) = -\frac{\pi}{aN_t}, \quad \omega_0 = \frac{2\pi}{aN_t}\left(0 + \frac{1}{2}\right) = \frac{\pi}{aN_t}, \tag{8.15}$$

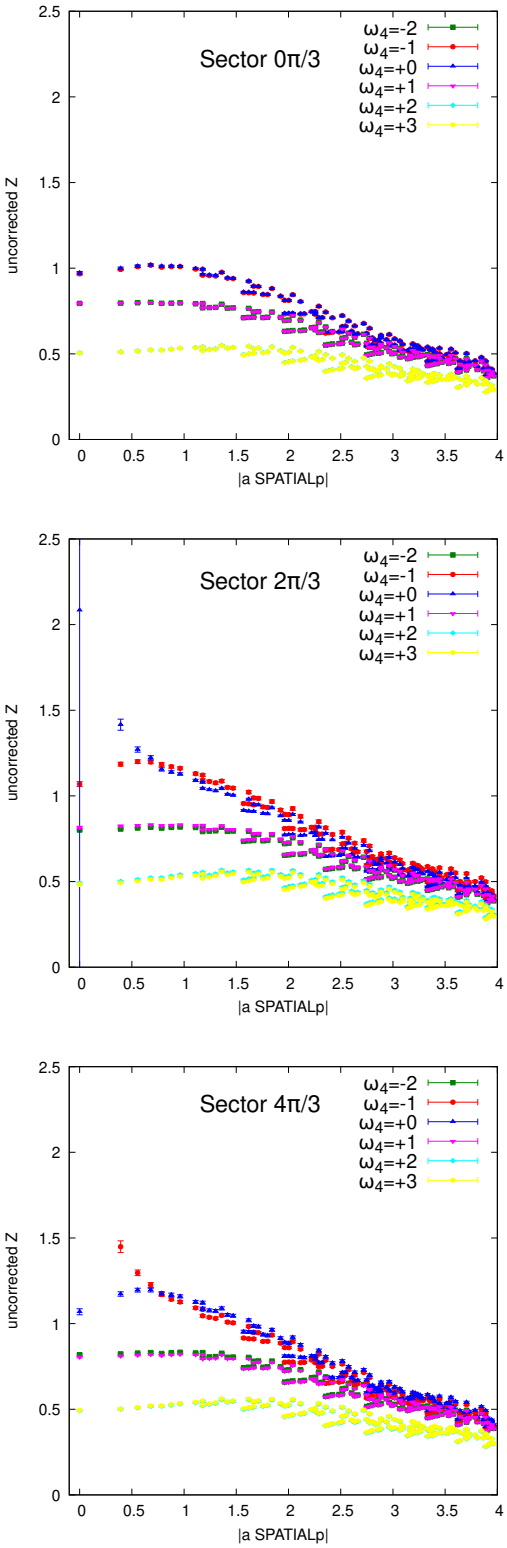

Figure 7 – The uncorrected form factors $Z(p)$ for the different Matsubara frequencies and the three different Polyakov loop sectors. Results for a 16×6 lattice with $\beta = 6.0$ and $\kappa = 0.1342$.

Source: By the author..

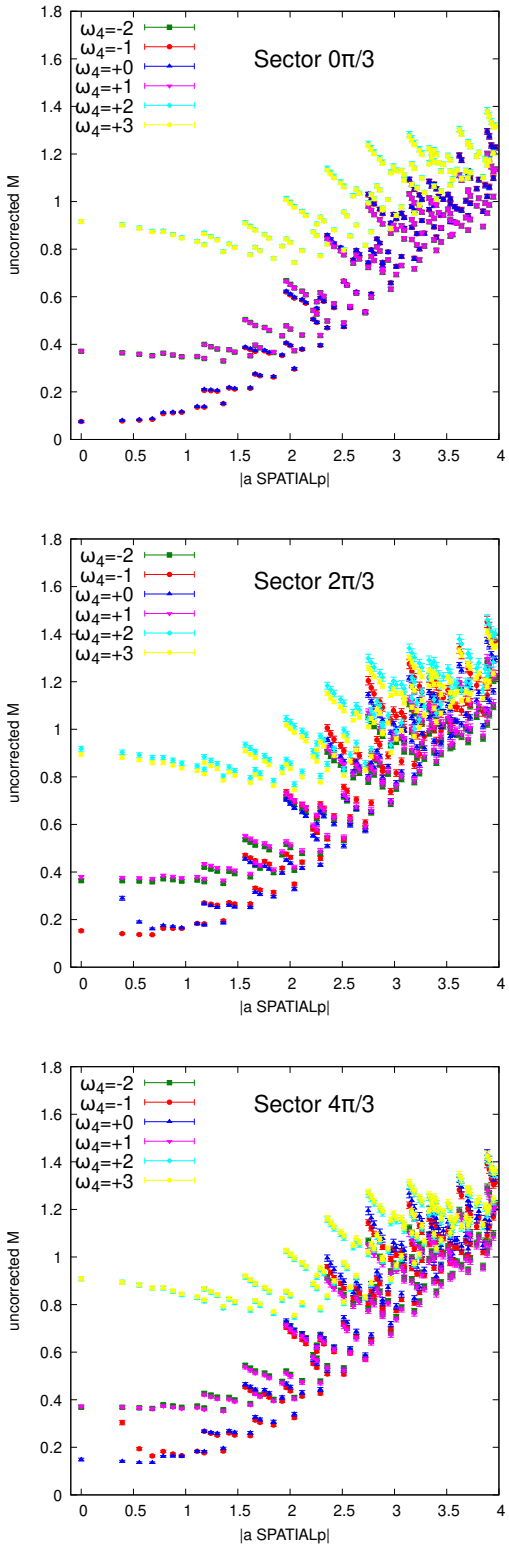

Figure 8 – The uncorrected form factors $M(p)$ for the different Matsubara frequencies and the three different Polyakov loop sectors. Results for a 16×6 lattice with $\beta = 6.0$ and $\kappa = 0.1342$.

Source: By the author..

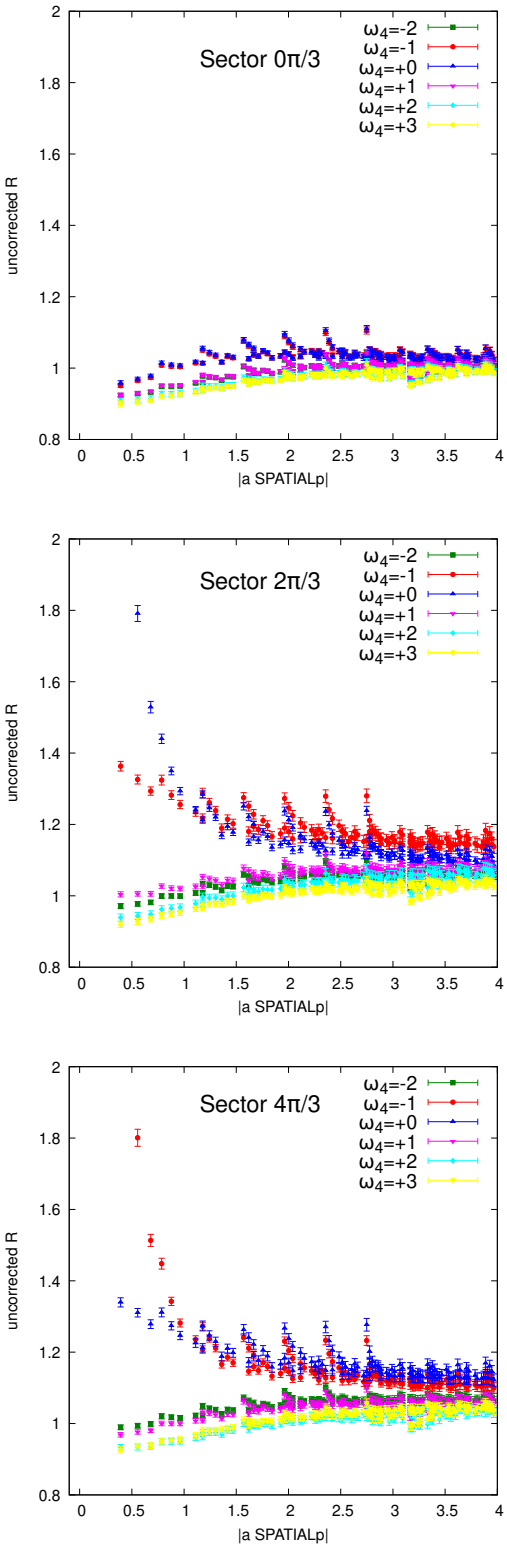

Figure 9 – The form factor $R(p)$ for the different Matsubara frequencies and the three different Polyakov loop sectors. Results for a 16×6 lattice with $\beta = 6.0$ and $\kappa = 0.1342$.

Source: By the author..

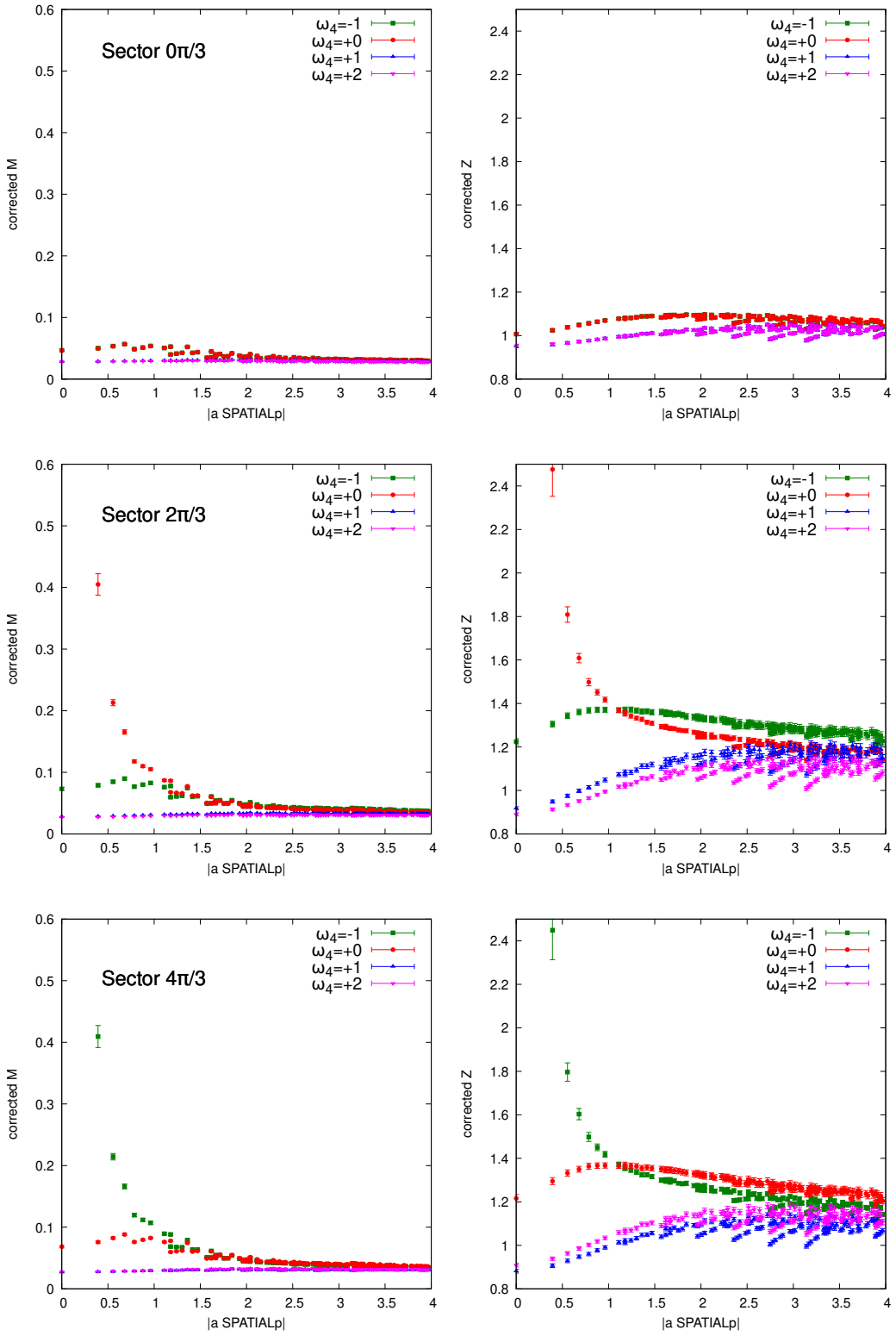

Figure 10 – The corrected form factors $M(p)$ and $Z(p)$, with our preferred corrections, for the different Matsubara frequencies and the three different Polyakov loop sectors. Results for a 16×4 lattice with $\beta = 6.0$ and $\kappa = 0.1342$.

Source: By the author..

which have the same absolute value. Indeed, for the $0\pi/3$ sector we see a pairing of Matsubara frequencies for ($n_t = 2$, $n_t = 3$), ($n_t = -2$, $n_t = 1$) and ($n_t = 0$ and $n_t = -1$). When we compute the Matsubara frequency, we see that the values in each pair are the same except for a sign, meaning that for this sector, the form factors depend solely on the absolute value of the Matsubara frequency*.

For most Matsubara frequencies and most sectors, the $Z(p)$ function preserves a dip in the infrared and goes to a constant in the ultraviolet.

We also observe that the pairing of Matsubara frequencies does not hold for the $2\pi/3$ and $4\pi/3$ sectors, and is maximally broken in the infrared for the lowest frequencies ω_0 and ω_{-1}. There is however, a symmetry: for all form factors, one of the frequencies of the pairing in one of these sectors takes has the behavior of the other one in the other sector.

The Matsubara frequency which we are most interested in is the ω_0 as is probes deeper into the infrared. We plot the values of the corrected $M(p)$ and $Z(p)$ functions for the different sectors for the single ω_0 frequency in Fig. 11. We see that even though for

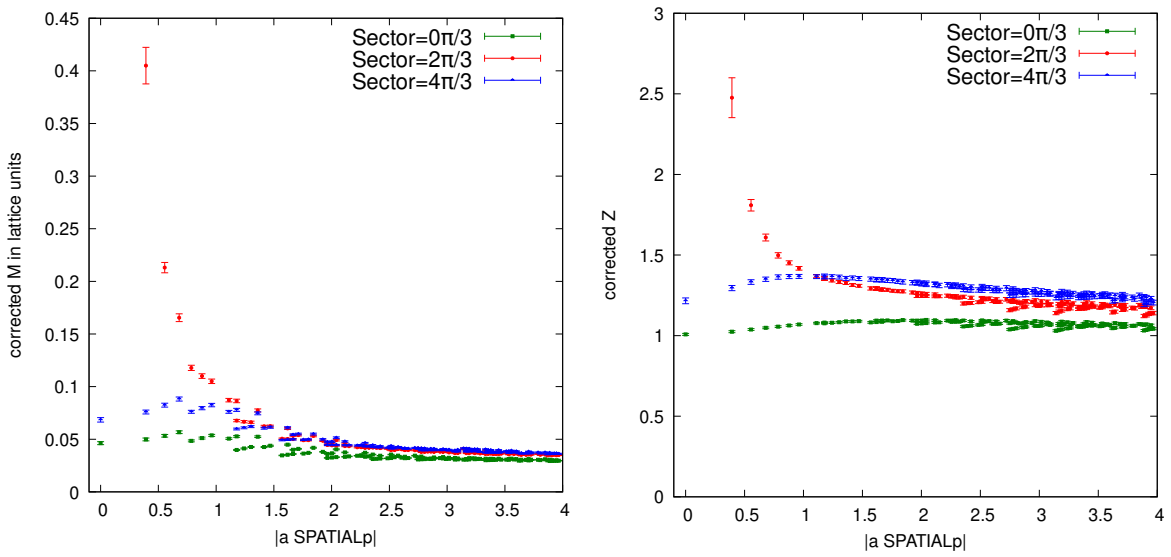

Figure 11 – The corrected form factors $M(p)$ and $Z(p)$, with our preferred corrections, for the different sectors and Matsubara frequency $\omega_{n_4=0}$. Results for a 16×4 lattice with $\beta = 6.0$ and $\kappa = 0.1342$.

Source: By the author..

the $0\pi/3$ sector the mass generation is not efficient in the infrared, the other sectors have large values, specially the $2\pi/3$ sector. In the case that we plot the ω_{-1} frequency, then

* For this to work with the pair $n_t = 2$ and $n_t = 3$, one must actually interpret the latter as $n_t = -3$, which is correct in the context of discrete Fourier transforms, since the frequency $2\pi(-n_t)/aN_t$ is the same as the frequency $2\pi(N_t - n_t)/aN_t$.

the $4\pi/3$ sector shows the large increase for low momenta, as displayed in Fig. 12. There is also a large increase in the $Z(p)$ function for the $2\pi/3$ sector.

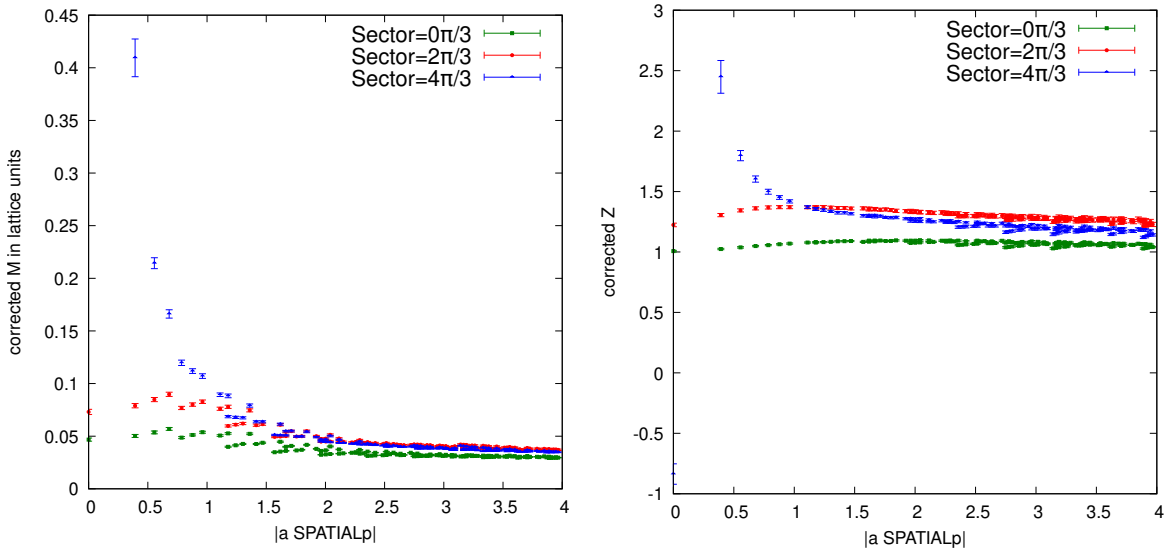

Figure 12 – The corrected form factors $M(p)$ and $Z(p)$, with our preferred corrections, for the different sectors and Matsubara frequency $\omega_{n_4=-1}$. Results for a 16×4 lattice with $\beta = 6.0$ and $\kappa = 0.1342$.

Source: By the author..

The same results are displayed for the temperature of 353.06 MeV associated to $N_t = 6$ in Figs.13 and 14 for comparison.

The actual temperature dependence of the corrected form factors $Z(p)$ and $M(p)$ is shown in Fig.15. Since no sector can be defined at zero temperature, we show the same data in all three plots.

The $M(p)$ temperature dependence for the $0\pi/3$ sector shows that as the temperature is raised the mass generation is less effective. In the other sectors, the situation is more complex. For the $4\pi/3$ sector, there is a crossing of the data at medium momentum: the order in the ultraviolet, from highest to lowest, is $N_t = 4, 6$ and then 48. In the infrared this gets inverted. In the $2\pi/3$ sector, the ordering is preserved. In the ultraviolet the data mostly agrees.

As for the $Z(p)$ form factor, the infrared dip is not strongly sensitive to the temperature difference between $N_t = 4, 6$, corresponding to a difference of about 170 MeV in physical units. The behavior, however, is quite different from the zero temperature data, which shows quite a strong suppression. In the ultraviolet the data also agrees, as was the case for the mass form factor. For the other sectors, there is no agreement over the momentum range plotted in the graph, with the $2\pi/3$ behavior being starkly different, depending on the temperature. The $R(p)$ form factor in Fig. 16 shows that the degree

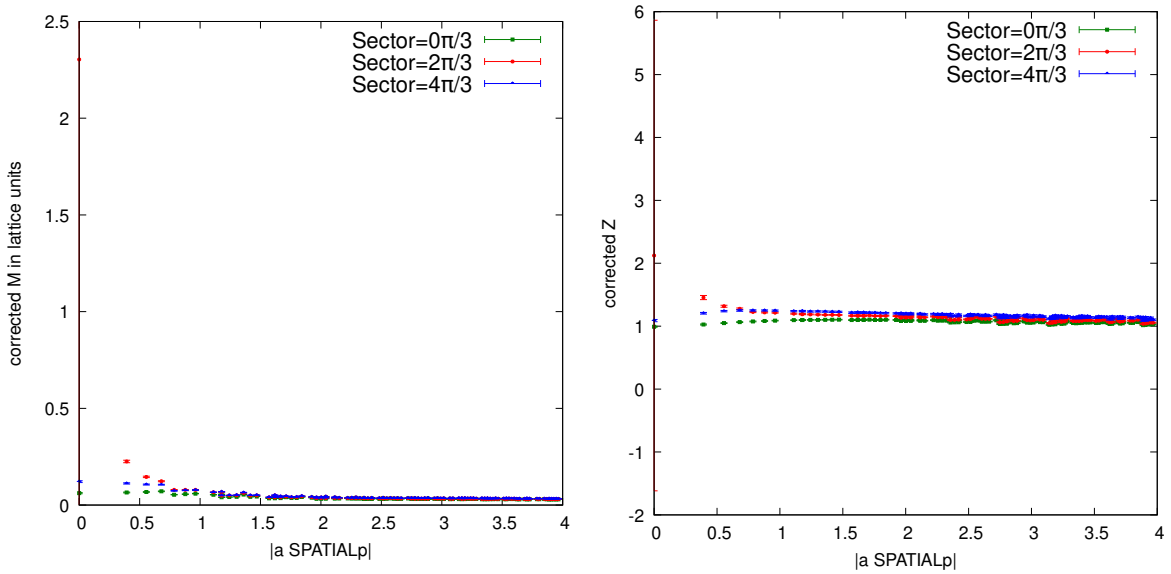

Figure 13 – The corrected form factors $M(p)$ and $Z(p)$, with our preferred corrections, for the different sectors and Matsubara frequency $\omega_{n_4=0}$. Results for a 16×6 lattice with $\beta = 6.0$ and $\kappa = 0.1342$.

Source: By the author..

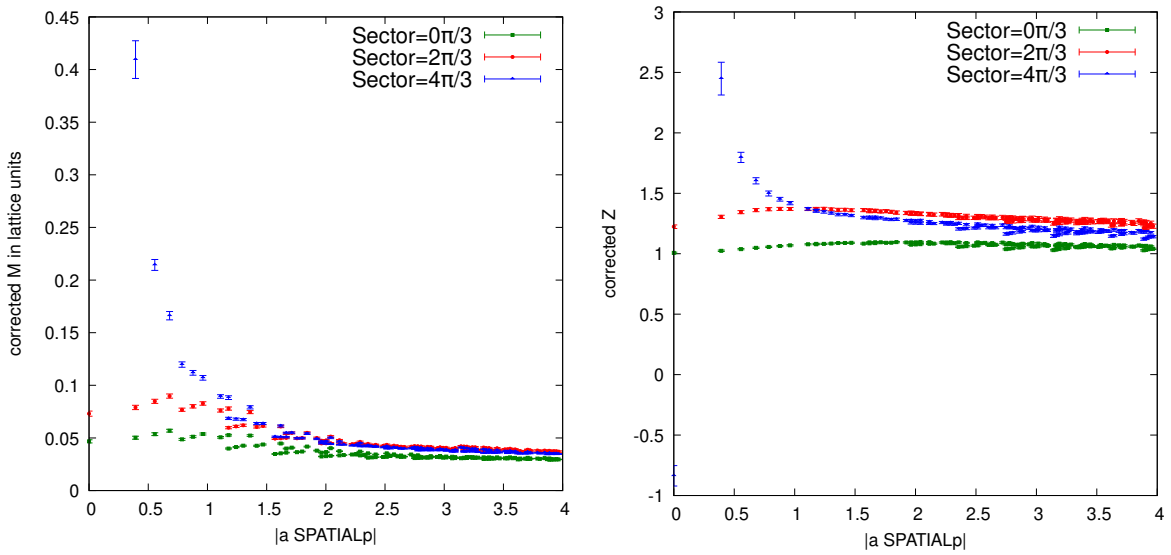

Figure 14 – The corrected form factors $M(p)$ and $Z(p)$, with our preferred corrections, for the different sectors and Matsubara frequency $\omega_{n_4=-1}$. Results for a 16×6 lattice with $\beta = 6.0$ and $\kappa = 0.1342$.

Source: By the author..

of assymmetry between the spatial and temporal components of the non-scalar part of the propagator increases as the temperature increases for the $2\pi/3$ and $4\pi/3$ sectors, and remains almost the same for the $0\pi/3$ form factor.

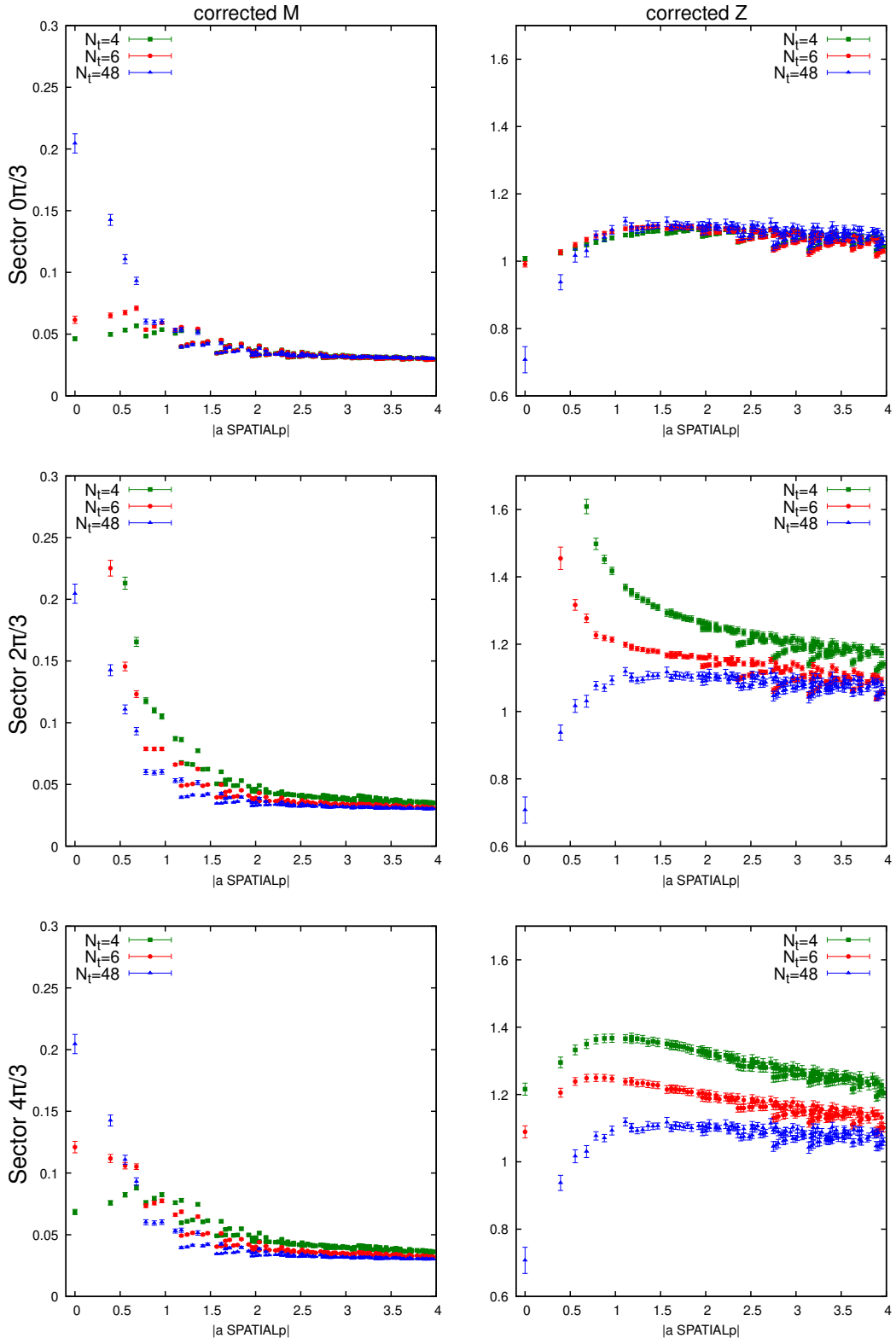

Figure 15 – The corrected form factors $M(p)$ and $Z(p)$, with our preferred corrections, for different temperatures and sectors and Matsubara frequency $\omega_{n_4=0}$. Results for lattices with $N_s = 16$, $\beta = 6.0$ and $\kappa = 0.1342$.

Source: By the author..

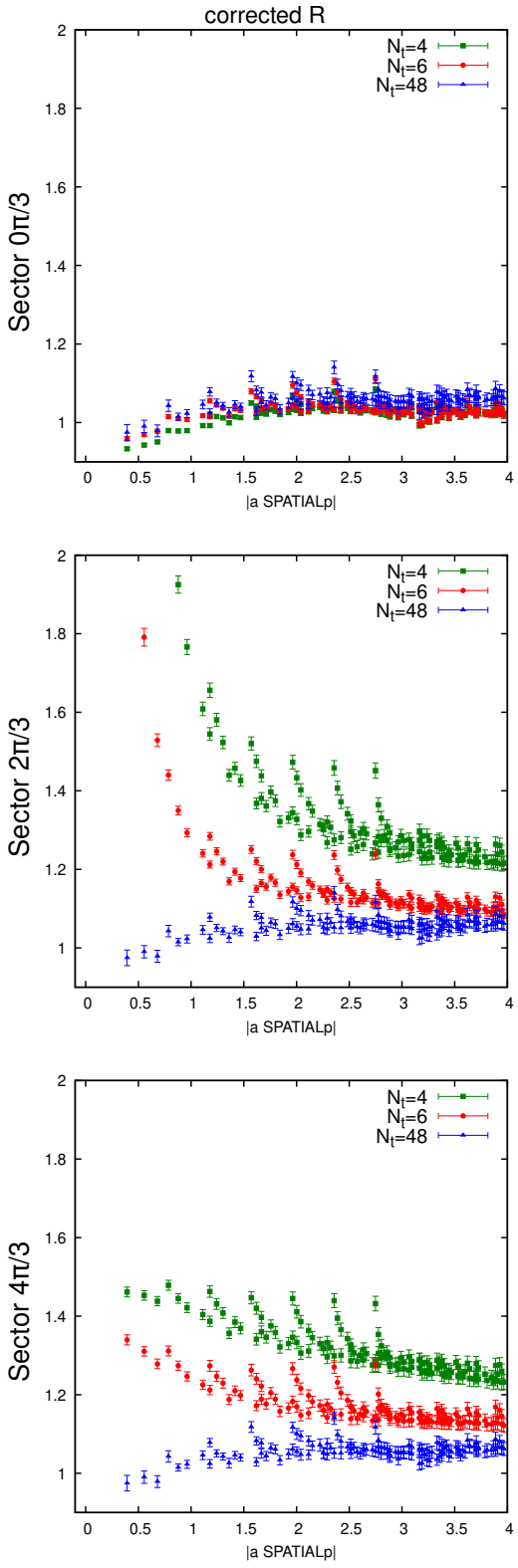

Figure 16 – The form factor $R(p)$ for different temperatures and sectors and Matsubara frequency $\omega_{n_4=0}$. Results for lattices with $N_s = 16$, $\beta = 6.0$ and $\kappa = 0.1342$.

Source: By the author..

Lastly, we examine the volume dependence of the finite temperature form factors. The corrected $M(p)$ and $Z(p)$ functions are displayed in Figs. 17 and 18 for $N_t = 4$ and $N_t = 6$ respectively, and likewise the $R(p)$ function in Figs.19 and 20.

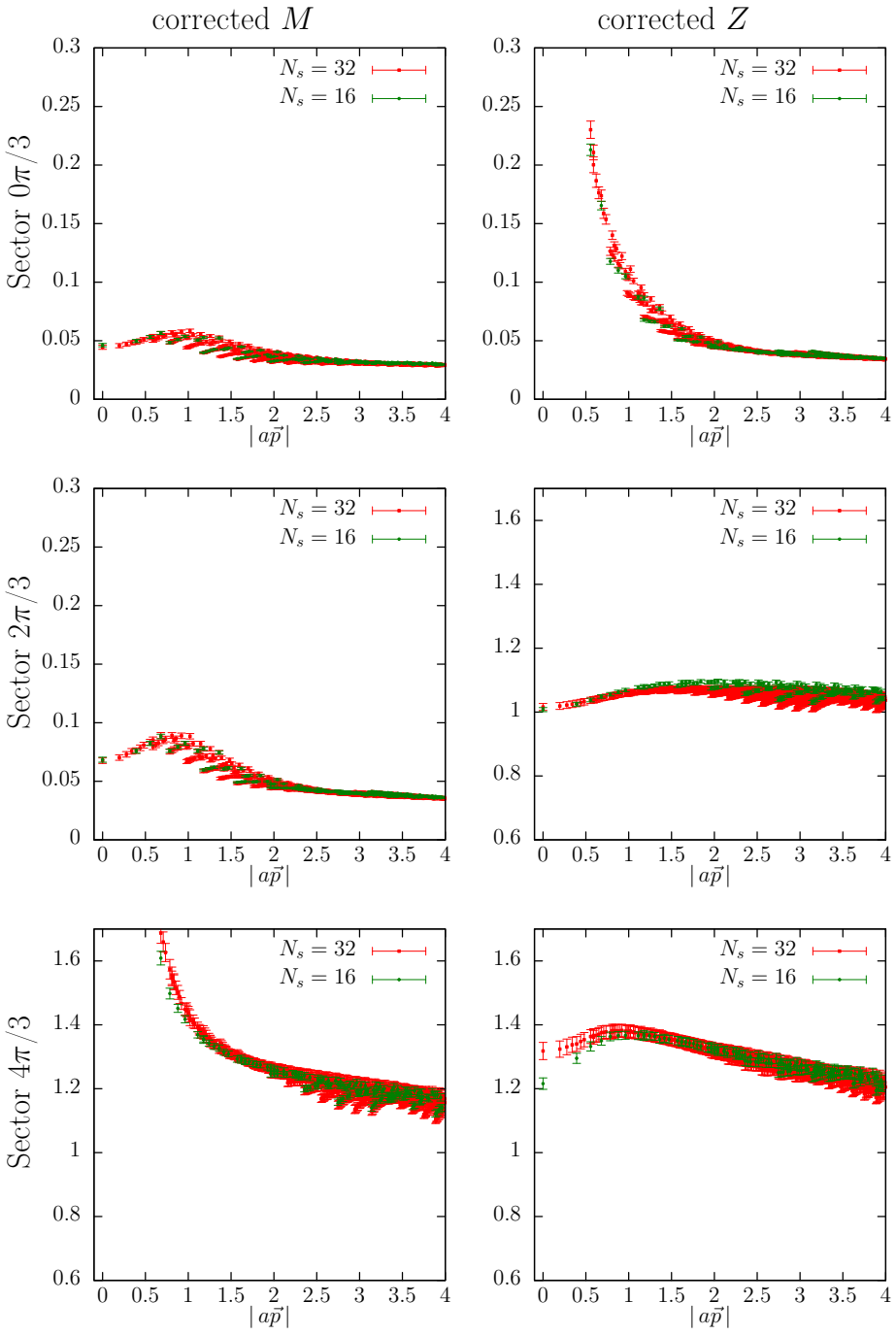

Figure 17 – The form factors $M(p)$ and $Z(p)$ for different volumes and sectors and Matsubara frequency $\omega_{n_4=0}$. Results for lattices with $N_t = 4$, $\beta = 6.0$ and $\kappa = 0.1342$.

Source: By the author..

For most form factors and sectors, the volume dependence seems rather mild. An exception is $4\pi/3$ sector in the case of the corrected Z, which shows some volume

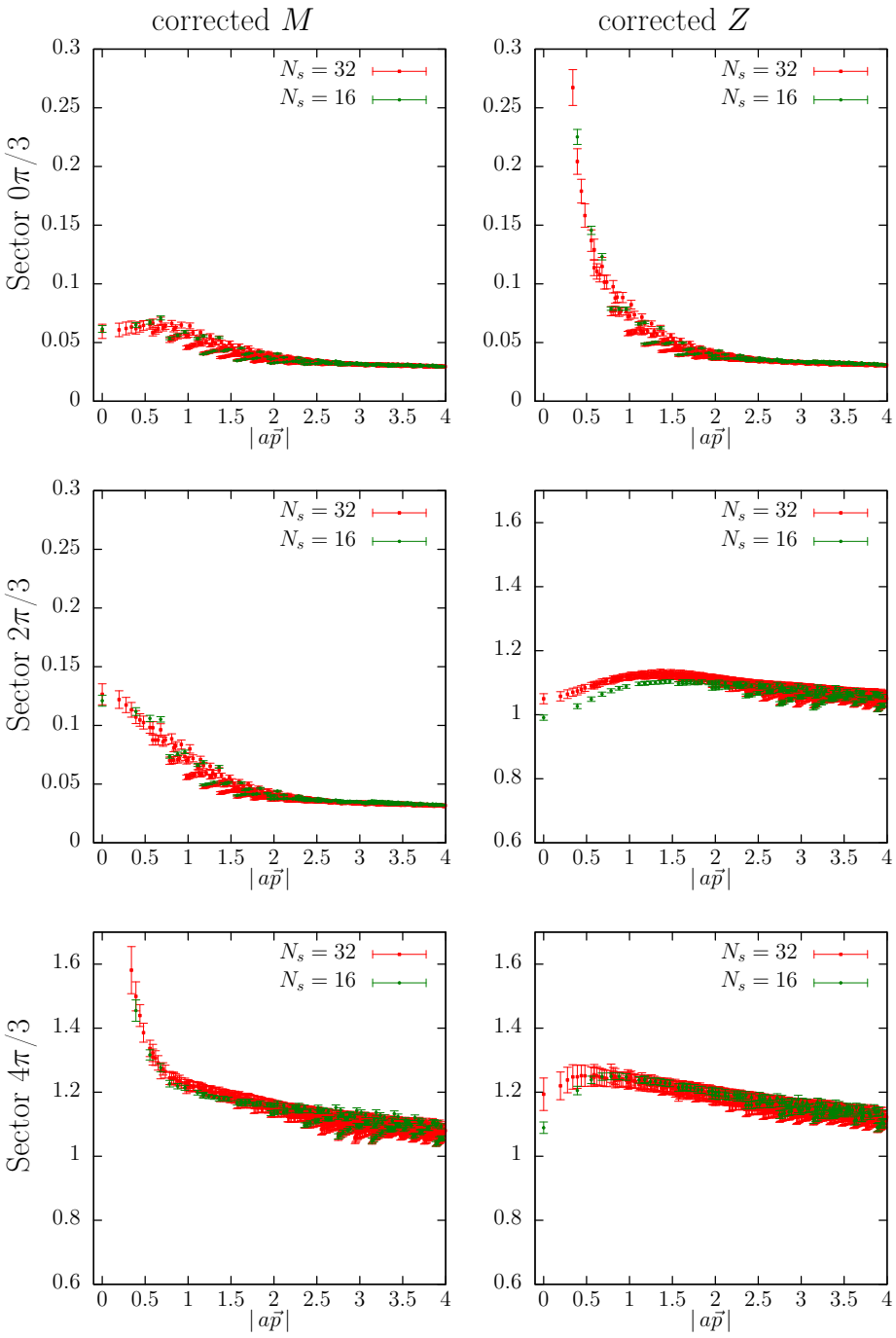

Figure 18 – The form factors $M(p)$ and $Z(p)$ for different volumes and sectors and Matsubara frequency $\omega_{n_4=0}$. Results for lattices with $N_t = 6$, $\beta = 6.0$ and $\kappa = 0.1342$.

Source: By the author..

dependence in the infrared for both temperatures.

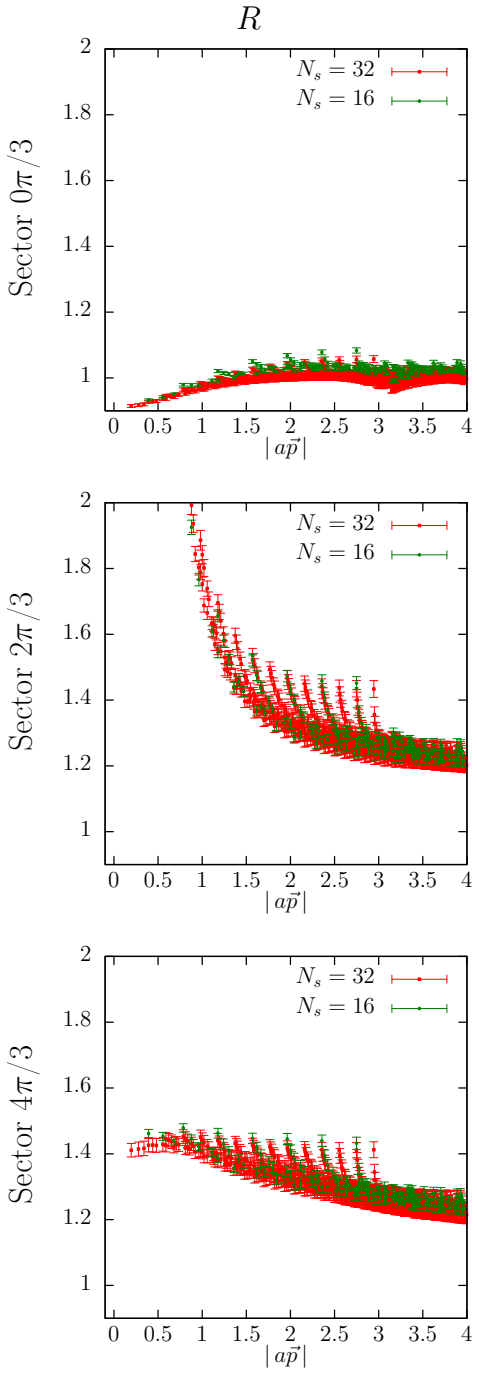

Figure 19 – The form factors $R(p)$ for different volumes and sectors and Matsubara frequency $\omega_{n_4=0}$. Results for lattices with $N_t = 4$, $\beta = 6.0$ and $\kappa = 0.1342$.

Source: By the author..

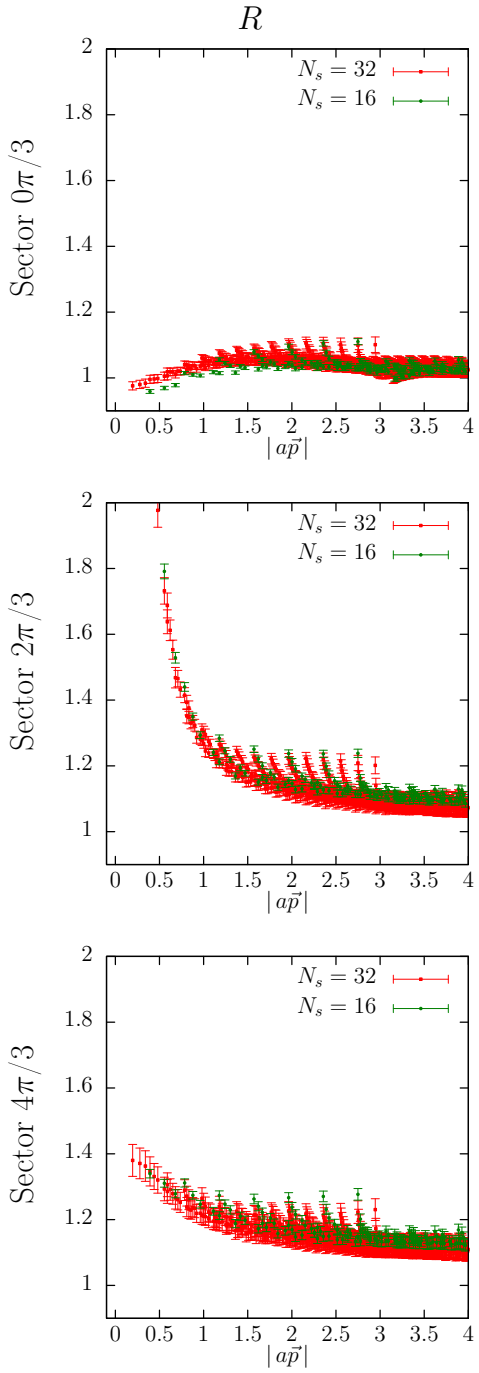

Figure 20 – The form factors $R(p)$ for different volumes and sectors and Matsubara frequency $\omega_{n_4=0}$. Results for lattices with $N_t = 6$, $\beta = 6.0$ and $\kappa = 0.1342$.

Source: By the author..

8.2.3 H4 extrapolation

On the lattice, we necessarily reduce the continuum 4-dimensional spherical symmetry group O(4) to the discrete rotations of the hypercubic group H(4). One of the consequences of this is that quantities which were restricted to depend only on invariants of O(4) will now, in general, depend on the invariants of H(4) which are higher in number. For example, the quark propagator, which can be described in the continuum as a function of p^2, where p_μ is the 4-momentum, will on the lattice depend on the H(4) invariants $p^{[2]} = p^2$, $p^{[4]}$, $p^{[6]}$ and $p^{[8]}$, where

$$p^{[2i]} = \sum_\mu p_\mu^{2i}. \tag{8.16}$$

That these are invariants of H(4) can be seen by noting that the hypercubic transformations simply shuffle the components of the p_μ vector, possibly changing their signs if a rotation or a reflection is involved, but since the powers in the summands are always even, these sign changes will not change the sum.

The fact that we only considered i up to 8 above, comes from a result in group-invariant theory, which states that any polynomial function of p which is invariant under the action of H(4) is a function of the 4 invariants above, (97, 149).

One example can help in elucidating the difference between the continuum and lattice results in regards to the H(4) artifacts is the following.

The possible momenta p_μ for a fermion on the lattice, with anti-periodic boundary conditions in the time direction, is restricted due to the finiteness of the lattice as well as from the discretization of the space-time itself. The set of allowed values are

$$\tilde{\Lambda} = \left\{ p = (p_1, p_2, p_3, p_4) \mid a\, p_\mu = \frac{2\pi}{N_\mu}(n_\mu + \theta_\mu), n_\mu = -\frac{N_\mu}{2} + 1, ..., \frac{N_\mu}{2} \right\}, \tag{8.17}$$

where $\theta_0 = 1/2$ and $\theta_i = 0$, which comes from the anti-periodic boundary condition in the time direction.

Consider a $16^3 \times 48$ lattice. A few lattice momenta with the same a^2p^2 and different values for the other H(4) invariants are shown in Table 14. If we had O(4) symmetry, then the quantities of interest would only depend on $(ap)^2$, and would therefore be the same for all momenta with the same value $(ap)^2$, but this is not the case: this manifests itself in plots of the said quantities against $(ap)^2$ in the form of bands instead of a single curve, with data with the same or close values of $(ap)^2$ giving somewhat different values, due to the artifacts, complicating the unambiguous determination of the values of interest.

What we can do, since we are ultimately interested in the continuum results, which should depend only on p^2, is to try to extrapolate out the other invariants. We make the supposition that we can write the quantities of interest extracted from the lattice as

Table 14 – H(4) invariants for a few lattice momenta and a measurement of the distance to the diagonal in momentum space.

n_μ	$a^2p^{[2]}$	$a^4p^{[4]}$	$a^6p^{[6]}$	Δap
(0, 1, 2, 2)	1.39220	0.78481	0.47310	0.60253
(8, 0, 0, 1)	1.39220	1.55639	1.90101	0.90867
(0, 0, 0, 3)	1.39220	1.92632	2.67354	1.00279
(7, 2, 2, 2)	2.81438	2.07048	1.59951	0.17004
(1, 0, 3, 3)	2.81438	3.85409	5.34714	1.08881
(10, 1, 1, 2)	2.81438	3.99678	6.98372	0.80356
(1, 1, 1, 4)	2.81438	6.13712	15.0291	1.08881
(4, 0, 0, 4)	2.81438	6.20846	15.0635	1.28380
(7,1,2,3)	3.12281	3.25955	3.80729	0.58081
(4,0,3,3)	3.12281	3.97300	5.38886	0.97683
(10,0,2,2)	3.12281	4.32972	7.21110	0.97683
(4,1,1,4)	3.12281	6.25603	15.0708	0.97683
(1,0,2,4)	3.12281	6.47006	15.2565	1.22227
(13,0,0,0)	3.12281	9.75191	30.45330	1.53039

Source: By the author.

following (97),

$$Q_L(a,p) = Q((ap)^2) + a^4p^{[4]}f_4((ap)^2) + a^6p^{[6]}f_6((ap)^2) + a^8p^{[8]}f_8((ap)^2). \tag{8.18}$$

We will eventually need to worry about the continuum limit of $Q((ap)^2)$, but if this is a sound procedure, the H(4) lattice artifacts will have been eliminated.

We could try to fit for each value of $(ap)^2$ separately, but the momenta in Table 14 is the exception rather than the rule: in the majority of the cases, we have one single representative for each $(ap)^2$ and therefore, if the f_4, f_6 and f_8 in Eq. 8.18 are not constants, we would not be able to obtain a reliable extrapolation for all values of $(ap)^2$, as we would have more parameters to be fitted than data points. We proceed differently and try a global fit with all data points contributing information.

In order to fit the functions $f_4((ap)^2)$ and $f_6((ap)^2)$, we rely on an Ansatz motivated by the $\mathcal{O}(a^2)$ expansion of the trace of the 1-loop Wilson quark propagator, whose term associated to $a^4p^{[4]}$ has the form (97, 178)

$$f_4^{\text{1-loop}}((ap)^2) = \frac{c(g^2) + c_{\log}(g^2)\log((ap)^2)}{(ap)^2}. \tag{8.19}$$

We take the same form for f_6 as well, but we have set $f_8 = 0$, as we have observed that these contributions did not change the results significantly.

An alternative method which aims at reducing these H(4) artifacts is the so-called 'cylinder cut'. In this approach, one aims to keep only data corresponding to momentum which lies close to the diagonal in momentum space $\hat{n} = \frac{1}{2}(1,1,1,1)$, eliminating the rest of the points. One selects points which satisfy the condition that they are contained

in a cylinder of a given radius. More concretely, for each momentum, one calculates $\Delta ap = |ap| \sin(\theta(ap))$, where the angle is computed by

$$\cos(\theta(ap)) = \frac{ap.\hat{n}}{|ap|}, \tag{8.20}$$

and keep only momenta that satisfy $\Delta ap < r_{\text{cut}}$. The original proponents of this scheme (179) used $r_{\text{cut}} = 1 \times \frac{2\pi}{N_s}$, which is a radius of 1 lattice spacing from the diagonal. In this formula, N_s is the number of points in the spatial direction. For the data in Table 14, this would eliminate all but the point corresponding to $(7, 2, 2, 2)$. One can observe that there is a correlation between low values of Δap and lower values of $a^4 p^{[4]}$, although this is not a strict rule, as can be seen comparing the rows of $(1, 0, 3, 3)$ and $(10, 1, 1, 2)$. This correlation goes in the direction of implying that by taking momenta close to the diagonal, we are effectively taking values close to $Q((ap)^2)$ of Eq. 8.18, without doing any extrapolation of the data. This procedure, however, throws away all the information contained corresponding to momenta which do not survive the cut criterion. It does not take into account, for example, what the trend is between values associated to momenta with the same $(ap)^2$ but different $a^4 p^{[4]}$. This is what the extrapolation aims to improve upon. For our quantities, therefore, we will prefer to use the H(4) extrapolation method. We first average over the signed permutations of our momenta.

For example, data corresponding to momentum $(0, 1, 2, 2)$, and its permutations $(0, 2, 1, 2)$ and $(0, 2, 2, 1)$ as well as $(0, -1, 2, 2)$ and its permutations, with all possible placements of the minus signs will give the same invariants in H(4), therefore the data can be safely combined in order to increase the statistics. This is sometimes referred to as an orbit average. The time component, however, cannot be permutated around, because of the θ term in 8.17, which would give a different value for the invariants.

We perform a non-linear fit, with the model

$$Q_L(a, p) = Q((ap)^2) + a^4 p^{[4]} \left(\frac{c_4 + c_{\log 4} \log((ap)^2)}{(ap)^2} \right) + a^6 p^{[6]} \left(\frac{c_6 + c_{\log 6} \log((ap)^2)}{(ap)^2} \right), \tag{8.21}$$

i.e, we find the constants c_4, $c_{\log 4}$, c_6, $c_{\log 6}$ and the set of $Q((ap)^2)$ which minimize the residual sum of squares, given our data.

Due to time constraints this analysis could not be completed at the time of the submission of this thesis, but work on it is underway.

9 CONCLUSION

In our gauge fixing results we found that it is possible to reduce critical slowing down in Landau gauge fixing algorithms for $SU(3)$ using overrelaxation and stochastic overrelaxation, bringing the critical exponents down from approximately 2 to close to 1. In order to attain these improvements, one can use two steps of maximization per site for the calulation of the improvement matrix and then use the optimal ω or p parameters for the algorithms, as shown in the text.

Encouraged by studies that found unquenching effects on the quark propagator to have a small effect on the final results we calculated the quark propagator on pure-gauge ensembles of various volumes and temperatures with the aim of understanding the thermal effects on this correlator.

At zero temperature, we are able to reproduce the qualitative features found in all studies for the form factors in Landau gauge, namely, dynamical mass generation for the mass form factor in the infrared, which can be attributed to the mechanism of chiral symmetry breaking. We also found the characteristic dip for low momenta for the quark wave-function renormalization function in Landau gauge. The $R(p)$ form factor, which measures the level of asymmetry between the spatial and temporal non-scalar components of the propagator, show some deviation from 1, which we attribute to the anti-periodic boundary conditions of the quark field in the time direction and the asymmetry of our lattice, which is larger in the time direction. Some volume dependence shows up and this needs to be addressed more carefully, perhaps by producing ensembles with spatial volumes in between the ones considered here, to be able to investigate how the data is approaching the infinite volume limit. Likewise, some finite spacing dependence shows that we are not as close to the continuum limit as we would like.

At finite temperature, we found that, depending on the the Polyakov loop sector that one is, the results change dramatically. For the ω_0 Matsubara frequency, in the $0\pi/3$ sector, we get a suppression of dynamical mass generation, however for the $2\pi/3$ sector, we get higher values for the mass form factor than at zero temperature. The dip for low momenta of the Z function in the $0\pi/3$ sector is not as deep as in the vacuum, and for the other sectors there is actually an enhancement. Lastly, finite volume effects at non-zero temperature seem milder than what we found at zero temperature.

REFERENCES

1 PESKIN, M.; SCHROEDER, D. **An introduction to quantum field theory**. Philadelphia: Westview Press, 1995. (Frontiers in physics). ISBN 978-0-813-34543-7.

2 SCHWARTZ, M. D. **Quantum field theory and the standard model**. Cambridge: Cambridge University Press, 2014. ISBN 978-1-107-03473-0, 978-1-107-03473-0.

3 MANDL, F.; SHAW, G. **Quantum field theory**. 2nd ed. Hoboken: Wiley, 2010. ISBN 978-0-471-49683-0.

4 WEINBERG, S. **The quantum theory of fields**: vol. 1: foundations. Cambridge: Cambridge University Press, 2005. ISBN 978-0-521-67053-1, 978-0-511-25204-4.

5 MUTA, T. **Foundations of quantum chromodynamics**: an introduction to perturbative methods in gauge theories. 3rd ed. Hackensack: World Scientific, 2010. (World scientific lecture notes in physics, v. 78). ISBN 978-981-279-353-9.

6 GREINER, W.; SCHRAMM, S.; STEIN, E. **Quantum chromodynamics**. Berlin: Springer, 2002. ISBN 978-3-540-66610-3.

7 GROSS, D. J.; WILCZEK, F. Ultraviolet behavior of non-Abelian gauge theories. **Physical Review Letters**, v. 30, n. 26, p. 1343–1346, 1973.

8 POLITZER, H. D. Reliable perturbative results for strong interactions? **Physical Review Letters**, v. 30, n. 26, p. 1346–1349, 1973.

9 DÜRR, S. *et al.* Ab-initio determination of light hadron masses. **Science**, v. 322, n. 5905, p. 1224–1227, 2008.

10 BORSÁNYI, S. *et al.* Leading hadronic contribution to the muon magnetic moment from lattice QCD. **Nature**, v. 593, n. 7857, p. 51–55, 2021.

11 CAPITANI, S. *et al.* Nucleon electromagnetic form factors in two-flavor QCD. **Physical Review D**, v. 92, n. 5, p. 054511, 2015.

12 AOKI, Y. *et al.* FLAG review 2021. **European Physical Journal C**, v. 82, n. 10, p. 869, 2022.

13 KUGO, T.; OJIMA, I. Local covariant operator formalism of non-Abelian gauge theories and quark confinement problem. **Progress of Theoretical Physics Supplement**, v. 66, p. 1–130, 1979.

14 MARINARI, E. *et al.* The string tension in gauge theories: a suggestion for a new measurement method. **Physics Letters B**, v. 298, n. 3-4, p. 400–404, 1993.

15 GRIBOV, V. N. Quantization of non-Abelian gauge theories. **Nuclear Physics B**, v. 139, n. 1-2, p. 1–19, 1978.

16 VANDERSICKEL, N.; ZWANZIGER, D. The Gribov problem and QCD dynamics. **Physics Reports**, v. 520, n. 4, p. 175–251, 2012.

17 CUCCHIERI, A.; MENDES, T. Numerical test of the Gribov-Zwanziger scenario in Landau gauge. **Proceedings of Science**, v. 087, p. 026, 2009. DOI: 10.22323/1.087.0026.

18 GREENSITE, J. **An introduction to the confinement problem**. Berlin: Springer, 2011. (Lecture notes in physics, v. 821). ISBN 978-3-642-14382-3.

19 LACHINI, N. P. **Confinement, ghost sector and geometry in lattice gauge theories**. Dissertação (Mestrado em Ciências) — Instituto de Física de São Carlos, Universidade de São Paulo, São Carlos, 2019.

20 NAMBU, Y. Strings, monopoles and gauge fields. **Physical Review D**, v. 10, n. 12, p. 4262–4268, 1974.

21 HOOFT, G. 't. Topology of the gauge condition and new confinement phases in non-Abelian gauge theories. **Nuclear Physics B**, v. 190, n. 3, p. 455–478, 1981.

22 POLYAKOV, A. M. Compact gauge fields and the infrared catastrophe. **Physics Letters B**, v. 59, n. 1, p. 82–84, 1975.

23 HOOFT, G. 't. On the phase transition towards permanent quark confinement. **Nuclear Physics B**, v. 138, n. 1, p. 1–25, 1978.

24 MACK, G. Predictions of a theory of quark confinement. **Physical Review Letters**, v. 45, n. 17, p. 1378–1381, 1980.

25 ROTHE, H. J. **Lattice gauge theories**: an introduction. 4th ed. Singapore, Singapore: World Scientific Publishing Company, 2012. (World scientific lecture notes in physics, v. 43). ISBN 978-981-4365-87-1.

26 BELAVIN, A. A. *et al.* Pseudoparticle solutions of the Yang-Mills equations. **Physics Letters B**, v. 59, n. 1, p. 85–87, 1975.

27 GATTRINGER, C. *et al.* Searching for KvBLL calorons in SU(3) lattice gauge field ensembles. **Nuclear Physics B** - proceedings supplements, v. 129, p. 653–658, 2004. DOI: 10.1016/S0920-5632(03)02671-9.

28 SCHÄFER, T.; SHURYAK, E. V. Instantons in QCD. **Reviews of Modern Physics**, v. 70, n. 2, p. 323–426, 1998.

29 CLAY MATHEMATICS INSTITUTE. **Yang-Mills & the mass gap**. Available at: https://www.claymath.org/millennium/yang-mills-the-maths-gap/. Accessible at: 19 Jan. 2024.

30 ABBOTT, B. P. *et al.* GW170817: observation of gravitational waves from a binary neutron star inspiral. **Physical Review Letters**, v. 119, n. 16, p. 161101, 2017.

31 COLLINS, J. C.; PERRY, M. J. Superdense matter: neutrons or asymptotically free quarks? **Physical Review Letters**, v. 34, n. 21, p. 1353–1356, 1975.

32 CABIBBO, N.; PARISI, G. Exponential hadronic spectrum and quark liberation. **Physics Letters B**, v. 59, n. 1, p. 67–69, 1975.

33 KOGUT, J. B.; STEPHANOV, M. A. **The phases of quantum chromodynamics**: from confinement to extreme environments. Cambridge: Cambridge University Press, 2004. (Cambridge monographs on particle physics, nuclear physics and cosmology, v. 21). ISBN 978-0-511-05738-0.

34 HEINZ, U. W.; JACOB, M. **Evidence for a new state of matter**: an assessment of the results from the CERN lead beam program. 2000. Available at: https://arxiv.org/abs/nucl-th/0002042. Accessible at: 18 Jan. 2024.

35 ARSENE, I.-C. *et al.* Quark gluon plasma and color glass condensate at RHIC? The perspective from the BRAHMS experiment. **Nuclear Physics A**, v. 757, n. 1-2, p. 1–27, 2005.

36 SHURYAK, E. Strongly coupled quark-gluon plasma in heavy ion collisions. **Reviews of Modern Physics**, v. 89, n. 3, p. 035001, 2017.

37 LUO, X.; XU, N. Search for the QCD critical point with fluctuations of conserved quantities in relativistic heavy-ion collisions at RHIC : an overview. **Nuclear Science and Techniques**, v. 28, n. 8, p. 112, 2017.

38 MATSUI, T.; SATZ, H. J/ψ Suppression by quark-gluon plasma formation. **Physics Letters B**, v. 178, n. 4, p. 416–422, 1986.

39 BAZAVOV, A. *et al.* Chiral crossover in QCD at zero and non-zero chemical potentials. **Physics Letters B**, v. 795, p. 15–21, 2019. DOI: 10.1016/j.physletb.2019.05.013.

40 BHATTACHARYA, T. *et al.* QCD phase transition with chiral quarks and physical quark masses. **Physical Review Letters**, v. 113, n. 8, p. 082001, 2014.

41 BERNHARDT, J.; FISCHER, C. S. QCD phase transitions in the light quark chiral limit. **Physical Review D**, v. 108, n. 11, p. 114018, 2023.

42 BRAUN, J. *et al.* Chiral susceptibility in (2+1)-flavor QCD. **Physical Review D**, v. 102, n. 5, p. 056010, 2020.

43 GOTTLIEB, S. A. *et al.* Thermodynamics of lattice QCD with two light quark flavors on a 16**3 x 8 lattice. 2. **Physical Review D**, v. 55, n. 11, p. 6852–6860, 1997.

44 GLOZMAN, L. Y. Three regimes of QCD. **International Journal of Modern Physics A**, v. 36, n. 25, p. 2044031, 2021.

45 AOKI, Y. *et al.* The QCD transition temperature: results with physical masses in the continuum limit. **Physics Letters B**, v. 643, n. 1, p. 46–54, 2006.

46 GATTRINGER, C.; LANG, C. B. **Quantum chromodynamics on the lattice**. Berlin: Springer, 2010. (Lecture notes in physics, v. 788). ISBN 978-3-642-01849-7.

47 OSTERWALDER, K.; SCHRADER, R. Axioms for Euclidean Green's functions. **Communications in Mathematical Physics**, v. 31, p. 83–112, 1973. DOI: 10.1007/BF01645738.

48 OSTERWALDER, K.; SCHRADER, R. Axioms for Euclidean Green's functions. II. **Communications in Mathematical Physics**, v. 42, p. 281–305, 1975. DOI: 10.1007/BF01608978.

49 OSTERWALDER, K. Euclidean Green's functions and Wightman distributions. *In*: VELO, G.; WIGHTMAN, A. (ed.). **Constructive quantum field theory**. Berlin: Springer, 1973, (Lecture notes in physics, v. 25).

50 MONTVAY, I.; MÜNSTER, G. **Quantum fields on a lattice**. Cambridge: Cambridge University Press, 1997. (Cambridge monographs on mathematical physics). ISBN 978-0-521-59917-7.

51 WORKMAN, R. L. *et al.* Review of particle physics. **Progress of Theoretical and Experimental Physics**, v. 2022, n. 8, p. 083C01, 2022.

52 NE'EMAN, Y. Derivation of strong interactions from a gauge invariance. **Nuclear Physics**, v. 26, n. 2, p. 222–229, 1961.

53 GELL-MANN, M. **The eightfold way**: A theory of strong interaction symmetry. 1961. (Technical Report of the California Institute of Technology TID-12608; CTSL-20.). Available at: https://inspirehep.net/files/d8e242837fb067f401f31c1e5a118df6. Accessible at: 20 Jan. 2024.

54 EICHMANN, G. **Lecture notes of introduction to hadron physics**. 2014. Available at: http://cftp.tecnico.ulisboa.pt/~gernot.eichmann/2014-hadron-physics/hadron-part-7.pdf. Accessible at: 22 Jan. 2024.

55 GELL-MANN, M.; LÉVY, M. The axial vector current in beta decay. **Il Nuovo Cimento**, v. 16, n. 4, p. 705, 1960.

56 GOLDSTONE, J. Field theories with superconductor solutions. **Il Nuovo Cimento**, v. 19, p. 154–164, 1961. DOI: 10.1007/BF02812722.

57 TANABASHI, M. *et al.* Review of particle physics. **Physical Review D**, v. 98, n. 3, p. 030001, 2018.

58 GIUSTI, L.; HOELBLING, C.; REBBI, C. Light quark masses with overlap fermions in quenched QCD. **Physical Review D**, v. 64, n. 11, p. 114508, 2001. [Erratum: Phys.Rev.D 65, 079903 (2002)].

59 ALLTON, C. *et al.* Physical results from 2+1 flavor domain wall QCD and SU(2) chiral perturbation theory. **Physical Review D**, v. 78, n. 11, p. 114509, 2008.

60 FUKAYA, H. *et al.* Determination of the chiral condensate from QCD Dirac spectrum on the lattice. **Physical Review D**, v. 83, n. 7, p. 074501, 2011.

61 WILSON, K. G. Confinement of quarks. **Physical Review D**, v. 10, n. 8, p. 2445–2459, 1974.

62 LÜSCHER, M.; WEISZ, P. On-shell improved lattice gauge theories. **Communications in Mathematical Physics**, v. 98, n. 3, p. 433, 1985. [Erratum: Commun.Math.Phys. 98, 433 (1985)].

63 AOKI, S. *et al.* Light hadron spectrum and quark masses from quenched lattice QCD. **Physical Review D**, v. 67, n. 3, p. 034503, 2003.

64 SMIT, J. **Introduction to quantum fields on a lattice**. Cambridge: Cambridge University Press, 2002. (Cambridge lecture notes in physics, v. 15). ISBN 978-0-521-89051-9.

65 HELLER, U. M.; KARSCH, F. One loop perturbative calculation of Wilson loops on finite lattices. **Nuclear Physics B**, v. 251, p. 254–278, 1985. DOI: 10.1016/0550-3213(85)90261-5.

66 HASENFRATZ, A.; HASENFRATZ, P. The connection between the lambda parameters of lattice and continuum QCD. **Physics Letters B**, v. 93, n. 1-2, p. 165, 1980.

67 PARISI, G. On the relation between the renormalized and the bare coupling constant on the lattice. **Physics Letters B**, v. 92, n. 1-2, p. 133–134, 1980.

68 LEPAGE, G. P.; MACKENZIE, P. B. On the viability of lattice perturbation theory. **Physical Review D**, v. 48, n. 5, p. 2250–2264, 1993.

69 CAPITANI, S. *et al.* Non-perturbative quark mass renormalization in quenched lattice QCD. **Nuclear Physics B**, v. 544, n. 3, p. 669–698, 1999. [Erratum: Nucl.Phys.B 582, 762–762 (2000)].

70 LÜSCHER, M. **Advanced lattice QCD**. 1998. Available at: https://arxiv.org/pdf/hep-lat/9802029.pdf. Accessible at: 22 Jan. 2024.

71 CUCCHIERI, A.; MENDES, T. Critical slowing down in SU(2) Landau gauge fixing algorithms at beta = infinity. **Computer Physics Communications**, v. 154, n. 1, p. 1–48, 2003.

72 SOMMER, R. A new way to set the energy scale in lattice gauge theories and its applications to the static force and α_s in SU(2) Yang-Mills theory. **Nuclear Physics B**, v. 411, n. 2-3, p. 839–854, 1994.

73 NECCO, S.; SOMMER, R. The N(f) = 0 heavy quark potential from short to intermediate distances. **Nuclear Physics B**, v. 622, n. 1-2, p. 328–346, 2002.

74 BELLAC, M. L. **Thermal field theory**. Cambridge: Cambridge University Press, 2011. (Cambridge monographs on mathematical physics). ISBN 978-0-511-88506-8.

75 MAAS, A. Describing gauge bosons at zero and finite temperature. **Physics Reports**, v. 524, p. 203–300, 2013. DOI: 10.1016/j.physrep.2012.11.002.

76 KARSCH, F. Lattice QCD at high temperature and the QGP. **AIP Conference Proceedings**, v. 842, n. 1, p. 20–28, 2006.

77 MCLERRAN, L. D.; SVETITSKY, B. Quark liberation at high temperature: a Monte Carlo study of SU(2) gauge theory. **Physical Review D**, v. 24, n. 2, p. 450, 1981.

78 PHILIPSEN, O. Lattice QCD at non-zero temperature and baryon density. *In*: LELLOUCH, L. *et al.* (ed.). **Modern perspectives in lattice QCD**: quantum field theory and high performance computing. Oxford: Oxford University Press, 2011, (Lecture notes of the Les Houches summer school, v. 93).

79 SVETITSKY, B.; YAFFE, L. G. Critical behavior at finite temperature confinement transitions. **Nuclear Physics B**, v. 210, n. 4, p. 423–447, 1982.

80 BAZAVOV, A. *et al.* The chiral and deconfinement aspects of the QCD transition. **Physical Review D**, v. 85, n. 5, p. 054503, 2012.

81 DIRAC, P. **Lectures on quantum mechanics**. Mineola: Dover Publications, 2001. (Dover books on physics).

82 CERQUEIRA, M. C. **Estudo numérico de correlações gluônicas em teorias de Yang-Mills a temperatura finita**. Tese (Doutorado em Ciências) — Instituto de Física de São Carlos, Universidade de São Paulo, São Carlos, 2023.

83 ELITZUR, S. Impossibility of spontaneously breaking local symmetries. **Physical Review D**, v. 12, n. 12, p. 3978–3982, 1975.

84 MARTINELLI, G. *et al.* A general method for nonperturbative renormalization of lattice operators. **Nuclear Physics B**, v. 445, n. 1, p. 81–108, 1995.

85 GIUSTI, L. *et al.* Problems on lattice gauge fixing. **International Journal of Modern Physics A**, v. 16, n. 21, p. 3487–3534, 2001.

86 SEMENOV-TYAN-SHANSKII, M. A.; FRANKE, V. A. A variational principle for the Lorentz condition and restriction of the domain of path integration in non-Abelian gauge theory. **Journal of Soviet Mathematics**, v. 34, p. 1999–2004, 1986. DOI: 10.1007/BF01095108.

87 SKULLERUD, J.-I.; WILLIAMS, A. G. Quark propagator in Landau gauge. **Physical Review D**, v. 63, n. 5, p. 054508, 2001.

88 SADOOGHI, N.; ROTHE, H. J. Continuum behavior of lattice QED, discretized with one sided lattice differences, in one loop order. **Physical Review D**, v. 55, n. 11, p. 6749–6759, 1997.

89 NIELSEN, H. B.; NINOMIYA, M. No go theorem for regularizing chiral fermions. **Physics Letters B**, v. 105, n. 2-3, p. 219–223, 1981.

90 CREUTZ, M. Confinement, chiral symmetry, and the lattice. **Acta Physica Slovaca**, v. 61, n. 1, p. 1–127, 2011.

91 WILCZEK, F. On lattice fermions. **Physical Review Letters**, v. 59, n. 21, p. 2397, 1987.

92 GINSPARG, P. H.; WILSON, K. G. A remnant of chiral symmetry on the lattice. **Physical Review D**, v. 25, n. 10, p. 2649, 1982.

93 GATTRINGER, C. A new approach to Ginsparg-Wilson fermions. **Physical Review D**, v. 63, n. 11, p. 114501, 2001.

94 SHARATCHANDRA, H. S.; THUN, H. J.; WEISZ, P. Susskind fermions on a Euclidean lattice. **Nuclear Physics B**, v. 192, n. 1, p. 205–236, 1981.

95 CHODOS, A.; HEALY, J. B. Spectral degeneracy of the lattice Dirac equation as a function of lattice shape. **Nuclear Physics B**, v. 127, n. 3, p. 426–446, 1977.

96 LÜSCHER, M. *et al.* Nonperturbative O(a) improvement of lattice QCD. **Nuclear Physics B**, v. 491, n. 1-2, p. 323–343, 1997.

97 OLIVEIRA, O. *et al.* Quark propagator with two flavors of O(a)-improved Wilson fermions. **Physical Review D**, v. 99, n. 9, p. 094506, 2019.

98 CELMASTER, W.; GONSALVES, R. J. The renormalization prescription dependence of the QCD coupling constant. **Physical Review D**, v. 20, n. 6, p. 1420–1434, 1979.

99 FRANCO, E.; LUBICZ, V. Quark mass renormalization in the MS-bar and RI schemes up to the NNLO order. **Nuclear Physics B**, v. 531, n. 1-3, p. 641–651, 1998.

100 CHETYRKIN, K. G.; RETEY, A. Renormalization and running of quark mass and field in the regularization invariant and MS-bar schemes at three loops and four loops. **Nuclear Physics B**, v. 583, n. 1-2, p. 3–34, 2000.

101 SOKAL, A. D. Monte carlo methods in statistical mechanics: foundations and new algorithms. *In*: DEWITT-MORETTE, C.; CARTIER, P.; FOLACCI, A. (ed.). **Functional integration**: basics and applications. Boston: Springer, 1997. p. 131–192. ISBN 978-1-4899-0319-8.

102 TOMÉ, T.; OLIVEIRA, M. J. de. **Stochastic dynamics and irreversibility**. Cham: Springer, 2014. (Graduate texts in physics). ISBN 978-3-319-11769-0.

103 LÜSCHER, M. A Portable high quality random number generator for lattice field theory simulations. **Computer Physics Communications**, v. 79, n. 1, p. 100–110, 1994.

104 KENNEDY, A. D.; PENDLETON, B. J. Improved heat bath method for Monte Carlo calculations in lattice gauge theories. **Physics Letters B**, v. 156, n. 5-6, p. 393–399, 1985.

105 VISCARDI, L. A. M. **Férmions em QCD na rede**. Dissertação (Mestrado em Ciências) — Instituto de Física de São Carlos, Universidade de São Paulo, São Carlos, 2019.

106 SERENONE, W. M. **Landau's two-component superfluid model and the quark-gluon plasma**. Tese (Doutorado em Ciências) — Instituto de Física de São Carlos, Universidade de São Paulo, São Carlos, 2019.

107 CABIBBO, N.; MARINARI, E. A new method for updating SU(N) matrices in computer simulations of gauge theories. **Physics Letters B**, v. 119, n. 4-6, p. 387–390, 1982.

108 MANDULA, J. E.; OGILVIE, M. Efficient gauge fixing via overrelaxation. **Physics Letters B**, v. 248, n. 1-2, p. 156–158, 1990.

109 VORST, H. A. van der. Bi-CGSTAB: a fast and smoothly converging variant of Bi-CG for the solution of nonsymmetric linear systems. **SIAM Journal on Scientific and Statistical Computing**, v. 13, n. 2, p. 631–644, 1992.

110 SAAD, Y. **Iterative methods for sparse linear systems**. Philadelphia: Society for Industrial and Applied Mathematics, 2003. ISBN 978-0-89871-534-7.

111 LÜSCHER, M. Computational strategies in lattice QCD. *In*: LELLOUCH, L. *et al.* (ed.). **Modern perspectives in lattice QCD**: quantum field theory and high performance computing. Oxford: Oxford University Press, 2011. p. 331–399. (Lecture notes of the Les Houches summer school, v. 93).

112 MARQUES, J. **Github repository - PhD code**. Available at: https://github.com/jesuel-marques/GaugeFix-Coulomb/tree/gfix_with_configgen. Accessible at: 4 Feb. 2024.

113 FRIGO, M.; JOHNSON, S. G. The design and implementation of FFTW3. **Proceedings of the IEEE**, v. 93, n. 2, p. 216–231, 2005.

114 BERNARD, C. W. *et al.* Lattice quark propagator in fixed gauges. **Nuclear Physics B** - proceedings supplements, v. 17, p. 593–598, 1990. DOI: 10.1016/0920-5632(90)90321-K.

115 BERNARD, C. W.; SONI, A.; YEE, K. K. Applications of gauge fixed correlation functions of quarks and gluons. **Nuclear Physics B** - proceedings supplements, v. 20, p. 410–416, 1991. DOI: 10.1016/0920-5632(91)90951-A.

116 BERNARD, C. W.; SONI, A.; YEE, K. K. **Introduction to lattice gauge fixing and effective quark and gluon masses**. 1992. Available at: https://arxiv.org/pdf/hep-lat/9208007.pdf. Accessible at: 31 Jan. 2024.

117 SKULLERUD, J.-I. A lattice study of the quark propagator and vertex function. **Nuclear Physics B** - proceedings supplements, v. 42, n. 1-3, p. 364–366, 1995.

118 SKULLERUD, J.-I.; WILLIAMS, A. G. The quark propagator in momentum space. **Nuclear Physics B** - proceedings supplements, v. 83, p. 209–211, 2000. DOI: 10.1016/S0920-5632(00)91625-6.

119 SKULLERUD, J.-I.; LEINWEBER, D. B.; WILLIAMS, A. G. Nonperturbative improvement and tree level correction of the quark propagator. **Physical Review D**, v. 64, n. 7, p. 074508, 2001.

120 BONNET, F. D. R. *et al.* Quark propagator in a covariant gauge. **Nuclear Physics B** - proceedings supplements, v. 109, n. 1, p. 158–162, 2002.

121 BOWMAN, P. O. *et al.* Modeling the quark propagator. **Nuclear Physics B** - proceedings supplements, v. 119, p. 323–325, 2003. DOI: 10.1016/S0920-5632(03)01533-0.

122 BOWMAN, P. O.; HELLER, U. M.; WILLIAMS, A. G. Lattice quark propagator in Landau and Laplacian gauges. **Nuclear Physics B** - proceedings supplements, v. 106, p. 820–822, 2002. DOI: 10.1016/S0920-5632(01)01854-0.

123 BOWMAN, P. O.; HELLER, U. M.; WILLIAMS, A. G. Quark propagator from an improved staggered action in Laplacian and Landau gauges. **Nuclear Physics B** - proceedings supplements, v. 109, n. 1, p. 163–167, 2002.

124 BOWMAN, P. O. *et al.* Infrared and ultraviolet properties of the Landau gauge quark propagator. **Nuclear Physics B** - proceedings supplements, v. 128, p. 23–29, 2004. DOI: 10.1016/S0920-5632(03)02454-X.

125 BOWMAN, P. O. *et al.* Unquenched quark propagator in Landau gauge. **Physical Review D**, v. 71, n. 5, p. 054507, 2005.

126 PARAPPILLY, M. B. *et al.* Scaling behavior of quark propagator in full QCD. **Physical Review D**, v. 73, n. 5, p. 054504, 2006.

127 PARAPPILLY, M. B. *et al.* Effects of dynamical sea-quarks on quark and gluon propagators. **AIP Conference Proceedings**, v. 842, n. 1, p. 237–239, 2006.

128 BOWMAN, P. O. *et al.* Role of center vortices in chiral symmetry breaking in SU(3) gauge theory. **Physical Review D**, v. 84, n. 3, p. 034501, 2011.

129 BONNET, F. D. R. *et al.* Overlap quark propagator in Landau gauge. **Physical Review D**, v. 65, n. 11, p. 114503, 2002.

130 ZHANG, J. B. *et al.* Towards the continuum limit of the overlap quark propagator in Landau gauge. **Nuclear Physics B** - proceedings supplements, v. 119, p. 831–833, 2003. DOI: 10.1016/S0920-5632(03)80474-7.

131 ZHANG, J. B. *et al.* Scaling behavior of the overlap quark propagator in Landau gauge. **Physical Review D**, v. 70, n. 3, p. 034505, 2004.

132 ZHANG, J. B. *et al.* Scaling behavior of the Landau gauge overlap quark propagator. **Nuclear Physics B** - proceedings supplements, v. 129, p. 495–497, 2004. DOI: 10.1016/S0920-5632(03)02620-3.

133 ZHANG, J. B. *et al.* Quark propagator in Landau and Laplacian gauges with overlap fermions. **Physical Review D**, v. 71, n. 1, p. 014501, 2005.

134 KAMLEH, W. *et al.* The fat link irrelevant clover overlap quark propagator. **Physical Review D**, v. 71, n. 9, p. 094507, 2005.

135 KAMLEH, W. *et al.* Unquenching effects in the quark and gluon propagator. **Physical Review D**, v. 76, n. 9, p. 094501, 2007.

136 ZHANG, J. B. *et al.* Stout-link smearing in lattice fermion actions. **Physical Review D**, v. 80, n. 7, p. 074503, 2009.

137 MORAN, P. J. *et al.* Impact of stout-link smearing in lattice fermion actions. **Proceedings of Science**, v. 091, p. 023, 2009. DOI: 10.22323/1.091.0023.

138 TREWARTHA, D. *et al.* The influence of instantons on the quark propagator. **Proceedings of Science**, v. 164, p. 247, 2012. DOI: 10.22323/1.164.0247.

139 TREWARTHA, A. *et al.* Quark propagation in the instantons of lattice QCD. **Physical Review D**, v. 88, n. 3, p. 034501, 2013.

140 TREWARTHA, D.; KAMLEH, W.; LEINWEBER, D. Centre vortex effects on the overlap quark propagator. **Proceedings of Science**, v. 214, p. 357, 2014. DOI: 10.22323/1.214.0357.

141 TREWARTHA, A.; KAMLEH, W.; LEINWEBER, D. Evidence that centre vortices underpin dynamical chiral symmetry breaking in SU(3) gauge theory. **Physics Letters B**, v. 747, p. 373–377, 2015. DOI: 10.1016/j.physletb.2015.06.025.

142 TREWARTHA, A.; KAMLEH, W.; LEINWEBER, D. Connection between center vortices and instantons through gauge-field smoothing. **Physical Review D**, v. 92, n. 7, p. 074507, 2015.

143 VIRGILI, A.; KAMLEH, W.; LEINWEBER, D. Impact of centre vortex removal on the Landau-gauge quark propagator in dynamical QCD. **Proceedings of Science**, v. 396, p. 082, 2021. DOI: 10.22323/1.396.0082.

144 VIRGILI, A.; KAMLEH, W.; LEINWEBER, D. B. Overlap quark propagator near the physical pion mass. **Physics Letters B**, v. 840, p. 137865, 2023. DOI: 10.1016/j.physletb.2023.137865.

145 LEINWEBER, D. *et al.* Dynamical fermions, centre vortices, and emergent phenomena. **EPJ Web of Conferences**, v. 274, p. 01002, 2022. DOI: 10.1051/epjconf/202227401002.

146 KAMLEH, W.; LEINWEBER, D. B.; VIRGILI, A. **Evidence that center vortices drive dynamical mass generation in QCD**. 2023. Available at: https://arxiv.org/pdf/2305.18690. Accessible at: 20 Feb. 2024.

147 BOWMAN, P. O.; HELLER, U. M.; WILLIAMS, A. G. Lattice quark propagator with staggered quarks in Landau and Laplacian gauges. **Physical Review D**, v. 66, n. 1, p. 014505, 2002.

148 OLIVEIRA, O. *et al.* Lattice Landau gauge quark propagator and the quark-gluon vertex. **Acta Physica Polonica B** - supplements, v. 9, p. 363–368, 2016. DOI: 10.5506/APhysPolBSupp.9.363.

149 SOTO, F. de; ROIESNEL, C. On the reduction of hypercubic lattice artifacts. **Journal of High Energy Physics**, v. 2007, n. 9, p. 007, 2007.

150 OLIVEIRA, O.; FALCÃO, A. F.; SILVA, P. J. Looking at the analytic structure of Landau gauge propagators. **Proceedings of Science**, v. 396, p. 457, 2022. DOI: 10.22323/1.396.0457.

151 FALCÃO, A. F.; OLIVEIRA, O. Analytic structure of the Landau gauge quark propagator from Padé analysis. **Physical Review D**, v. 106, n. 11, p. 114022, 2022.

152 MARQUES, J. *et al.* The quark propagator and quark-gluon vertex from lattice QCD at finite temperature. **Proceedings of Science**, v. 430, p. 280, 2023. DOI: 10.22323/1.430.0280.

153 NAKAJIMA, H.; FURUI, S. Color confinement in lattice Landau gauge with unquenched Wilson and KS fermions. **Proceedings of Science**, v. 020, p. 302, 2006. DOI: 10.22323/1.020.0302.

154 FURUI, S.; NAKAJIMA, H. Unquenched Kogut-Susskind quark propagator in lattice Landau gauge QCD. **Physical Review D**, v. 73, n. 7, p. 074503, 2006.

155 LAVELLE, M. J.; SCHADEN, M. Propagators and condensates in QCD. **Physics Letters B**, v. 208, n. 2, p. 297–302, 1988.

156 ARRIOLA, E. R.; BOWMAN, P. O.; BRONIOWSKI, W. Landau-gauge condensates from the quark propagator on the lattice. **Physical Review D**, v. 70, n. 9, p. 097505, 2004.

157 FURUI, S. Propagator of the lattice domain wall fermion and the staggered fermion. **Few-Body Systems**, v. 45, n. 11, p. 51–63, 2009. [Erratum: Few Body Syst. 46, 73–74 (2009)].

158 BURGIO, G. *et al.* Propagators in lattice Coulomb gauge and confinement mechanisms. **Proceedings of Science**, v. 105, p. 272, 2011. DOI: 10.22323/1.105.0272.

159 SCHRÖCK, M. The chirally improved quark propagator and restoration of chiral symmetry. **Physics Letters B**, v. 711, n. 2, p. 217–224, 2012.

160 SCHRÖCK, M. Chiral restoration of the momentum space quark propagator through Dirac low-mode truncation. **Proceedings of Science**, v. 171, p. 080, 2013. DOI: 10.22323/1.171.0080.

161 BURGIO, G. *et al.* Running mass, effective energy and confinement: the lattice quark propagator in Coulomb gauge. **Physical Review D**, v. 86, n. 1, p. 014506, 2012.

162 BURGIO, G. *et al.* Lattice Coulomb propagators, effective energy and confinement. **Proceedings of Science**, v. 171, p. 075, 2012. DOI: 10.22323/1.171.0075.

163 MERCADO, Y. D.; PAK, M.; SCHRÖCK, M. Overlap quark propagator in Coulomb gauge QCD. **Proceedings of Science**, v. 214, p. 346, 2014. DOI: 10.22323/1.214.0346.

164 PAK, M.; SCHRÖCK, M. Overlap quark propagator in Coulomb gauge QCD and the interrelation of confinement and chiral symmetry breaking. **Physical Review D**, v. 91, n. 7, p. 074515, 2015.

165 SCHRÖCK, M.; VOGT, H. Lattice QCD Green's functions in maximally Abelian gauge: Infrared Abelian dominance and the quark sector. **Physical Review D**, v. 93, n. 1, p. 014501, 2016.

166 BECIREVIC, D. *et al.* Quark masses and renormalization constants from quark propagator and three point functions. **Nuclear Physics B** - proceedings supplements, v. 83, p. 863–865, 2000. DOI: 10.1016/S0920-5632(00)91828-0.

167 BECIREVIC, D. *et al.* Light quark masses from lattice quark propagators at large momenta. **Physical Review D**, v. 61, n. 11, p. 114507, 2000.

168 CONSTANTINOU, M. *et al.* Non-perturbative renormalization of quark bilinear operators with $N_f = 2$ (tmQCD) Wilson fermions and the tree-level improved gauge action. **Journal of High Energy Physics**, v. 2010, n. 08, p. 068, 2010.

169 BURGER, F. *et al.* Quark mass and chiral condensate from the Wilson twisted mass lattice quark propagator. **Physical Review D**, v. 87, n. 3, p. 034514, 2013.

170 GIUSTI, L. *et al.* Quark and gluon propagators in covariant gauges. **Nuclear Physics B** - proceedings supplements, v. 106, p. 995–997, 2002. DOI: 10.1016/S0920-5632(01)01908-9.

171 BLUM, T. C. *et al.* Nonperturbative renormalization of domain wall fermions: quark bilinears. **Physical Review D**, v. 66, n. 1, p. 014504, 2002.

172 HAMADA, M. *et al.* Quark propagators at finite temperature with the clover action. **Proceedings of Science**, v. 032, p. 136, 2006. DOI: 10.22323/1.032.0136.

173 HAMADA, M. *et al.* Quark propagators in confinement and deconfinement phases. **Physical Review D**, v. 81, n. 9, p. 094506, 2010.

174 SILVA, P. J.; OLIVEIRA, O. Lattice Landau gauge quark propagator at finite temperature. **Proceedings of Science**, v. 336, p. 163, 2019. DOI: 10.22323/1.336.0163.

175 OLIVEIRA, O.; SILVA, P. J. Finite temperature Landau gauge lattice quark propagator. **European Physical Journal C**, v. 79, n. 9, p. 793, 2019.

176 SILVA, P. J.; OLIVEIRA, O. Lattice computation of the quark propagator in Landau gauge at finite temperature. **Proceedings of Science**, v. 363, p. 047, 2020.

177 HUDSPITH, R. J. Fourier accelerated conjugate gradient lattice gauge fixing. **Computer Physics Communications**, v. 187, p. 115–119, 2015. DOI: 10.1016/j.cpc.2014.10.017.

178 CONSTANTINOU, M. *et al.* O(a**2) corrections to the one-loop propagator and bilinears of clover fermions with Symanzik improved gluons. **Journal of High Energy Physics**, v. 2009, n. 10, p. 064, 2009.

179 LEINWEBER, D. B. *et al.* Asymptotic scaling and infrared behavior of the gluon propagator. **Physical Review D**, v. 60, n. 9, p. 094507, 1999. [Erratum: Phys.Rev.D 61, 079901 (2000)].